

NUMERICAL STUDIES OF THE  
KLEIN-GORDON-SCHRÖDINGER  
EQUATIONS

LI YANG

*(M.Sc., Sichuan University)*

A THESIS SUBMITTED  
FOR THE DEGREE OF MASTER OF SCIENCE  
DEPARTMENT OF MATHEMATICS  
NATIONAL UNIVERSITY OF SINGAPORE  
2006

---

# Acknowledgements

---

I would like to thank my advisor, Associate Professor Bao Weizhu, who gave me the opportunity to work on such an interesting research project, paid patient guidance to me, reviewed my thesis and gave me much invaluable help and constructive suggestions on it.

It is also my pleasure to express my appreciation and gratitude to Zhang Yanzhi, Wang Hanquan, and Lim Fongyin, from whom I got valuable suggestions and great help on my research project.

I would also wish to thank the National University of Singapore for her financial support by awarding me the Research Scholarship during the period of my MSc candidature.

My sincere thanks go to the Mathematics Department of NUS for its kind help during my two-year study here.

**Li Yang**  
**June 2006**

---

# Contents

---

<b>Acknowledgements</b>	<b>ii</b>
<b>Summary</b>	<b>vi</b>
<b>List of Tables</b>	<b>ix</b>
<b>List of Figures</b>	<b>x</b>
<b>1 Introduction</b>	<b>1</b>
1.1 Physical background . . . . .	1
1.2 The problem . . . . .	2
1.3 Contemporary studies . . . . .	3
1.4 Overview of our work . . . . .	5
<b>2 Numerical studies of the Klein-Gordon equation</b>	<b>8</b>
2.1 Derivation of the Klein-Gordon equation . . . . .	8
2.2 Conservation laws of the Klein-Gordon equation . . . . .	10
2.3 Numerical methods for the Klein-Gordon equation . . . . .	12

---

2.3.1	Existing numerical methods . . . . .	13
2.3.2	Our new numerical method . . . . .	14
2.4	Numerical results of the Klein-Gordon equation . . . . .	15
2.4.1	Comparison of different methods . . . . .	15
2.4.2	Applications of CN-LF-SP . . . . .	18
<b>3</b>	<b>The Klein-Gordon-Schrödinger equations</b>	<b>26</b>
3.1	Derivation of the Klein-Gordon-Schrödinger equations . . . . .	26
3.2	Conservation laws of the Klein-Gordon-Schrödinger equations . . . . .	28
3.3	Dynamics of mean value of the meson field . . . . .	30
3.4	Plane wave and soliton wave solutions of KGS . . . . .	31
3.5	Reduction to the Schrödinger-Yukawa equations (S-Y) . . . . .	32
<b>4</b>	<b>Numerical studies of the Klein-Gordon-Schrödinger equations</b>	<b>34</b>
4.1	Numerical methods for the Klein-Gordon-Schrödinger equations . . . . .	34
4.1.1	Time-splitting for the nonlinear Schrödinger equation . . . . .	36
4.1.2	Phase space analytical solver+time-splitting spectral discretizations (PSAS-TSSP) . . . . .	36
4.1.3	Crank-Nicolson leap-frog time-splitting spectral discretizations (CN-LF-TSSP) . . . . .	40
4.2	Properties of numerical methods . . . . .	42
4.2.1	For plane wave solution . . . . .	42
4.2.2	Conservation and decay rate . . . . .	43
4.2.3	Dynamics of mean value of meson field . . . . .	45
4.2.4	Stability analysis . . . . .	49
4.3	Numerical results of the Klein-Gordon-Schrödinger equation . . . . .	52
4.3.1	Comparisons of different methods . . . . .	52

---

4.3.2	Application of our numerical methods . . . . .	57
<b>5</b>	<b>Application to the Schrödinger-Yukawa equations</b>	<b>70</b>
5.1	Introduction to the Schrödinger-Yukawa equations . . . . .	70
5.2	Numerical method for the Schrödinger-Yukawa equations . . . . .	72
5.3	Numerical results of the Schrödinger-Yukawa equations . . . . .	73
5.3.1	Convergence of KGS to S-Y in “nonrelativistic limit” regime .	73
5.3.2	Applications . . . . .	74
<b>6</b>	<b>Conclusion</b>	<b>78</b>

---

# Summary

---

In this thesis, we present a numerical method for the nonlinear Klein-Gordon equation and two numerical methods for studying solutions of the Klein-Gordon-Schrödinger equations. We begin with the derivation of the Klein-Gordon equation (KG) which describes scalar (or pseudoscalar) spinless particles, analyze its properties and present Crank-Nicolson leap-frog spectral method (CN-LF-SP) for numerical discretization of the nonlinear Klein-Gordon equation. Numerical results for the Klein-Gordon equation demonstrate that the method is of spectral-order accuracy in space and second-order accuracy in time and it is much better than the other numerical methods proposed in the literature. It also preserves the system energy, linear momentum and angular momentum very well in the discretized level. We continue with the derivation of the Klein-Gordon-Schrödinger equations (KGS) which describes a system of conserved scalar nucleons interacting with neutral scalar mesons coupled through the Yukawa interaction and analyze its properties. Two efficient and accurate numerical methods are proposed for numerical discretization of the Klein-Gordon-Schrödinger equations. They are phase space analytical solver+time-splitting spectral method (PSAS-TSSP) and Crank-Nicolson leap-frog time-splitting spectral method (CN-LF-TSSP). These methods are explicit, unconditionally stable, of spectral accuracy in space and second order accuracy in time, easy to extend

to high dimensions, easy to program, less memory-demanding, and time reversible and time transverse invariant. Furthermore, they conserve (or keep the same decay rate of) the wave energy in KGS when there is no damping (or a linear damping) term, give exact results for plane-wave solutions of KGS, and keep the same dynamics of the mean value of the meson field in discretized level. We also apply our new numerical methods to study numerically soliton-soliton interaction of KGS in 1D and dynamics of KGS in 2D. We numerically find that, when a large damping term is added to the Klein-Gordon equation, bound state of KGS can be obtained from the dynamics of KGS when time goes to infinity. Finally, we extend our numerical method, time-splitting spectral method (TSSP) to the Schrödinger-Yukawa equations and present the numerical results of the Schrödinger-Yukawa equations in 1D and 2D cases.

The thesis is organized as follows: Chapter 1 introduces the physical background of the Klein-Gordon equation and the Klein-Gordon-Schrödinger equations. We also review some existing results of them and report our main results. In Chapter 2, the Klein-Gordon equation, which describes scalar (or pseudoscalar) spinless particles, is derived and its analytical properties are analyzed. The Crank-Nicolson leap-frog spectral method for the nonlinear Klein-Gordon equation is presented and other existing numerical methods are introduced. We also report the numerical results of the nonlinear Klein-Gordon equation, i.e., the breather solution of KG, soliton-soliton collision in 1D and 2D problems. In Chapter 3, the Klein-Gordon-Schrödinger equations, describing a system of conserved scalar nucleons interacting with neutral scalar mesons coupled through the Yukawa interaction, is derived and its analytical properties are analyzed. In Chapter 4, two new efficient and accurate numerical methods are proposed to discretize KGS and the properties of these two numerical methods are studied. We test the accuracy and stability of our methods for KGS with a solitary wave solution, and apply them to study numerically dynamics of a plane wave, soliton-soliton collision in 1D with/without damping terms and a 2D

problem of KGS. In Chapter 5, we extend our methods to the Schrödinger-Yukawa equations and report some numerical results of them. Finally, some conclusions based on our findings and numerical results are drawn in Chapter 6.

---

## List of Tables

---

2.1	Spatial discretization errors $e(t)$ at time $t = 1$ for different mesh sizes $h$ under $k = 0.001$ . . . . .	18
2.2	Temporal discretization errors $e(t)$ at time $t = 1$ for different time steps $k$ under $h = 1/16$ . . . . .	18
2.3	Conserved quantities analysis: $k = 0.001$ and $h = 1/16$ . . . . .	19
4.1	Spatial discretization errors $e_1(t)$ and $e_2(t)$ at time $t = 2$ for different mesh sizes $h$ under $k = 0.0001$ . I: For $\gamma = 0$ . . . . .	53
4.1	(cont'd): II: For $\gamma = 0.5$ . . . . .	54
4.2	Temporal discretization errors $e_1(t)$ and $e_2(t)$ at time $t = 1$ for different time steps $k$ . I: For $\gamma = 0$ . . . . .	55
4.2	(cont'd): II. For $\gamma = 0.5$ and $h = 1/4$ . . . . .	56
4.3	Conserved quantities analysis: $k = 0.0001$ and $h = \frac{1}{8}$ . . . . .	56
5.1	Error analysis between KGS and its reduction S-Y: Errors are computed at time $t = 1$ under $h = 5/128$ and $k = 0.00005$ . . . . .	74

---

# List of Figures

---

2.1 Time evolution of soliton-soliton collision in Example 2.1. a): surface plot; b): contour plot. . . . . 17

2.2 Time evolution of a stationary Klein-Gordon’s breather solution in Example 2.2. a): surface plot; b): contour plot. . . . . 20

2.3 Circular and elliptic ring solitons in Example 2.3 (from top to bottom:  $t = 0, 4, 8, 11.5$  and  $15$ ). . . . . 23

2.4 Collision of two ring solitons in Example 2.4 (from top to bottom :  $t = 0, 2, 4, 6$  and  $8$ ). . . . . 24

2.5 Collision of four ring solitons in Example 2.5 (from top to bottom:  $t = 0, 2.5, 5, 7.5$  and  $10$ ). . . . . 25

4.1 Numerical solutions of the meson field  $\phi$  (left column) and the nucleon density  $|\psi|^2$  (right column) at  $t = 1$  for Example 1 with Type 1 initial data in the “nonrelativistic” limit regime by PSAS-TSSP. ‘-’: exact solution given in (4.96), ‘+ + +’: numerical solution. I. With the meshing strategy  $h = O(\varepsilon)$  and  $k = O(\varepsilon)$ : (a)  $\Gamma_0 = (\varepsilon_0, h_0, k_0) = (0.125, 0.25, 0.04)$ , (b)  $\Gamma_0/4$ , and (c)  $\Gamma_0/16$ . . . . . 58

4.1	(cont'd): II. With the meshing strategy $h = O(\varepsilon)$ and $k = 0.04$ -independent of $\varepsilon$ : (d) $\Gamma_0 = (\varepsilon_0, h_0) = (0.125, 0.25)$ , (e) $\Gamma_0/4$ , and (f) $\Gamma_0/16$ . . . . .	59
4.2	Numerical solutions of the density $ \psi(x, t) ^2$ and the meson field $\phi(x, t)$ at $t = 1$ in the nonrelativistic limit regime by PSAS-TSSP with the same mesh ( $h = 1/2$ and $k = 0.005$ ). '-': 'exact' solution, '+ + +': numerical solution. The left column corresponds to the meson field $\phi(x, t)$ : (a) $\varepsilon = 1/2$ , (c) $\varepsilon = 1/16$ . (e) $\varepsilon = 1/128$ . The right column corresponds to the density $ \psi(x, t) ^2$ : (b) $\varepsilon = 1/2$ , (d) $\varepsilon = 1/16$ . (f) $\varepsilon = 1/128$ . . . . .	60
4.3	Numerical solutions for plane wave of KGS in Example 4.2 at time $t = 2$ (left column) and $t = 4$ (right column). '-': exact solution given in (4.96), '+ + +': numerical solution. (a): Real part of nucleon field $Re(\psi(x, t))$ ; (b): imaginary part of nucleon field $Im(\psi(x, t))$ ; (c): meson field $\phi$ . . . . .	61
4.4	Numerical solutions of soliton-soliton collision in standard KGS in Example 4.3 I: Nucleon density $ \psi(x, t) $ . . . . .	62
4.5	(cont'd): II. Meson field $\phi(x, t)$ . . . . .	63
4.6	Time evolution of nucleon density $ \psi(x, t) ^2$ (left column) and meson field $\phi(x, t)$ (right column) for soliton-soliton collision of KGS in Example 4.4 for different values of $\gamma$ . . . . .	65
4.7	Time evolution of the Hamiltonian $H(t)$ ('left') and mean value of the meson field $N(t)$ ('right') in Example 4.4 for different values of $\gamma$ . . . . .	66
4.8	Time evolution of the Hamiltonian $H(t)$ ('left') and mean value of the meson field $N(t)$ ('right') in Example 4.6 for different values of $\gamma$ . . . . .	66
4.9	Numerical solutions of the nucleon density $ \psi(x, y, t) ^2$ (right column) and meson field $\phi(x, y, t)$ (left column) in Example 4.5 at $t = 1$ . 1th row: $\varepsilon = 1/2$ ; 2nd row: $\varepsilon = 1/8$ ; 3rd row : $\varepsilon = 1/32$ . . . . .	67

4.10	Numerical solutions of the nucleon density $ \psi(x, y, t) ^2$ (right column) and meson field $\phi(x, y, t)$ (left column) in Example 4.5 at $t = 2$ . 1th row: $\varepsilon = 1/2$ ; 2nd row: $\varepsilon = 1/8$ ; 3rd row : $\varepsilon = 1/32$ . . . . .	68
4.11	Surface plots of the nucleon density $ \psi(x, y, t) ^2$ (left column) and meson field $\phi(x, y, t)$ (right column) in Example 4.6 with $\gamma = 0$ at different times. . . . .	69
5.1	Numerical results for different scales of the $X\alpha$ term in Example 5.2, i.e., $\alpha = 1, \sqrt{\varepsilon}, \varepsilon, 0$ . a) and b) : small time $t = 0.25$ , pre-break, a) for $\varepsilon = 0.05$ , b) for $\varepsilon = 0.0125$ . c)-f): large time, $t = 4.0$ , post-break. c) for $\varepsilon = 0.1$ , d) for $\varepsilon = 0.05$ , e) for $\varepsilon = 0.0375$ , f) $\varepsilon = 0.025$ . . . . .	76
5.2	Time evolution of the position density for $X\alpha$ term at $O(1)$ in Example 5.2, i.e., $\alpha = 0.5$ , with $\varepsilon = 0.025$ , $h = 1/512$ and $k = 0.0005$ . a) surface plot; b) pseudocolor plot. . . . .	77
5.3	Time evolution of the position density for attractive Hartree interaction in Example 5.2. $C = -1$ , $\alpha = 0.5$ , $\varepsilon = 0.025$ , $k = 0.00015$ . a) surface plot; b) pseudocolor plot. . . . .	77

# Introduction

In this chapter, we introduce the physical background of the nonlinear Klein-Gordon equation (KG) and the Klein-Gordon-Schrödinger equations (KGS) and review some existing analytical and numerical results of them and report our main results of these two problems.

## 1.1 Physical background

The Klein-Gordon equation (or Klein-Fock-Gordon equation) is a relativistic version of the Schrödinger equation, which describes scalar (or pseudoscalar) spinless particles. The Klein-Gordon equation was actually first found by Schrödinger, before he made the discovery of the equation that now bears his name. He rejected it because he couldn't make it fit the data (the equation doesn't take into account the spin of the electron); the way he found his equation was by making simplification in the Klein-Gordon equation. Later, it was revived and it has become commonly accepted that Klein-Gordon equation is the appropriate model to describe the wave function of the particle that is charge-neutral, spinless and relativistic effects can't be ignored. It has important applications in plasma physics, together with Zakharov equation describing the interaction of Langmuir wave and the ion acoustic wave in a plasma

[57], in astrophysics together with Maxwell equation describing a minimally coupled charged boson field to a spherically symmetric space time [21], in biophysics together with another Klein-Gordon equation describing the long wave limit of a lattice model for one-dimensional nonlinear wave processes in a bi-layer [47] and so on. Furthermore, Klein-Gordon equation coupled with Schrödinger equation (Klein-Gordon-Schrödinger equations or KGS) is introduced in [54, 29] and it describes a system of conserved scalar nucleons interacting with neutral scalar mesons coupled through the Yukawa interaction. As is well known, KGS is not exactly integrable, so the numerical study on it is very important.

## 1.2 The problem

One of the problems we will study numerically is the general nonlinear Klein-Gordon equation (KG)

$$\partial_{tt}\phi - \Delta\phi + F(\phi) = 0, \quad \mathbf{x} \in \mathbb{R}^d, \quad t > 0, \quad (1.1)$$

$$\phi(\mathbf{x}, 0) = \phi^{(0)}(\mathbf{x}), \quad \partial_t\phi(\mathbf{x}, 0) = \phi^{(1)}(\mathbf{x}), \quad \mathbf{x} \in \mathbb{R}^d, \quad (1.2)$$

with the requirements

$$|\partial_t\phi|, \quad |\nabla\phi| \longrightarrow 0, \quad \text{as } |\mathbf{x}| \longrightarrow \infty, \quad (1.3)$$

where  $t$  is time,  $\mathbf{x}$  is the spatial coordinate, the real-valued function  $\phi(\mathbf{x}, t)$  is the wave function in relativistic regime,  $G'(\phi) = F(\phi)$ .

The general form of (1.1) covers many different generalized Klein-Gordon equations arising in various physical applications. For example: a) when  $F(\phi) = \pm(\phi - \phi^3)$ , (1.1) is referred as the  $\phi^4$  equation, which describes the motion of the system in field theory [23]; b) when  $F(\phi) = \sin(\phi)$ , (1.1) becomes the well-known sine-Gordon equation, which is widely used in physical world. It can be found in the motion of a rigid pendulum attached to an extendible string [60], in rapidly rotating fluids [31], in the physics of Josephson junctions and other applications [14, 49].

Another specific problem we study numerically is the Klein-Gordon-Schrödinger (KGS) equations describing a system of conserved scalar nucleons interacting with neutral scalar mesons coupled through the Yukawa interaction [54, 29]:

$$i \partial_t \psi + \Delta \psi + \phi \psi + i\nu \psi = 0, \quad \mathbf{x} \in \mathbb{R}^d, \quad t > 0, \quad (1.4)$$

$$\varepsilon^2 \partial_{tt} \phi + \gamma \varepsilon \partial_t \phi - \Delta \phi + \phi - |\psi|^2 = 0, \quad \mathbf{x} \in \mathbb{R}^d, \quad t > 0, \quad (1.5)$$

$$\psi(\mathbf{x}, 0) = \psi^{(0)}(\mathbf{x}), \quad \phi(\mathbf{x}, 0) = \phi^{(0)}(\mathbf{x}), \quad \partial_t \phi(\mathbf{x}, 0) = \phi^{(1)}(\mathbf{x}), \quad \mathbf{x} \in \mathbb{R}^d; \quad (1.6)$$

where  $t$  is time,  $\mathbf{x}$  is the spatial coordinate, the complex-valued function  $\psi = \psi(\mathbf{x}, t)$  represents a scalar nucleon field, the real-valued function  $\phi = \phi(\mathbf{x}, t)$  represents a scalar meson field,  $\varepsilon > 0$  is a parameter inversely proportional to the speed of light, and  $\gamma \geq 0$  and  $\nu \geq 0$  are two nonnegative parameters.

The general form of (1.4) and (1.5) covers many different generalized Klein-Gordon-Schrödinger equations arising in many various physical applications. In fact, when  $\varepsilon = 1$ ,  $\gamma = 0$  and  $\nu = 0$ , it reduces to the standard KGS [29]. When  $\nu > 0$ , a linear damping term is added to the nonlinear Schrödinger equation (1.4) for arresting blowup. When  $\gamma > 0$ , a damping mechanism is added to the Klein-Gordon equation (1.5). When  $\varepsilon \rightarrow 0$  (corresponding to infinite speed of light or ‘nonrelativistic’ limit regime) in (1.5), formally, we get the well-known Schrödinger-Yukawa (S-Y) equations without ( $\nu = 0$ ) or with ( $\nu > 0$ ) a linear damping term:

$$i \partial_t \psi + \Delta \psi + \phi \psi + i\nu \psi = 0, \quad \mathbf{x} \in \mathbb{R}^d, \quad t > 0, \quad (1.7)$$

$$-\Delta \phi + \phi = |\psi|^2, \quad \mathbf{x} \in \mathbb{R}^d, \quad t > 0. \quad (1.8)$$

### 1.3 Contemporary studies

There was a series of mathematical study from partial differential equations for the KG (1.1). J. Ginibre et al. [32] studied the Cauchy problem for a class of nonlinear Klein-Gordon equations by a contraction method and proved the existence and uniqueness of strongly continuous global solutions in the energy space

$H^1(\mathbb{R}^n) \oplus L^2(\mathbb{R}^n)$  for arbitrary space dimension  $n$ . In [68], Weder developed the scattering theory for the Klein-Gordon equation and proved the existence and completeness of the wave operators, and invariance principle as well.

On the other hand, numerical methods for the nonlinear Klein-Gordon equation were studied in the last fifty years. Strauss et al. [62] proposed a finite difference scheme for the one-dimensional (1D) nonlinear Klein-Gordon equation, which is based on radial coordinate and second-order central difference for the terms  $\phi_{tt}$  and  $\phi_{rr}$ . In [40], Jiménez presented four explicit finite difference methods to integrate the nonlinear Klein-Gordon equation and compared the properties of these four numerical methods. Numerical treatment for damped nonlinear Klein-Gordon equation, based on variational method and finite element approach, is studied in [45, 65]. In [45], Khalifa et al. established the existence and uniqueness of the solution and a numerical scheme was developed based on finite element method. In [36], Guo et al. proposed a Legendre spectral scheme for solving the initial boundary value problem of the nonlinear Klein-Gordon equation, which also kept the conservation. There are also some other numerical methods for solving it [44, 66]. In particular, the Sine-Gordon equation is a typical example of the nonlinear Klein-Gordon equation. There has been a considerable amount of recent discussions on computations of sine-Gordon type solitons, in particular via finite difference and predictor-corrector scheme [2, 18, 19], finite element approaches [2, 4], perturbation methods [48] and symplectic integrators [52].

There was also a series of mathematical study from partial differential equations for the KGS (1.4)-(1.5) in the last two decades. For the standard KGS, i.e.  $\varepsilon = 1$ ,  $\gamma = 0$  and  $\nu = 0$ , Fukuda and Tsutsumi [28, 29, 30] established the existence and uniqueness of global smooth solutions, Biler [17] studied attractors of the system, Guo [33] established global solutions, Hayashi and Von Wahl [37] proved the existence of global strong solution, Guo and Miao [34] studied asymptotic behavior of

the solution, Ohta [56] studied the stability of stationary states for KGS. For plane, solitary and periodic wave solutions of the standard KGS, we refer to [22, 38, 51, 67]. For dissipative KGS, i.e.  $\varepsilon = 1$ ,  $\gamma > 0$  and  $\nu > 0$ , Guo and Li [35, 50], Ozawa and Tsutsumi [58] studied attractor of the system and asymptotic smoothing effect of the solution, Lu and Wang [53] found global attractors. For the nonrelativistic limit of the Klein-Gordon equation, we refer to [15, 16, 64, 20].

In order to study effectively the dynamics and wave interaction of the KGS, especially in 2D & 3D, an efficient and accurate numerical method is one of the key issues. However, numerical methods and simulation for the KGS in the literature remain very limited. Xiang [69] proposed a conservative spectral method for discretizing the standard KGS and established error estimate for the method. Zhang [70] studied a conservative finite difference method for the standard KGS in 1D. Due to that both methods are implicit, it is a little complicated to apply the methods for simulating wave interactions in KGS, especially in 2D & 3D. Usually very tedious iterative method must be adopted at every time step for solving nonlinear system in the above discretizations for KGS and thus they are not very efficient. In fact, there was **no** numerical result for KGS based on their numerical methods in [69, 70]. To our knowledge, there is **no** numerical simulation results for the KGS reported in the literature. Thus it is of great interests to develop an efficient, accurate and unconditionally stable numerical method for the KGS.

## 1.4 Overview of our work

In this thesis, we propose a Crank-Nicolson leap-frog spectral discretization (CN-LF-SP) for the nonlinear Klein-Gordon equation and we also present two different numerical methods, i.e., phase space analytical solver+time-splitting spectral discretization (PSAS-TSSP) and Crank-Nicolson leap-frog time-splitting spectral discretization (CN-LF-TSSP) for the damped Klein-Gordon-Schrödinger equations.

Our numerical method for the KG is based on discretizing spatial derivatives in the Klein-Gordon equation (1.1) by Fourier pseudospectral method and then applying Crank-Nicolson/leap-frog for linear/nonlinear terms for time derivatives. The key points in designing our new numerical methods for the KGS are based on: (i) discretizing spatial derivatives in the Klein-Gordon equation (1.5) by Fourier pseudospectral method, and then solving the ordinary differential equations (ODEs) in phase space analytically under appropriate chosen transmission conditions between different time intervals or applying Crank-Nicolson/leap-frog for linear/nonlinear terms for time derivatives [12, 10]; and (ii) solving the nonlinear Schrödinger equation (1.4) in KGS by a time-splitting spectral method [63, 26, 5, 8, 9], which was demonstrated to be very efficient and accurate and applied to simulate dynamics of Bose-Einstein condensation in 2D & 3D [6, 7]. Our extensive numerical results demonstrate that the methods are very efficient and accurate for the KGS. In fact, similar techniques were already used for discretizing the Zakharov system [11, 12, 42] and the Maxwell-Dirac system [10, 39].

This thesis consists of six chapters arranged as following. Chapter 1 introduces the physical background of the Klein-Gordon equation and the Klein-Gordon-Schrödinger equations. We also review some existing results of them and report our main results. In Chapter 2, the Klein-Gordon equation, which describes scalar (or pseudoscalar) spinless particles, is derived and its analytical properties are analyzed. The Crank-Nicolson leap-frog spectral method for the nonlinear Klein-Gordon equation is presented and other existing numerical methods are introduced. We also report the numerical results of the nonlinear Klein-Gordon equation, i.e., the breather solution of KG, soliton-soliton collision in 1D and 2D problems. In Chapter 3, the Klein-Gordon-Schrödinger equations, describing a system of conserved scalar nucleons interacting with neutral scalar mesons coupled through the Yukawa interaction, is derived and its analytical properties are analyzed. In Chapter 4, two new efficient and accurate numerical methods are proposed to discretize KGS and the properties

---

of these two numerical methods are studied. We test the accuracy and stability of our methods for KGS with a solitary wave solution, and apply them to study numerically the dynamics of a plane wave, soliton-soliton collision in 1D with/without damping terms and a 2D problem of KGS. In Chapter 5, we extend our methods to the Schrödinger-Yukawa equations and report some numerical results of it. Finally, some conclusions based on our findings and numerical results are drawn in Chapter 6.

# Numerical studies of the Klein-Gordon equation

In this chapter, the Klein-Gordon equation, which is the relativistic quantum mechanical equation for a free particle, is derived and its properties are analyzed. We present the Crank-Nicolson leap-frog spectral discretization (CN-LF-SP) for the nonlinear Klein-Gordon equation (1.1) with the periodic boundary conditions, show the numerical simulations of (1.1) in 1D and 2D examples, and compare our method with other existing numerical methods.

## 2.1 Derivation of the Klein-Gordon equation

This section is devoted to derive the Klein-Gordon equation. From elementary quantum mechanics [60], we know that the Schrödinger equation for free particle is

$$i\hbar\frac{\partial}{\partial t}\phi = \frac{\mathbf{P}^2}{2m}\phi, \quad (2.1)$$

where  $\phi$  is the wave function,  $m$  is the mass of the particle,  $\hbar$  is Planck's constant, and  $\mathbf{P} = -i\hbar\nabla$  is the momentum operator.

The Schrödinger equation suffers from not being relativistically covariant, meaning

that it does not take into account Einstein's special relativity. It is natural to try to use the identity from special relativity

$$E = \sqrt{\mathbf{P}^2 c^2 + m^2 c^4} \phi, \quad (2.2)$$

for the energy ( $c$  is the speed of light); then, plugging into the quantum mechanical momentum operator, yields the equation

$$i \hbar \frac{\partial}{\partial t} \phi = \sqrt{(-i \hbar \nabla)^2 c^2 + m^2 c^4} \phi. \quad (2.3)$$

This, however, is a cumbersome expression to work with because of the square root. In addition, this equation, as it stands, is nonlocal. Klein and Gordon instead worked with more general square of this equation (the Klein-Gordon equation for a free particle), which in covariant notation reads

$$(\square^2 + \mu^2)\phi = 0, \quad (2.4)$$

where  $\mu = \frac{mc}{\hbar}$  and  $\square^2 = \frac{1}{c^2} \frac{\partial^2}{\partial t^2} - \nabla^2$ . This operator ( $\square^2$ ) is called as the d'Alembert operator. This wave equation (2.4) is called as the Klein-Gordon equation. It was in the middle 1920's by E. Schrödinger, as well as by O. Klein and W. Gordon, as a candidate for the relativistic analog of the nonrelativistic Schrödinger equation for a free particle.

In order to obtain a dimensionless form of the Klein-Gordon equation (2.4), we define the normalized variables

$$\tilde{t} = \mu c t, \quad \tilde{x} = \mu x. \quad (2.5)$$

Then plugging (2.5) into (2.4) and omitting all ' $\sim$ ', we get the following dimensionless standard Klein-Gordon equation

$$\partial_{tt}\phi - \Delta\phi + \phi = 0. \quad (2.6)$$

For more general case, we consider the nonlinear Klein-Gordon equation

$$\partial_{tt}\phi - \Delta\phi + F(\phi) = 0, \quad (2.7)$$

where  $G(\phi) = \int_0^\phi F(\phi) d\phi$ .

## 2.2 Conservation laws of the Klein-Gordon equation

There are at least three invariants in the nonlinear Klein-Gordon equation (1.1).

**Theorem 2.1.** The nonlinear Klein-Gordon equation (1.1) preserves the conserved quantities. They are the energy

$$\begin{aligned}
H(t) &:= H(\phi(\cdot, t)) = \int_{\mathbb{R}^d} \left[ \frac{1}{2} (\partial_t \phi(\mathbf{x}, t))^2 + \frac{1}{2} |\nabla \phi(\mathbf{x}, t)|^2 + G(\phi(\mathbf{x}, t)) \right] d\mathbf{x} \\
&\equiv \int_{\mathbb{R}^d} \left[ \frac{1}{2} (\phi^{(1)}(\mathbf{x}))^2 + \frac{1}{2} |\nabla \phi^{(0)}(\mathbf{x})|^2 + G(\phi^{(0)}(\mathbf{x})) \right] d\mathbf{x} \\
&:= H(0), \quad t \geq 0,
\end{aligned} \tag{2.8}$$

the linear momentum

$$\begin{aligned}
\mathbf{P}(t) &:= \mathbf{P}(\phi(\cdot, t)) = \int_{\mathbb{R}^d} (\partial_t \phi(\mathbf{x}, t)) (\nabla \phi(\mathbf{x}, t)) d\mathbf{x} \\
&\equiv \int_{\mathbb{R}^d} \phi^{(1)}(\mathbf{x}) (\nabla \phi^{(0)}(\mathbf{x})) d\mathbf{x} := \mathbf{P}(0), \quad t \geq 0,
\end{aligned} \tag{2.9}$$

and angular momentum

$$\begin{aligned}
\mathbf{A}(t) &:= \mathbf{A}(\phi(\cdot, t)) = \int_{\mathbb{R}^d} \left[ \mathbf{x} \left( \frac{1}{2} (\partial_t \phi(\mathbf{x}, t))^2 + \frac{1}{2} (\nabla \phi(\mathbf{x}, t))^2 + G(\phi(\mathbf{x}, t)) \partial_t \phi(\mathbf{x}, t) \right) \right. \\
&\quad \left. + t \partial_t \phi(\mathbf{x}, t) \nabla \phi(\mathbf{x}, t) \right] d\mathbf{x} \\
&\equiv \int_{\mathbb{R}^d} \left[ \mathbf{x} \left( \frac{1}{2} (\phi^{(1)}(\mathbf{x}))^2 + \frac{1}{2} (\nabla \phi^{(0)}(\mathbf{x}))^2 + G(\phi^{(0)}(\mathbf{x})) \phi^{(1)}(\mathbf{x}) \right) \right. \\
&\quad \left. + t \phi^{(1)}(\mathbf{x}) \nabla \phi^{(0)}(\mathbf{x}) \right] d\mathbf{x} \\
&:= \mathbf{A}(0), \quad t \geq 0.
\end{aligned} \tag{2.10}$$

**Proof.** Multiplying (1.1) by  $\phi_t$ , and integrating over  $\mathbb{R}^d$ , we can get

$$\int_{\mathbb{R}^d} \frac{\partial}{\partial t} \left[ \frac{1}{2} (\phi_t)^2 + \frac{1}{2} |\nabla \phi|^2 + G(\phi) \right] d\mathbf{x} - \int_{\mathbb{R}^d} \nabla \cdot (\nabla \phi \phi_t) d\mathbf{x} = 0. \tag{2.11}$$

From (2.11), noting (1.3), we can have the conservation of energy

$$\frac{d}{dt} H = \int_{\mathbb{R}^d} \frac{\partial}{\partial t} \left[ \frac{1}{2} (\phi_t)^2 + \frac{1}{2} |\nabla \phi|^2 + G(\phi) \right] d\mathbf{x} = 0. \tag{2.12}$$

Multiplying (1.1) by  $\nabla\phi$ , and integrating over  $\mathbb{R}^d$ , we can get

$$\int_{\mathbb{R}^d} (\nabla\phi\phi_t)_t d\mathbf{x} - \int_{\mathbb{R}^d} \nabla \left[ \frac{1}{2}(\phi_t)^2 + \frac{1}{2}|\nabla\phi|^2 - G(\phi) \right] d\mathbf{x} = 0. \quad (2.13)$$

From (2.13), noting (1.3), we can obtain the conservation of linear momentum

$$\frac{d}{dt} \mathbf{P} = \int_{\mathbb{R}^d} (\nabla\phi\phi_t)_t d\mathbf{x} = 0. \quad (2.14)$$

Multiplying (1.1) by  $\mathbf{x}\phi_t$ , we get

$$\mathbf{x}\phi_t(\phi_{tt} - \Delta\phi + G(\phi)) = 0. \quad (2.15)$$

Multiplying (1.1) by  $t\nabla\phi$ , we get

$$t\nabla\phi(\phi_{tt} - \Delta\phi + G(\phi)) = 0. \quad (2.16)$$

Subtracting (2.15) by (2.16) and integrating over  $\mathbb{R}^d$ , we can obtain

$$\begin{aligned} & \int_{\mathbb{R}^d} \left[ \mathbf{x} \left( \frac{1}{2}(\phi_t)^2 + \frac{1}{2}|\nabla\phi|^2 + G(\phi)\phi_t \right) + t\phi_t\nabla\phi \right]_t d\mathbf{x} \\ & - \int_{\mathbb{R}^d} \nabla \left[ (\mathbf{x} \cdot \nabla\phi)\phi_t + t \left( \frac{1}{2}(\phi_t)^2 + \frac{1}{2}|\nabla\phi|^2 - G(\phi) \right) \right] d\mathbf{x} = 0. \end{aligned} \quad (2.17)$$

From (2.17), noting (1.3), we can obtain the conservation of angular momentum

$$\frac{d}{dt} \mathbf{A} = \int_{\mathbb{R}^d} \frac{\partial}{\partial t} \left[ \mathbf{x} \left( \frac{1}{2}(\phi_t)^2 + \frac{1}{2}(\nabla\phi)^2 + G(\phi)\phi_t \right) + t\phi_t\nabla\phi \right] d\mathbf{x} = 0. \quad (2.18)$$

□

In one dimension case, the above conserved quantities become

$$H = \int_{-\infty}^{\infty} \left[ \frac{1}{2}(\phi_t(x,t))^2 + \frac{1}{2}(\phi_x(x,t))^2 + G(\phi(x,t)) \right] dx, \quad (2.19)$$

$$P = \int_{-\infty}^{\infty} [\phi_t(x,t)\phi_x(x,t)] dx, \quad (2.20)$$

$$\begin{aligned} A = & \int_{-\infty}^{\infty} \left[ x \left( \frac{1}{2}(\phi_t(x,t))^2 + \frac{1}{2}(\phi_x(x,t))^2 + G(\phi)\phi_t(x,t) \right) \right. \\ & \left. + t\phi_t(x,t)\phi_x(x,t) \right] dx. \end{aligned} \quad (2.21)$$

## 2.3 Numerical methods for the Klein-Gordon equation

In this section, we review some existing numerical methods for the nonlinear Klein-Gordon equation and present a new method for it. For simplicity of notation, we shall introduce the methods in one spatial dimension ( $d = 1$ ). Generalization to  $d > 1$  is straightforward by tensor product grids and the results remain valid without modification. For  $d = 1$ , the problem becomes

$$\partial_{tt}\phi - \partial_{xx}\phi + F_{\text{lin}}(\phi) + F_{\text{non}}(\phi) = 0, \quad a < x < b, \quad t > 0, \quad (2.22)$$

$$\phi(a, t) = \phi(b, t), \quad \partial_x\phi(a, t) = \partial_x\phi(b, t), \quad t \geq 0, \quad (2.23)$$

$$\phi(x, 0) = \phi^{(0)}(x), \quad \partial_t\phi(x, 0) = \phi^{(1)}(x), \quad a \leq x \leq b, \quad t \geq 0, \quad (2.24)$$

where  $F_{\text{lin}}(\phi)$  represents the linear part of  $F(\phi)$  and  $F_{\text{non}}(\phi)$  represents the nonlinear part of it. As it is known in Section 2.2, the KG equation has the properties

$$H(t) = \int_a^b \left[ \frac{1}{2}\phi_t(x, t)^2 + \frac{1}{2}\phi_x(x, t)^2 + G(\phi) \right] dx = H(0), \quad (2.25)$$

$$P(t) = \int_a^b [\phi_t(x, t)\phi_x(x, t)] dx = P(0), \quad (2.26)$$

$$A(t) = \int_a^b \left[ x \left( \frac{1}{2}\phi_t(x, t)^2 + \frac{1}{2}\phi_x(x, t)^2 + G(\phi)\phi_t(x, t) \right) + t\phi_t(x, t)\phi_x(x, t) \right] dx = A(0). \quad (2.27)$$

In some cases, the boundary condition (2.23) may be replaced by

$$\phi(a, t) = \phi(b, t) = 0, \quad t \geq 0. \quad (2.28)$$

We choose the spatial mesh size  $h = \Delta x > 0$  with  $h = (b - a)/M$  for  $M$  being an even positive integer, the time step being  $k = \Delta t > 0$  and let the grid points and the time step be

$$x_j := a + jh, \quad j = 0, 1, \dots, M; \quad t_m := mk, \quad m = 0, 1, 2, \dots. \quad (2.29)$$

Let  $\phi_j^m$  be the approximation of  $\phi(x_j, t_m)$ .

### 2.3.1 Existing numerical methods

There are several numerical methods proposed in the literature [3, 27, 41] for discretizing the nonlinear Klein-Gordon equation. We will review these numerical schemes for it. The schemes are the following

**A).** This is the simplest scheme for the nonlinear Klein-Gordon equation and has had wide use [27]:

$$\frac{\phi_j^{n+1} - 2\phi_j^n + \phi_j^{n-1}}{k^2} - \frac{\phi_{j+1}^n - 2\phi_j^n + \phi_{j-1}^n}{h^2} + F(\phi_j^n) = 0, \\ j = 0, \dots, M-1, \quad (2.30)$$

$$\phi_M^{n+1} = \phi_0^{n+1}, \quad \phi_{-1}^{n+1} = \phi_{M-1}^{n+1}. \quad (2.31)$$

The initial conditions are discretized as

$$\phi_j^0 = \phi^{(0)}(x_j), \quad \frac{\phi_j^1 - \phi_j^{-1}}{2k} = \phi^{(1)}(x_j), \quad 0 \leq j \leq M-1. \quad (2.32)$$

**B).** This scheme was proposed by Ablowitz, Kruskal, and Ladik [3]:

$$\frac{\phi_j^{n+1} - 2\phi_j^n + \phi_j^{n-1}}{k^2} - \frac{\phi_{j+1}^n - 2\phi_j^n + \phi_{j-1}^n}{h^2} + F\left(\frac{\phi_{j+1}^n + \phi_{j-1}^n}{2}\right) = 0, \\ j = 0, \dots, M-1, \quad (2.33)$$

$$\phi_M^{n+1} = \phi_0^{n+1}, \quad \phi_{-1}^{n+1} = \phi_{M-1}^{n+1}. \quad (2.34)$$

The initial conditions are discretized as

$$\phi_j^0 = \phi^{(0)}(x_j), \quad \frac{\phi_j^1 - \phi_j^{-1}}{2k} = \phi^{(1)}(x_j), \quad 0 \leq j \leq M-1. \quad (2.35)$$

**C).** This scheme has been studied by Jiménez [41]:

$$\frac{\phi_j^{n+1} - 2\phi_j^n + \phi_j^{n-1}}{k^2} - \frac{\phi_{j+1}^n - 2\phi_j^n + \phi_{j-1}^n}{h^2} + \frac{G(\phi_{j+1}^n) - G(\phi_{j-1}^n)}{\phi_{j+1}^n - \phi_{j-1}^n} = 0. \\ j = 0, \dots, M-1, \quad (2.36)$$

$$\phi_M^{n+1} = \phi_0^{n+1}, \quad \phi_{-1}^{n+1} = \phi_{M-1}^{n+1}. \quad (2.37)$$

The initial conditions are discretized as

$$\phi_j^0 = \phi^{(0)}(x_j), \quad \frac{\phi_j^1 - \phi_j^{-1}}{2k} = \phi^{(1)}(x_j), \quad 0 \leq j \leq M-1. \quad (2.38)$$

The existing numerical methods are of second-order accuracy in space and second-order accuracy in time. Our new method shown in the next section is of spectral-order accuracy in space, which is much more accurate than them.

### 2.3.2 Our new numerical method

We discretize the Klein-Gordon equation (1.1) by using a pseudospectral method for spatial derivatives, followed by application of a Crank-Nicolson/leap-frog method for linear/nonlinear terms for time derivative.

$$\begin{aligned} & \frac{\phi_j^{m+1} - 2\phi_j^m + \phi_j^{m-1}}{k^2} - D_{xx}^f [\beta\phi_j^{m+1} + (1 - 2\beta)\phi_j^m + \beta\phi_j^{m-1}] \\ & + F_{\text{lin}}(\beta\phi_j^{m+1} + (1 - 2\beta)\phi_j^m + \beta\phi_j^{m-1}) + F_{\text{non}}(\phi_j^m) = 0 \\ & j = 0, \dots, M, \quad m = 1, 2, \dots \end{aligned} \quad (2.39)$$

where  $0 \leq \beta \leq 1/2$  is a constant;  $D_{xx}^f$ , a spectral differential operator approximation of  $\partial_{xx}$ , is defined as

$$D_{xx}^f U|_{x=x_j} = - \sum_{l=-M/2}^{M/2-1} \mu_l^2 (\tilde{U})_l e^{i\mu_l(x_j-a)}, \quad (2.40)$$

where  $(\tilde{U})_l$ , the Fourier coefficient of a vector  $U = (U_0, U_1, U_2, \dots, U_M)^T$  with  $U_0 = U_M$ , is defined as

$$(\tilde{U})_l = \frac{1}{M} \sum_{j=0}^{M-1} U_j e^{-i\mu_l(x_j-a)}, \quad \mu_l = \frac{2\pi l}{b-a}, \quad l = -\frac{M}{2}, \dots, \frac{M}{2} - 1. \quad (2.41)$$

The initial condition (2.24) are discretized as

$$\phi_j^0 = \phi^0(x_j), \quad \frac{\phi_j^1 - \phi_j^{-1}}{2k} = \phi^{(1)}, \quad j = 0, 1, 2, \dots, M-1. \quad (2.42)$$

**Remark 2.1.** If the periodic boundary condition (2.23) is replaced by (2.28), then the Fourier basis used in the above algorithm can be replaced by the sine basis. In fact, the generalized nonlinear Klein Gordon equation (2.22) with the homogeneous Dirichlet boundary condition (2.28) and initial condition (2.24) can be discretized

by

$$\begin{aligned} & \frac{\phi_j^{m+1} - 2\phi_j^m + \phi_j^{m-1}}{k^2} - D_{xx}^s [\beta\phi_j^{m+1} + (1 - 2\beta)\phi_j^m + \beta\phi_j^{m-1}] \\ & + F_{\text{lin}}(\beta\phi_j^{m+1} + (1 - 2\beta)\phi_j^m + \beta\phi_j^{m-1}) + F_{\text{non}}(\phi_j^m) = 0 \\ & j = 0, \dots, M, \quad m = 1, 2, \dots \end{aligned} \quad (2.43)$$

where  $D_{xx}^f$ , a spectral differential operator approximation of  $\partial_{xx}$  based on sine-basis, is defined as

$$D_{xx}^s U|_{x=x_j} = - \sum_{l=-M/2}^{M/2-1} \eta_l^2 (\tilde{U})_l \sin(\eta_l(x_j - a)), \quad (2.44)$$

where  $(\tilde{U})_l$ , the sine coefficient of a vector  $U = (U_0, U_1, U_2, \dots, U_M)^T$  with  $U_0 = U_M = 0$ , is defined as

$$(\tilde{U})_l = \frac{2}{M} \sum_{j=1}^{M-1} U_j \sin(\eta_l(x_j - a)), \quad \eta_l = \frac{\pi l}{b - a}, \quad l = 1, 2, \dots, M - 1. \quad (2.45)$$

## 2.4 Numerical results of the Klein-Gordon equation

In this section, we report numerical results of the nonlinear Klein-Gordon equation with interaction of two solitary wave solutions in 1D to compare the accuracy and stability of different methods described in the previous section. We also present numerical examples including breather solution, soliton-soliton collisions in 1D, as well as ring solitary solutions and soliton-soliton collisions in 2D to demonstrate the efficiency and spectral accuracy of the Crank-Nicolson leap-frog spectral method (CN-LF-SP) for the nonlinear Klein-Gordon equation.

### 2.4.1 Comparison of different methods

**Example 2.1** The nonlinear Klein-Gordon equation with the interaction between two solitary solutions in 1D, i.e.,  $d = 1$ ,  $F(\phi) = \sin(\phi)$  in (1.1)-(1.2). The well-known

kink solitary solution for the Klein-Gordon equation is

$$\phi(x, t) = 4 \tan^{-1} \left[ \exp \left( \pm \frac{x - \theta t}{\sqrt{1 - \theta^2}} \right) \right], \quad (2.46)$$

where  $|\theta| < 1$ .

We consider the collision of two solitons, one with the + sign (kink) and the other with the - sign (antikink). The two solitons have equal amplitude but opposite velocities. The initial condition in (2.24) is chosen as

$$\phi^{(0)}(x) = 4 \tan^{-1} \left[ \exp \left( \frac{x + x_0}{\sqrt{1 - \theta^2}} \right) \right] + 4 \tan^{-1} \left[ \exp \left( \frac{-x + x_0}{\sqrt{1 - \theta^2}} \right) \right], \quad (2.47)$$

$$\phi^{(1)}(x) = 0. \quad (2.48)$$

We solve the problem on the interval  $[-32, 32]$ , i.e.,  $a = -32$  and  $b = 32$  with mesh size  $h = 1/32$  and time step  $k = 0.0001$  by using our method CN-LF-SP method ( $\beta = 0.25$ ). For the numerical results shown in Figure 2.1, we choose  $x_0 = 5.0$ ,  $\theta = 0.3$ . The above numerical results can be compared with the previous ones for this problem in [3, 25].

There is no analytical solution in this case and we let  $\phi$  be the ‘exact’ solution which is obtained numerically by using our numerical method with a very fine mesh and small time step size, e.g.  $h = \frac{1}{32}$  and  $k = 0.0001$ . Let  $\phi_{h,k}$  be the numerical solution obtained by using a numerical method with mesh size  $h$  and time step  $k$ . To quantify the numerical methods, we define the error functions as  $e(t) = \|\phi(\cdot, t) - \phi_{h,k}(t)\|_{l^2}$ . First we test the discretization error in space. In order to do this, we choose a very small time step, e.g.,  $k = 0.001$ , such that the error from time discretization is negligible compared with to spatial discretization error, and solve the nonlinear Klein-Gordon equation with different methods under different mesh size  $h$ . Table 2.1 lists the numerical errors of  $e(t)$  at  $t = 2$  with different mesh size  $h$  for different numerical methods.

Then we test the discretization error in time. Table 2.2 shows the numerical errors  $e(t)$  under different time steps  $k$  for different numerical methods.

Finally we test the conservation of conserved quantities. Table 2.3 presents the

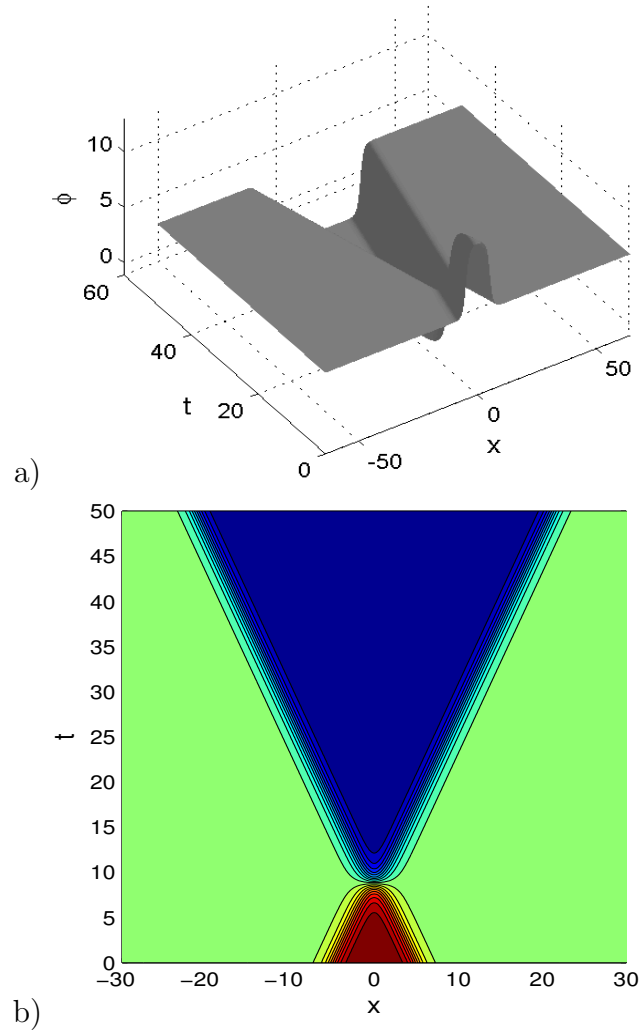


Figure 2.1: Time evolution of soliton-soliton collision in Example 2.1. a): surface plot; b): contour plot.

quantities at different times with mesh size  $h = 1/16$  and time step  $k = 0.001$  for different numerical methods.

From Tables 2.1-2.3, we can draw the following observations: our numerical method CN-LF-SP is of spectral-order accuracy in space discretization and second-order accuracy in time. Finite difference methods (A, B and C) are of second-order accuracy in space discretization. Moreover, CN-LF-SP with  $\beta = 1/2$  or  $\beta = 1/4$  are unconditionally stable, where CN-LF-SP with  $\beta = 0$  is conditionally stable. However finite

Mesh	$h = 1.0$	$h = 1/2$	$h = 1/4$
FDM A	0.131	4.659E-2	1.123E-2
FDM B	0.266	7.764E-2	1.986E-2
FDM C	0.173	5.608E-2	1.414E-2
CN-LF-SP ( $\beta = 0$ )	2.928E-2	5.037E-5	1.209E-7
CN-LF-SP ( $\beta = 1/4$ )	2.928E-2	5.033E-5	1.289E-7
CN-LF-SP ( $\beta = 1/2$ )	2.928E-2	5.030E-5	2.001E-7

Table 2.1: Spatial discretization errors  $e(t)$  at time  $t = 1$  for different mesh sizes  $h$  under  $k = 0.001$ .

Time Step	$k = \frac{1}{32}$	$k = \frac{1}{64}$	$k = \frac{1}{128}$	$k = \frac{1}{256}$	$k = \frac{1}{512}$
CN-LF-SP( $\beta = 0$ )	-	9.057E-6	2.273E-6	5.843E-7	1.868E-7
CN-LF-SP( $\beta = 1/4$ )	6.673E-5	1.668E-5	4.170E-6	1.044E-6	2.800E-7
CN-LF-SP( $\beta = 1/2$ )	1.669E-4	4.173E-5	1.043E-5	2.606E-6	6.568E-7

Table 2.2: Temporal discretization errors  $e(t)$  at time  $t = 1$  for different time steps  $k$  under  $h = 1/16$ .

difference methods (A, B and C) are all conditionally stable in time. All of these numerical methods conserve the energy  $H$ , the linear momentum  $P$  and angular momentum  $A$  very well.

## 2.4.2 Applications of CN-LF-SP

### Breather solution of the Klein-Gordon equation

**Example 2.2** The nonlinear Klein-Gordon equation with a breather solution, i.e., we choose  $d = 1$ ,  $F(\phi) = \sin(\phi)$  in (1.1)-(1.2) and consider the problem on the interval  $[a, b]$  with  $a = -40$  and  $b = 40$  with mesh size  $h = 5/256$ , time step  $k = 0.001$  and  $\beta = 0.25$  for CN-LF-SP. The well-known breather solution is of the

	Time	$H$	$P$	$A$
FDM A	1.0	16.1640	0.0000	0.0000
	2.0	16.1642	0.0000	0.0000
FDM B	1.0	16.1639	0.0000	0.0000
	2.0	16.1639	0.0000	0.0000
FDM C	1.0	16.1641	0.0000	0.0000
	2.0	16.1644	0.0000	0.0000
CN-LF-SP( $\beta = 0$ )	1.0	16.1641	0.0000	0.0000
	2.0	16.1644	0.0000	0.0000
CN-LF-SP( $\beta = 1/4$ )	1.0	1.61641	0.0000	0.0000
	2.0	16.1644	0.0000	0.0000
CN-LF-SP( $\beta = 1/2$ )	1.0	1.61641	0.0000	0.0000
	2.0	16.1644	0.0000	0.0000

Table 2.3: Conserved quantities analysis:  $k = 0.001$  and  $h = 1/16$ .

form [49]

$$\phi(x, t) = -4 \tan^{-1} \left[ \frac{m}{\sqrt{1-m^2}} \frac{\sin(t\sqrt{1-m^2}) + c_2}{\cosh(mx + c_1)} \right]. \quad (2.49)$$

The initial condition is taken as  $\phi^{(0)}(x) = \phi(x, 0)$ ,  $\phi^{(1)}(x) = \phi_t(x, 0)$  in (2.49). In the present example, we choose  $m = 0.5$ ,  $c_1 = 0$ ,  $c_2 = -10\sqrt{1-m^2}$ .

From the results shown in Figure 2.2, it is easy to see that they completely agree with those presented in [25].

### Ring solitary solution of the 2D Klein-Gordon equation

**Example 2.3** The Klein-Gordon equation with a circular ring soliton solution in 2D case, i.e., we choose  $d = 2$ ,  $F(\phi) = \sin(\phi)$  in (1.1)-(1.2). The initial condition is

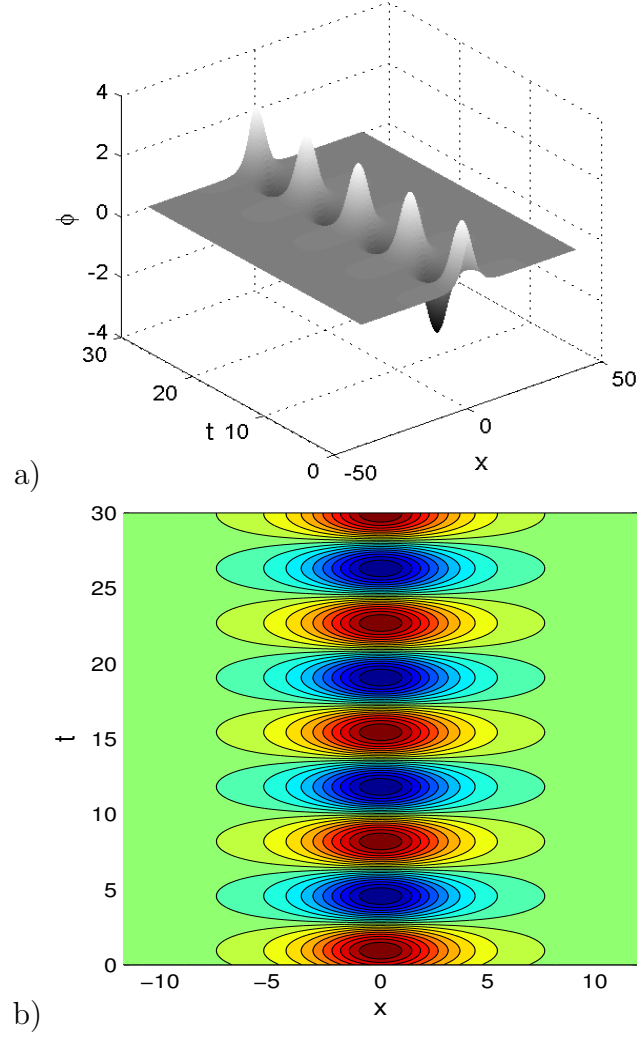


Figure 2.2: Time evolution of a stationary Klein-Gordon's breather solution in Example 2.2. a): surface plot; b): contour plot.

taken as

$$\phi(x, y, 0) = \alpha \tan^{-1} \left[ \exp(3 - \sqrt{x^2 + y^2}) \right], \quad (2.50)$$

$$\phi_t(x, y, 0) = 0, \quad (x, y) \in \mathbb{R}^2, \quad (2.51)$$

where  $\alpha = 4.0$  in our numerical simulation. We solve this problem on the rectangle  $[-16, 16]^2$  with mesh size  $h = 1/16$  and time step  $k = 0.001$  by using our method CN-LF-SP ( $\beta = 0.25$ ). Figure 2.3 shows the surface plots of  $\sin(\phi/2)$  (left column)

and the contour plots of it (right column) at different times, i.e.,  $t = 0, 4, 8, 11.5, 15$ . The resolution is outstanding as compared with the existing numerical solutions [4, 24]. It is found that the ring solitons shrink at the initial stage, but oscillations and radiations begin to form and continue slowly as time goes on. This can be clearly viewed in the contour plots.

**Example 2.4** Two circular soliton-soliton collision in 2D of Klein Gordon equation, i.e., we choose  $d = 2$ ,  $F(\phi) = \sin(\phi)$  in (1.1)-(1.2). The initial condition is taken as

$$\begin{aligned} \phi(x, y, 0) = & \alpha \tan^{-1} \left\{ \exp \left[ \gamma \left( 4 - \sqrt{(x+3)^2 + (y+7)^2} \right) \right] \right\} \\ & + \alpha \tan^{-1} \left\{ \exp \left[ \gamma \left( 4 - \sqrt{(x+3)^2 + (y+17)^2} \right) \right] \right\}, \end{aligned} \quad (2.52)$$

$$\begin{aligned} \phi_t(x, y, 0) = & \theta \operatorname{sech} \left[ \gamma \left( 4 - \sqrt{(x+3)^2 + (y+7)^2} \right) \right] \\ & + \theta \operatorname{sech} \left[ \gamma \left( 4 - \sqrt{(x+3)^2 + (y+17)^2} \right) \right], \quad (x, y) \in \mathbb{R}^2, \end{aligned} \quad (2.53)$$

where  $\alpha = 4.0$ ,  $\theta = 4.13$ ,  $\gamma = 2.29$  in our simulation. We solve this problem on the rectangle  $[-30, 10] \times [-27, 13]$  with mesh size  $h = 1/16$  and time step  $k = 0.001$  by using our method CN-LF-SP ( $\beta = 0.25$ ). Numerical simulation presented in Figure 2.4 is for  $\sin(\phi/2)$  at time  $t = 0, 2, 4, 6, 8$ , respectively. The solution shown includes the extension across  $x = -10$  and  $y = -7$  by symmetry properties of the problem [24]. Figure 2.4 demonstrates the collision between two expanding circular ring solitons in which two smaller ring solitons bounding an annular region merge into a large ring soliton. The simulated solution is again precisely consistent to existing results [24]. Contour plots are given to show more clearly the movement of solitons. Though minor disturbances can be observed in the middle of the numerical solution, probably due to the transactions following the symmetry features in computations, the overall simulation results match well with those described in [19, 24] with satisfaction.

**Example 2.5** The collision of four circular solitons in 2D of Klein Gordon equation,

i.e., we choose  $d = 2$ ,  $F(\phi) = \sin(\phi)$  in (1.1)-(1.2). The initial condition is taken as

$$\begin{aligned} \phi(x, y, 0) = & \alpha \tan^{-1} \left\{ \exp \left[ \gamma \left( 4 - \sqrt{(x+3)^2 + (y+3)^2} \right) \right] \right\} \\ & + \alpha \tan^{-1} \left\{ \exp \left[ \gamma \left( 4 - \sqrt{(x+3)^2 + (y+17)^2} \right) \right] \right\} \\ & + \alpha \tan^{-1} \left\{ \exp \left[ \gamma \left( 4 - \sqrt{(x+17)^2 + (y+3)^2} \right) \right] \right\} \\ & + \alpha \tan^{-1} \left\{ \exp \left[ \gamma \left( 4 - \sqrt{(x+17)^2 + (y+17)^2} \right) \right] \right\}, \quad (2.54) \end{aligned}$$

$$\begin{aligned} \phi_t(x, y, 0) = & \theta \operatorname{sech} \left[ \gamma \left( 4 - \sqrt{(x+3)^2 + (y+3)^2} \right) \right] \\ & + \theta \operatorname{sech} \left[ \gamma \left( 4 - \sqrt{(x+3)^2 + (y+17)^2} \right) \right] \\ & + \theta \operatorname{sech} \left[ \gamma \left( 4 - \sqrt{(x+17)^2 + (y+3)^2} \right) \right] \\ & + \theta \operatorname{sech} \left[ \gamma \left( 4 - \sqrt{(x+17)^2 + (y+17)^2} \right) \right], \quad (x, y) \in \mathbb{R}^2, \quad (2.55) \end{aligned}$$

where  $\alpha = 4.0$ ,  $\theta = 4.13$ ,  $\gamma = 2.29$  in our simulation. We solve this problem on the rectangle  $[-30, 10] \times [-27, 13]$  with mesh size  $h = 1/16$  and time step  $k = 0.001$  by using our method CN-LF-SP ( $\beta = 0.25$ ). Numerical simulation is presented in Figure 2.5 in terms of  $\sin(\phi/2)$  at  $t = 0, 2.5, 5, 7.5, 10$ . The simulation is based on an extension across  $x = -10$  and  $y = -10$  due to the symmetry [4, 24, 46]. The computation can be continued for  $t \geq 0$  without major boundary disturbances. This feature is significant in potential multi-dimensional applications. Figure 2.5 demonstrates precisely the collision between four expanding circular ring solitons in which the smaller ring solitons bounding an annular region merge into a large ring soliton. This matches known experimental results [18, 24]. Again, contour plots are given to illustrate more clearly the movement of the solitons.

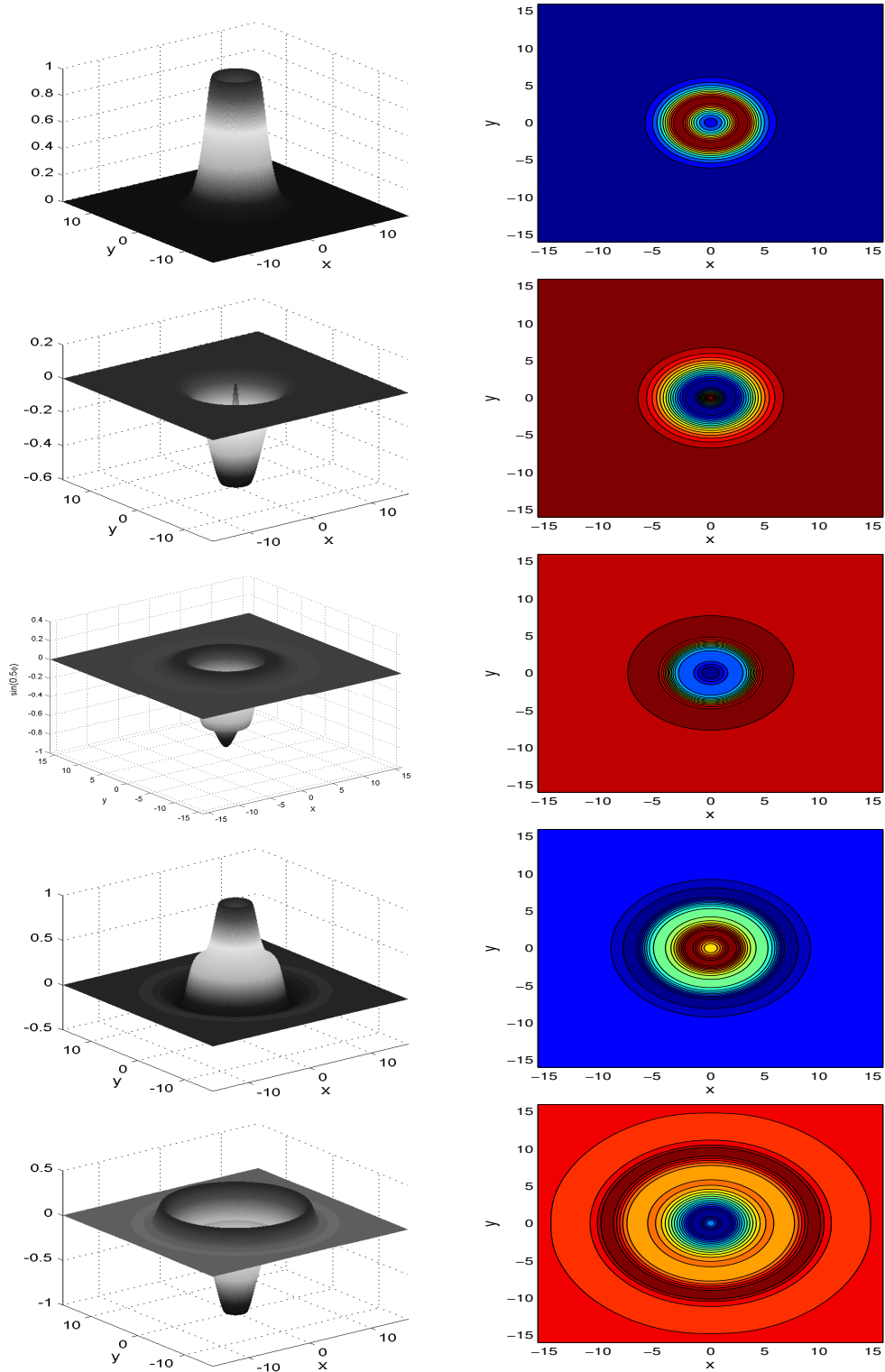


Figure 2.3: Circular and elliptic ring solitons in Example 2.3 (from top to bottom:  $t = 0, 4, 8, 11.5$  and  $15$ ).

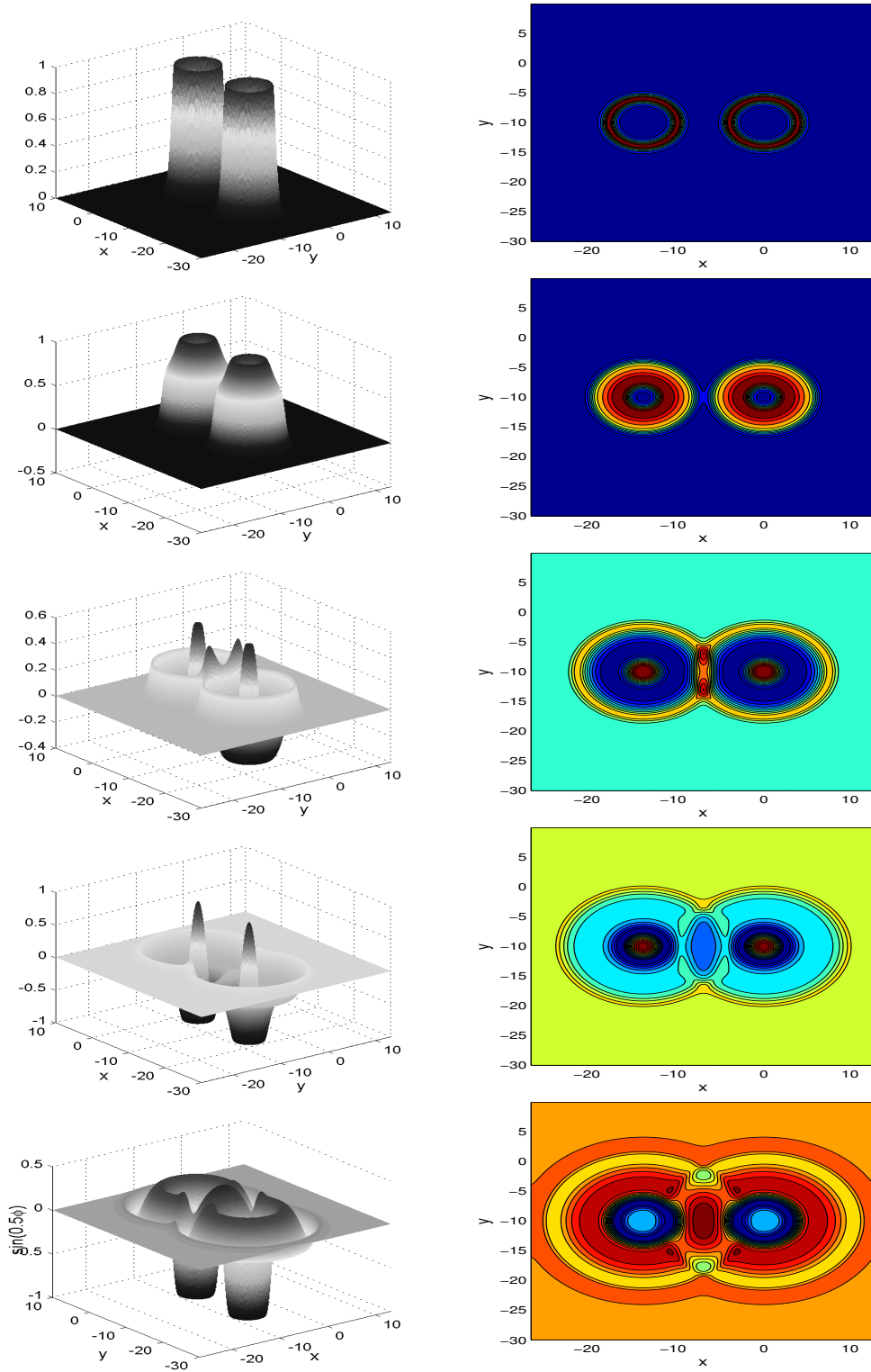


Figure 2.4: Collision of two ring solitons in Example 2.4 (from top to bottom :  $t = 0, 2, 4, 6$  and  $8$ ).

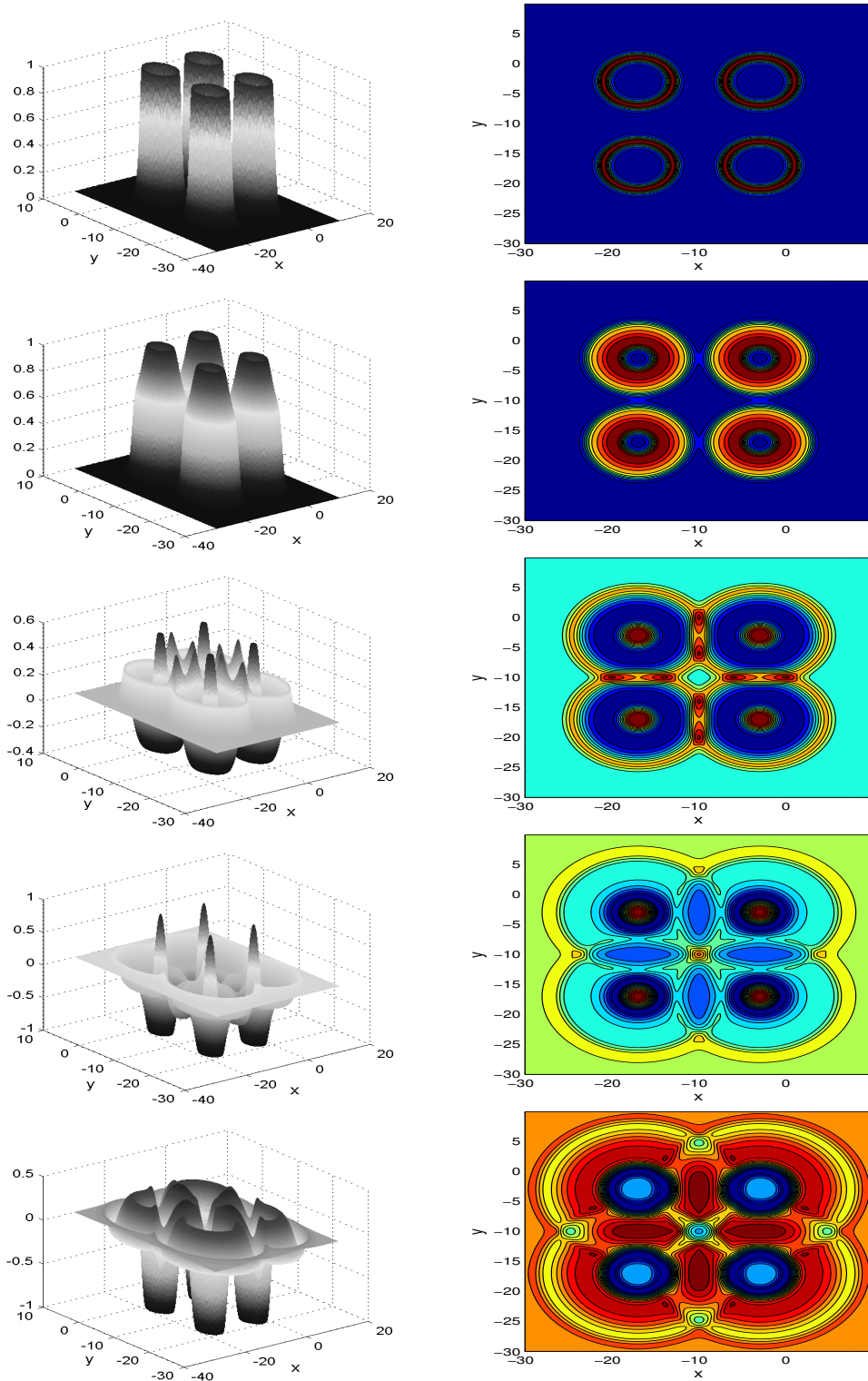


Figure 2.5: Collision of four ring solitons in Example 2.5 (from top to bottom:  $t = 0, 2.5, 5, 7.5$  and  $10$ ).

## The Klein-Gordon-Schrödinger equations

In this chapter, the Klein-Gordon-Schrödinger equations describing a system of conserved scalar nucleons interacting with neutral scalar mesons, are derived and its analytical properties are analyzed.

### 3.1 Derivation of the Klein-Gordon-Schrödinger equations

This section is devoted to derive the Klein-Gordon-Schrödinger equations. The Lagrangian density of the dynamic system that describes the interaction between the complex scalar nucleon field and real scalar meson field in one dimension (1D) is

$$\begin{aligned}\mathcal{L} &= \mathcal{L}_o + \mathcal{L}_{int} \\ &= i\hbar\psi^*\psi_t + \frac{\hbar^2}{2m}\psi^*\psi_{xx} + \frac{1}{2}(\phi_t^2 - \phi_x^2 - \mu^2\phi^2) + g^2\phi|\psi|^2,\end{aligned}\quad (3.1)$$

where  $\psi$  represents the complex scalar nucleon field,  $\phi$  describes the real scalar meson field,  $g^2\phi|\psi|^2$  is the Yukawa interaction potential, and  $m, \mu$  respectively describe the mass of nucleon and mass of meson.

Since the Lagrangian of the whole system must satisfy the Euler-Lagrange equation (that is,  $\frac{\partial}{\partial ct} \frac{\partial \mathcal{L}}{\partial(\frac{\partial \eta}{\partial ct})} + \frac{\partial}{\partial x} \frac{\partial \mathcal{L}}{\partial(\frac{\partial \eta}{\partial x})} - \frac{\partial \mathcal{L}}{\partial \eta} = 0$ ). Then we can get the equations of motion of the whole system.

Let  $\eta = \psi^*$ , we get the equation

$$i\hbar \psi_t + \frac{\hbar^2}{2m} \psi_{xx} + g^2 \psi \phi = 0. \quad (3.2)$$

Let  $\eta = \phi$ , we get another equation

$$\square \phi + \mu^2 \phi - g^2 |\psi|^2 = 0, \quad (3.3)$$

where  $\square = \frac{1}{c^2} \frac{\partial^2}{\partial t^2} - \partial_{xx}$ .

In general, we can obtain the equations of motion of the dynamic system in  $d$ -dimension ( $d = 1, 2, 3$ ).

$$i\hbar \psi_t + \frac{\hbar^2}{2m} \nabla^2 \psi + g^2 \psi \phi = 0, \quad (3.4)$$

$$\square \phi + \mu^2 \phi - g^2 |\psi|^2 = 0, \quad (3.5)$$

where  $\square = \frac{1}{c^2} \frac{\partial^2}{\partial t^2} - \nabla^2$ . In order to obtain a dimensionless form of the KGS (3.4)-(3.5), we define the normalized variables

$$\tilde{t} = \frac{\hbar \mu^2}{2m} t, \quad \tilde{x} = \mu x, \quad (3.6)$$

$$\tilde{\psi} = \frac{g^2 \sqrt{2m}}{\hbar \mu^2} \psi, \quad \tilde{\phi} = \frac{2mg^2}{\hbar^2 \mu^2} \phi. \quad (3.7)$$

Then defining

$$\varepsilon = \frac{\hbar \mu}{2mc}, \quad (3.8)$$

and plugging (3.6)-(3.7) into (3.4)-(3.5), and then removing all ‘ $\sim$ ’, we get the following dimensionless standard Klein-Gordon-Schrödinger equations

$$i \partial_t \psi + \Delta \psi + \phi \psi = 0, \quad (3.9)$$

$$\varepsilon^2 \partial_{tt} \phi - \Delta \phi + \phi - |\psi|^2 = 0. \quad (3.10)$$

Adding dissipative terms to (3.9), we can obtain the generalized Klein-Gordon-Schrödinger equations

$$i \partial_t \psi + \Delta \psi + \phi \psi + i\nu \psi = 0, \quad (3.11)$$

$$\varepsilon^2 \partial_{tt} \phi + \gamma \varepsilon \partial_t \phi - \Delta \phi + \phi - |\psi|^2 = 0. \quad (3.12)$$

## 3.2 Conservation laws of the Klein-Gordon-Schrödinger equations

Define the wave energy

$$D(t) := D(\psi(\cdot, t)) = \int_{\mathbb{R}^d} |\psi(\mathbf{x}, t)|^2 d\mathbf{x}, \quad t \geq 0, \quad (3.13)$$

and the Hamiltonian

$$\begin{aligned} H(t) = \int_{\mathbb{R}^d} & \left[ \frac{1}{2} (\phi^2(\mathbf{x}, t) + \varepsilon^2 (\partial_t \phi(\mathbf{x}, t))^2 + |\nabla \phi(\mathbf{x}, t)|^2) + |\nabla \psi(\mathbf{x}, t)|^2 \right. \\ & \left. - |\psi(\mathbf{x}, t)|^2 \phi(\mathbf{x}, t) \right] d\mathbf{x}, \quad t \geq 0. \end{aligned} \quad (3.14)$$

**Lemma 3.1.** Suppose  $(\psi, \phi)$  be the solution of the generalized Klein-Gordon-Schrödinger equations (1.4)-(1.5), its wave energy and Hamiltonian has the following properties

$$\frac{d}{dt} D(t) = \frac{d}{dt} \int_{\mathbb{R}^d} |\psi(\mathbf{x}, t)|^2 d\mathbf{x} = -2\nu \int_{\mathbb{R}^d} |\psi(\mathbf{x}, t)|^2 d\mathbf{x}, \quad t \geq 0, \quad (3.15)$$

$$\begin{aligned} \frac{d}{dt} H(t) &= \frac{d}{dt} \int_{\mathbb{R}^d} \left[ \frac{1}{2} (\phi^2(\mathbf{x}, t) + \varepsilon^2 (\partial_t \phi(\mathbf{x}, t))^2 + |\nabla \phi(\mathbf{x}, t)|^2) + |\nabla \psi(\mathbf{x}, t)|^2 \right. \\ & \quad \left. - |\psi(\mathbf{x}, t)|^2 \phi(\mathbf{x}, t) \right] d\mathbf{x} \\ &= - \int_{\mathbb{R}^d} \left[ \gamma \varepsilon (\partial_t \phi(\mathbf{x}, t))^2 + i\nu (\partial_t \psi^*(\mathbf{x}, t) \psi(\mathbf{x}, t) \right. \\ & \quad \left. - \partial_t \psi(\mathbf{x}, t) \psi^*(\mathbf{x}, t)) \right] d\mathbf{x}, \quad t \geq 0. \end{aligned} \quad (3.16)$$

**Proof.** Multiplying (1.4) by  $\psi^*$ , the conjugate of  $\psi$ , we get

$$i \psi_t \psi^* + \Delta \psi \psi^* + \phi |\psi|^2 + i\nu |\psi|^2 = 0. \quad (3.17)$$

Then taking the conjugate of (1.5) and multiplying it by  $\psi$ , we obtain

$$-i \psi_t^* \psi + \psi \Delta \psi^* + \phi |\psi|^2 - i\nu |\psi|^2 = 0. \quad (3.18)$$

Subtracting (3.18) from (3.17) and then multiplying both sides by  $-i$ , we can get

$$\psi_t \psi^* + \psi_t^* \psi + i(\psi \Delta \psi^* - \psi^* \Delta \psi) + 2\nu |\psi|^2 = 0. \quad (3.19)$$

Integrating over  $\mathbb{R}^d$ , integration by parts, (3.19) leads to

$$\frac{d}{dt} D(t) = \frac{d}{dt} \int_{\mathbb{R}^d} |\psi(\mathbf{x}, t)|^2 d\mathbf{x} = -2\nu \int_{\mathbb{R}^d} |\psi(\mathbf{x}, t)|^2 d\mathbf{x}, \quad t \geq 0, \quad (3.20)$$

which implies that  $D(t)$  preserves as a constant when  $\nu = 0$ .

Multiplying (1.4) by  $\psi_t^*$ , we get

$$i |\psi_t|^2 + \Delta \psi \psi_t^* + \phi \psi \psi_t^* + i \nu \psi \psi_t^* = 0. \quad (3.21)$$

Then taking the conjugate of (1.5) and multiplying it by  $\psi_t$ , we obtain

$$-i |\psi_t|^2 + \psi_t \Delta \psi^* + \phi \psi^* \psi_t - i \nu \psi^* \psi_t = 0. \quad (3.22)$$

Adding (3.21) to (3.22), we can get

$$(\psi \Delta \psi_t^* + \psi_t \Delta \psi^*) + \phi (|\psi|^2)_t + i \nu (\psi \psi_t^* - \psi^* \psi_t) = 0 \quad (3.23)$$

Integrating over  $\mathbb{R}^d$  (3.19) leads to

$$\int_{\mathbb{R}^d} [(\psi \Delta \psi_t^* + \psi_t \Delta \psi^*) + \phi (|\psi|^2)_t + i \nu (\psi \psi_t^* - \psi^* \psi_t)] d\mathbf{x} = 0. \quad (3.24)$$

Multiplying (1.5) by  $\phi_t$ , and integrating over  $\mathbb{R}^d$ , we can get

$$\int_{\mathbb{R}^d} [\varepsilon^2 \phi_{tt} \phi_t + \gamma \varepsilon (\phi_t)^2 - \Delta \phi \phi_t + \phi \phi_t - |\psi|^2 \phi_t] d\mathbf{x} = 0 \quad (3.25)$$

Noting (3.25), (3.24) and (3.20), we obtain

$$\begin{aligned} \frac{d}{dt} H(t) &= \int_{\mathbb{R}^d} [\phi \phi_t + \varepsilon^2 \phi_t \phi_{tt} + \nabla \phi \cdot \nabla \phi_t + (|\nabla \psi|^2 - |\psi|^2 \phi)_t] d\mathbf{x} \\ &= \int_{\mathbb{R}^d} [-\gamma \varepsilon (\phi_t)^2 + \Delta \phi \phi_t + |\psi|^2 \phi_t + \nabla \phi \cdot \nabla \phi_t + (|\nabla \psi|^2 - |\psi|^2 \phi)_t] d\mathbf{x} \\ &= \int_{\mathbb{R}^d} [\Delta \phi \phi_t + \nabla \phi \cdot \nabla \phi_t] d\mathbf{x} + \int_{\mathbb{R}^d} [-(|\psi|^2)_t \phi + (|\nabla \psi|^2)_t] d\mathbf{x} - \int_{\mathbb{R}^d} \gamma \varepsilon (\phi_t)^2 d\mathbf{x} \\ &= - \int_{\mathbb{R}^d} [\gamma \varepsilon (\phi_t)^2 + i \nu (\psi_t \psi^* - \psi_t^* \psi)] d\mathbf{x}, \quad t \geq 0, \end{aligned} \quad (3.26)$$

which implies that  $H(t)$  is decreasing if  $\nu = 0$  as time  $t$  is increasing and  $H(t)$  preserves as a constant when  $\nu = 0$  and  $\gamma = 0$ .  $\square$

From the above discussion, we find that when  $\gamma = 0$  and  $\nu = 0$  in (1.4)-(1.5), the KGS has at least two invariants.

**Theorem 3.1.** The generalized Klein-Gordon-Schrödinger equations (1.4)-(1.5) with  $\gamma = \nu = 0$  preserve the conserved quantities. They are the wave energy

$$D(t) := D(\psi(\cdot, t)) = \int_{\mathbb{R}^d} |\psi(\mathbf{x}, t)|^2 d\mathbf{x} \equiv \int_{\mathbb{R}^d} |\psi^{(0)}(\mathbf{x})|^2 d\mathbf{x} := D(0), \quad t \geq 0, \quad (3.27)$$

and the Hamiltonian

$$\begin{aligned} H(t) &= \int_{\mathbb{R}^d} \left[ \frac{1}{2} (\phi^2(\mathbf{x}, t) + \varepsilon^2 (\partial_t \phi(\mathbf{x}, t))^2 + |\nabla \phi(\mathbf{x}, t)|^2) + |\nabla \psi(\mathbf{x}, t)|^2 \right. \\ &\quad \left. - |\psi(\mathbf{x}, t)|^2 \phi(\mathbf{x}, t) \right] d\mathbf{x} \\ &\equiv \int_{\mathbb{R}^d} \left[ \frac{1}{2} ((\phi^{(0)}(\mathbf{x}))^2 + \varepsilon^2 (\phi^{(1)}(\mathbf{x}))^2 + |\nabla \phi^{(0)}(\mathbf{x})|^2) + |\nabla \psi^{(0)}(\mathbf{x})|^2 \right. \\ &\quad \left. - |\psi^{(0)}(\mathbf{x})|^2 \phi^{(0)}(\mathbf{x}) \right] d\mathbf{x} \\ &:= H(0), \quad t \geq 0. \end{aligned} \quad (3.28)$$

In one dimension case, the conserved quantities become

$$H = \int_{-\infty}^{\infty} \left[ \frac{1}{2} (\phi^2(x, t) + \varepsilon^2 (\phi_t(x, t))^2 + (\phi_x(x, t))^2) + |\psi(x, t)|^2 \right. \\ \left. - |\psi(x, t)|^2 \phi(x, t) \right] dx, \quad (3.29)$$

$$A = \int_{-\infty}^{\infty} |\psi(x, t)|^2 dx. \quad (3.30)$$

### 3.3 Dynamics of mean value of the meson field

When  $\nu = 0$ , the generalized KGS (1.4)-(1.5) collapses to

$$i \partial_t \psi + \Delta \psi + \phi \psi = 0, \quad \mathbf{x} \in \mathbb{R}^d, \quad t > 0, \quad (3.31)$$

$$\varepsilon^2 \partial_{tt} \psi + \gamma \varepsilon \partial_t \phi - \Delta \phi + \phi - |\psi|^2 = 0, \quad \mathbf{x} \in \mathbb{R}^d, \quad t > 0. \quad (3.32)$$

Define the mean value of the meson field as

$$N(t) := N(\phi(\cdot, t)) = \int_{\mathbb{R}^d} \phi(\mathbf{x}, t) d\mathbf{x}, \quad t \geq 0. \quad (3.33)$$

Integrating (3.32) over  $\mathbb{R}^d$ , integration by parts and noticing (3.27), we obtain

$$\varepsilon^2 N''(t) + \gamma \varepsilon N'(t) + N(t) = D(0), \quad t \geq 0, \quad (3.34)$$

with initial condition as

$$N(0) = N(\phi^{(0)}) := \int_{\mathbb{R}^d} \phi^{(0)}(\mathbf{x}) d\mathbf{x}, \quad N'(0) = N(\phi^{(1)}) := \int_{\mathbb{R}^d} \phi^{(1)}(\mathbf{x}) d\mathbf{x}. \quad (3.35)$$

Denote

$$\lambda_1^0 = \frac{-\gamma + \sqrt{\gamma^2 - 4}}{2\varepsilon}, \quad \lambda_2^0 = \frac{-\gamma - \sqrt{\gamma^2 - 4}}{2\varepsilon}, \quad \lambda_0 = \frac{-\gamma}{2\varepsilon}, \quad \beta_0 = \frac{\sqrt{4 - \gamma^2}}{2\varepsilon}. \quad (3.36)$$

Solving the ODE (3.34) with the initial data (3.35), we get the dynamics of the mean value of the meson field when  $\nu = 0$ :

(i) For  $\gamma > 2$

$$N(t) = D(0) + \frac{N(\phi^{(1)}) - \lambda_2^0(N(\phi^{(0)}) - D(0))}{\lambda_1^0 - \lambda_2^0} e^{\lambda_1^0 t} + \frac{-N(\phi^{(1)}) + \lambda_1^0(N(\phi^{(0)}) - D(0))}{\lambda_1^0 - \lambda_2^0} e^{\lambda_2^0 t};$$

(ii) for  $\gamma = 2$

$$N(t) = D(0) + (N(\phi^{(0)}) - D(0)) e^{\lambda_0 t} + (N(\phi^{(1)}) - \lambda_0(N(\phi^{(0)}) - D(0))) t e^{\lambda_0 t};$$

and (iii) for  $0 \leq \gamma < 2$

$$N(t) = D(0) + e^{\lambda_0 t} \left[ (N(\phi^{(0)}) - D(0)) \cos(\beta_0 t) + \frac{N(\phi^{(1)}) - \lambda_0(N(\phi^{(0)}) - D(0))}{\beta_0} \sin(\beta_0 t) \right].$$

These immediately imply that  $\lim_{t \rightarrow \infty} N(t) = D(0)$  when  $\gamma > 0$ , and  $N(t)$  is a periodic function with period  $T = 2\varepsilon\pi$  when  $\gamma = 0$ .

## 3.4 Plane wave and soliton wave solutions of KGS

When  $d = 1$ ,  $\gamma = 0$ ,  $\nu = 0$ , and  $\varepsilon = 1$ , the generalized KGS (1.4)-(1.5) collapses to

$$i \partial_t \psi + \Delta \psi + \phi \psi = 0, \quad x \in \mathbb{R}, \quad t > 0, \quad (3.37)$$

$$\partial_{tt} \phi - \Delta \phi + \phi - |\psi|^2 = 0, \quad x \in \mathbb{R}, \quad t > 0, \quad (3.38)$$

which admits plane and soliton wave solutions.

Firstly, it is instructive to examine some explicit solutions to (3.37) and (3.38). The initial data in (1.6) is chosen as

$$\phi^{(0)}(x) = d > 0, \quad \phi^{(1)}(x) = 0, \quad \psi^{(0)}(x) = \sqrt{d} \exp\left(i \frac{2\pi l x}{b-a}\right), \quad x \in \mathbb{R}, \quad (3.39)$$

with  $l$  an integer, and  $a$ ,  $b$  and  $d$  constants, the KGS admits the plane wave solution [22].

$$\phi(x, t) = d, \quad \psi(x, t) = \sqrt{d} \exp\left[i \left(\frac{2\pi l x}{b-a} - \omega t\right)\right], \quad x \in \mathbb{R}, \quad t \geq 0, \quad (3.40)$$

where

$$\omega = \left(\frac{2\pi l}{b-a}\right)^2 - d.$$

Secondly, as it is well known, the standard KGS is not completely integrable. Therefore the generalized KGS can not be exactly integrable either. However, it has one-soliton solutions to (3.37) and (3.38) for  $d = 1$ ,  $\gamma = 0$ ,  $\nu = 0$  [38]

$$\psi_{\pm}(x, t) = 3B \operatorname{sech}^2(Bx + c_{\pm}t) \exp\left[i(d_{\pm}x + (4B^2 - d_{\pm}^2)t)\right], \quad (3.41)$$

$$\phi_{\pm}(x, t) = 6B^2 \operatorname{sech}^2(Bx + c_{\pm}t), \quad x \in \mathbb{R}, \quad t \geq 0, \quad (3.42)$$

where

$$c_{\pm} = \pm \frac{\sqrt{4B^2 - 1}}{2\varepsilon}, \quad d_{\pm} = \mp \frac{\sqrt{4B^2 - 1}}{4B} = -\frac{c_{\pm}}{2B},$$

with  $B \geq 1/2$  a constant.

Note that the phase in  $\psi$  oscillates as  $O(\frac{1}{\varepsilon})$ . This exact solution is used in Chapter 4 to test the accuracy of our new numerical methods.

## **3.5 Reduction to the Schrödinger-Yukawa equations (S-Y)**

In the "nonrelativistic regime", i.e.,  $\varepsilon \rightarrow 0$  in (1.4)-(1.6), which corresponds to infinite speed of light, we can obtain the well-known Schrödinger-Yukawa equations

without ( $\nu = 0$ ) or with ( $\nu > 0$ ) a linear damping term:

$$i \partial_t \psi + \Delta \psi + \phi \psi + i \nu \psi = 0, \quad \mathbf{x} \in \mathbb{R}^d, \quad t > 0, \quad (3.43)$$

$$-\Delta \phi + \phi = |\psi|^2, \quad \mathbf{x} \in \mathbb{R}^d, \quad t > 0. \quad (3.44)$$

When  $\nu = 0$ , the S-Y equations (1.7)-(1.8) is time reversible, time transverse invariant, and preserves the following wave energy and Hamiltonian:

$$D^{\text{SY}} = \int_{\mathbb{R}^d} |\psi(\mathbf{x}, t)|^2 d\mathbf{x}, \quad (3.45)$$

$$H^{\text{SY}} = \int_{\mathbb{R}^d} \left[ \frac{1}{2} (\phi^2(\mathbf{x}, t) + |\nabla \phi(\mathbf{x}, t)|^2) + |\nabla \psi(\mathbf{x}, t)|^2 - |\psi(\mathbf{x}, t)|^2 \phi(\mathbf{x}, t) \right] d\mathbf{x} \quad (3.46)$$

Similarly, letting  $\varepsilon \rightarrow 0$  in (3.28), we get formally the quadratic convergence rate of the Hamiltonian from KGS with  $\nu = \gamma = 0$  to S-Y in the “nonrelativistic” limit regime, i.e.,  $0 < \varepsilon \ll 1$ :

$$\begin{aligned} H(t) &= \int_{\mathbb{R}^d} \left[ \frac{1}{2} (\phi^2(\mathbf{x}, t) + |\nabla \phi(\mathbf{x}, t)|^2) + |\nabla \psi(\mathbf{x}, t)|^2 - |\psi(\mathbf{x}, t)|^2 \phi(\mathbf{x}, t) \right] d\mathbf{x} \\ &\quad + \varepsilon^2 \int_{\mathbb{R}^d} (\partial_t \phi(\mathbf{x}, t))^2 d\mathbf{x} \\ &\approx H^{\text{SY}} + O(\varepsilon^2). \end{aligned} \quad (3.47)$$

Our numerical results in Chapter 5 confirm this asymptotic result.

# Numerical studies of the Klein-Gordon-Schrödinger equations

In this Chapter, we present two accurate and efficient numerical schemes, phase space analytical solver+time-splitting spectral method (PSAS-TSSP) and Crank-Nicolson leap-frog time-splitting spectral method (CN-LF-TSSP) for the Klein-Gordon-Schrödinger equations (1.4)-(1.5) with the periodic boundary conditions and analyze the numerical properties for these two numerical methods. Then we compare the accuracy and stability of different numerical methods for the Klein-Gordon-Schrödinger equations with a solitary wave solution, and also present the numerical results for plane waves, soliton-soliton collisions in 1D, 2D problems and the generalized KGS with a damping term.

## 4.1 Numerical methods for the Klein-Gordon-Schrödinger equations

In this section we present two new accurate and efficient numerical methods, i.e., phase space analytical+time-splitting spectral discretizations (PSAS-TSSP) and

Crank-Nicolson leap-frog spectral discretization (CN-LF-TSSP) for the Klein-Gordon-Schrödinger equations (1.4)-(1.6) with the periodic boundary conditions.

For simplicity of notation, we shall introduce the method in 1D of the KGS with periodic boundary conditions. Generalizations to higher dimensions are straightforward for tensor product grids and the results remain valid without modifications.

For  $d = 1$ , the problem becomes

$$i \partial_t \psi(x, t) + \partial_{xx} \psi + i\nu \psi + \phi \psi = 0, \quad a < x < b, \quad t > 0, \quad (4.1)$$

$$\varepsilon^2 \partial_{tt} \phi + \varepsilon \gamma \partial_t \phi - \partial_{xx} \phi + \phi - |\psi|^2 = 0, \quad a < x < b, \quad t > 0, \quad (4.2)$$

$$\psi(a, t) = \psi(b, t), \quad \partial_x \psi(a, t) = \partial_x \psi(b, t), \quad t \geq 0, \quad (4.3)$$

$$\phi(a, t) = \phi(b, t), \quad \partial_x \phi(a, t) = \partial_x \phi(b, t), \quad t \geq 0, \quad (4.4)$$

$$\psi(x, 0) = \psi^{(0)}(x), \quad \phi(x, 0) = \phi^{(0)}(x), \quad \partial_t \phi(x, 0) = \phi^{(1)}(x), \quad a \leq x \leq b. \quad (4.5)$$

As it is well known, the above KGS in 1D has the following properties:

$$D(t) = \int_a^b |\psi(x, t)|^2 dx = e^{-2\nu t} \int_a^b |\psi^{(0)}(x)|^2 dx = e^{-2\nu t} D(0), \quad t \geq 0. \quad (4.6)$$

So when  $\nu = 0$ ,  $D(t) \equiv D(0)$ , i.e., it is an invariant of the KGS. When  $\nu > 0$ , it decays to 0 exponentially. Furthermore, when  $\nu = 0$  and  $\gamma = 0$ , the KGS also conserves the Hamiltonian:

$$H(t) = \int_b^a \left[ \frac{1}{2} (\phi(x, t)^2 + \varepsilon^2 (\partial_t \phi(x, t))^2 + (\partial_x \phi(x, t))^2) + |\partial_x \psi(x, t)|^2 - |\psi(x, t)|^2 \phi(x, t) \right] dx \equiv H(0), \quad t \geq 0. \quad (4.7)$$

In some cases, the periodic boundary conditions (4.3) and (4.4) may be replaced by the homogeneous Dirichlet boundary conditions

$$\psi(a, t) = \psi(b, t) = 0, \quad \phi(a, t) = \phi(b, t) = 0, \quad t \geq 0. \quad (4.8)$$

We choose the spatial mesh size  $h = \Delta x > 0$  with  $h = (b - a)/M$  for  $M$  being an even positive integer, the time step size being  $k = \Delta t > 0$  and let the grid points and the time step be

$$x_j := a + jh, \quad j = 0, 1, \dots, M; \quad t_m := mk, \quad m = 0, 1, 2, \dots .$$

Let  $\psi_j^m$  and  $\phi_j^m$  be the approximations of  $\psi(x_j, t_m)$  and  $\phi(x_j, t_m)$ , respectively. Furthermore, let  $\psi^m$  and  $\phi^m$  be the solution vector at time  $t = t_m = mk$  with components  $\psi_j^m$  and  $\phi_j^m$ , respectively.

### 4.1.1 Time-splitting for the nonlinear Schrödinger equation

From time  $t = t_m$  and  $t = t_{m+1}$ , the first NLS-type equation (4.1) is solved in two splitting steps [5, 6, 8, 9, 63]. One solves first

$$i\partial_t\psi + \partial_{xx}\psi = 0, \tag{4.9}$$

for the time step of length  $k$ , followed by solving

$$i\partial_t\psi + i\nu\psi + \phi\psi = 0, \tag{4.10}$$

for the same time step. Equation (4.9) will be discretized in space by the Fourier spectral method and integrated in time *exactly*. For each fixed  $x \in [a, b]$ , integrating (4.10) from time  $t = t_m$  to  $t = t_{m+1} = t_m + k$ , and then approximating the integral on  $[t_m, t_{m+1}]$  via the trapezoidal rule [11, 12, 10], we obtain

$$\begin{aligned} \psi(x, t_{m+1}) &= \exp \left[ \int_{t_m}^{t_{m+1}} (-\nu + i\phi(x, \tau)) d\tau \right] \psi(x, t_m) \\ &= \exp \left[ -\nu k + ik \frac{\phi(x, t_m) + \phi(x, t_{m+1})}{2} \right] \psi(x, t_m), \quad a \leq x \leq b. \end{aligned} \tag{4.11}$$

### 4.1.2 Phase space analytical solver+time-splitting spectral discretizations (PSAS-TSSP)

The Klein-Gordon equation (4.2) in KGS is discretized by using a pseudospectral method for spatial derivatives and then solving the ODEs in phase space analytically under appropriate chosen transmission conditions between different time intervals. From time  $t = t_m$  to  $t = t_{m+1}$ , assume

$$\phi(x, t) = \sum_{l=-M/2}^{M/2-1} \tilde{\phi}_l^m(t) e^{i\mu_l(x-a)}, \quad a \leq x \leq b, \quad t_m \leq t \leq t_{m+1}, \tag{4.12}$$

where  $\mu_l = \frac{2\pi l}{b-a}$  and  $\widetilde{\phi}_l^m(t)$  is the Fourier coefficient of  $l$ th mode. Plugging (4.12) into (4.2) and noticing the orthogonality of the Fourier functions, we get the following ODEs for  $m \geq 0$  and  $t_m \leq t \leq t_{m+1}$ :

$$\varepsilon^2 \frac{d^2 \widetilde{\phi}_l^m(t)}{dt^2} + \varepsilon \gamma \frac{d \widetilde{\phi}_l^m(t)}{dt} + (\mu_l^2 + 1) \widetilde{\phi}_l^m(t) - (|\widetilde{\psi(t_m)}|^2)_l = 0, \quad (4.13)$$

$$\widetilde{\phi}_l^m(t_m) = \begin{cases} (\widetilde{\phi^{(0)}})_l, & m = 0, \\ \widetilde{\phi}_l^{m-1}(t_m), & m > 0, \end{cases} \quad l = -\frac{M}{2}, \dots, \frac{M}{2} - 1. \quad (4.14)$$

For each fixed  $l$  ( $-M/2 \leq l \leq M/2 - 1$ ), equation (4.13) is a second-order ODE. It needs two initial conditions such that the solution is unique. When  $m = 0$  in (4.13) and (4.14), we have the initial condition (4.14) and we can pose the other initial condition for (4.13) due to the initial condition (4.5):

$$\frac{d}{dt} \widetilde{\phi}_l^0(t_0) = \frac{d}{dt} \widetilde{\phi}_l^0(0) = (\widetilde{\phi^{(1)}})_l, \quad l = -\frac{M}{2}, \dots, \frac{M}{2} - 1. \quad (4.15)$$

Denote

$$\lambda_1 = \frac{-\gamma + \sqrt{\gamma^2 - 4(\mu_l^2 + 1)}}{2\varepsilon}, \quad \lambda_2 = \frac{-\gamma - \sqrt{\gamma^2 - 4(\mu_l^2 + 1)}}{2\varepsilon}, \quad \beta = \frac{\sqrt{4(\mu_l^2 + 1) - \gamma^2}}{2\varepsilon}. \quad (4.16)$$

Then the solution of (4.13), (4.14) with  $m = 0$  and (4.15) for  $l$  ( $-M/2 \leq l < M/2$ ) and  $0 \leq t \leq t_1$  is:

(i) For  $\gamma^2 - 4(\mu_l^2 + 1) > 0$

$$\begin{aligned} \widetilde{\phi}_l^0(t) &= \frac{(\widetilde{|\psi^{(0)}|^2})_l}{\mu_l^2 + 1} + \frac{\varepsilon}{\sqrt{\gamma^2 - 4(\mu_l^2 + 1)}} \left[ (\widetilde{\phi^{(1)}})_l - \left( (\widetilde{\phi^{(0)}})_l - \frac{(\widetilde{|\psi^{(0)}|^2})_l}{\mu_l^2 + 1} \right) \lambda_2 \right] e^{\lambda_1 t} \\ &\quad - \frac{\varepsilon}{\sqrt{\gamma^2 - 4(\mu_l^2 + 1)}} \left[ (\widetilde{\phi^{(1)}})_l - \left( (\widetilde{\phi^{(0)}})_l - \frac{(\widetilde{|\psi^{(0)}|^2})_l}{\mu_l^2 + 1} \right) \lambda_1 \right] e^{\lambda_2 t}; \end{aligned} \quad (4.17)$$

(ii) for  $\gamma^2 - 4(\mu_l^2 + 1) = 0$ ,

$$\widetilde{\phi}_l^0(t) = \frac{(\widetilde{|\psi^{(0)}|^2})_l}{\mu_l^2 + 1} + \left[ (\widetilde{\phi^{(0)}})_l - \frac{(\widetilde{|\psi^{(0)}|^2})_l}{\mu_l^2 + 1} + \left( (\widetilde{\phi^{(1)}})_l + \frac{\gamma}{2\varepsilon} \left( (\widetilde{\phi^{(0)}})_l - \frac{(\widetilde{|\psi^{(0)}|^2})_l}{\mu_l^2 + 1} \right) \right) t \right] e^{-\frac{\gamma t}{2\varepsilon}}; \quad (4.18)$$

and (iii) for  $\gamma^2 - 4(\mu_l^2 + 1) < 0$

$$\begin{aligned} \tilde{\phi}_l^0(t) = & e^{-\frac{\gamma t}{2\varepsilon}} \left[ \frac{1}{\beta} \left( (\widetilde{\phi^{(1)}})_l + \frac{\gamma}{2\varepsilon} ((\widetilde{\phi^{(0)}})_l - \frac{(|\psi^{(0)}|^2)_l}{\mu_l^2 + 1}) \right) \sin(\beta t) \right. \\ & \left. + \left( (\widetilde{\phi^{(0)}})_l - \frac{(|\psi^{(0)}|^2)_l}{\mu_l^2 + 1} \right) \cos(\beta t) \right] + \frac{(|\psi^{(0)}|^2)_l}{\mu_l^2 + 1}. \end{aligned} \quad (4.19)$$

But when  $m > 0$ , we only have one initial condition (4.14). One can't simply pose the continuity between  $\frac{d}{dt}\tilde{\phi}_l^m(t)$  and  $\frac{d}{dt}\tilde{\phi}_l^{m-1}(t)$  across the time  $t = t_m$ , because the last term in (4.13) is usually different in two adjacent time intervals  $[t_{m-1}, t_m]$  and  $[t_m, t_{m+1}]$ ; i.e.,  $(|\psi(t_{m-1})|^2)_l \neq (|\psi(t_m)|^2)_l$ . Since our goal is to develop an explicit scheme and we need to linearize the nonlinear term in (4.2) in our discretization (4.13), in general,

$$\begin{aligned} \frac{d}{dt}\tilde{\phi}_l^{m-1}(t_m^-) = \lim_{t \rightarrow t_m^-} \frac{d}{dt}\tilde{\phi}_l^{m-1}(t) \neq \lim_{t \rightarrow t_m^+} \frac{d}{dt}\tilde{\phi}_l^m(t) = \frac{d}{dt}\tilde{\phi}_l^m(t_m^+), \\ m = 1, 2, \dots, \quad l = -\frac{M}{2}, \dots, \frac{M}{2} - 1. \end{aligned} \quad (4.20)$$

Unfortunately, we don't know the jump  $\frac{d}{dt}\tilde{\phi}_l^m(t_m^+) - \frac{d}{dt}\tilde{\phi}_l^{m-1}(t_m^-)$  across the time  $t = t_m$ . In order to get a unique solution of (4.13) and (4.14) for  $m > 0$ , we pose here an additional condition:

$$\tilde{\phi}_l^m(t_{m-1}) = \tilde{\phi}_l^{m-1}(t_{m-1}), \quad l = -\frac{M}{2}, \dots, \frac{M}{2} - 1. \quad (4.21)$$

The condition (4.21) is equivalent to posing that the solution  $\tilde{\phi}_l^m(t)$  on the time interval  $[t_m, t_{m+1}]$  of (4.13)-(4.14) is also continuous at the time  $t = t_{m-1}$ . After a simple computation, we get the solution of (4.13), (4.14) and (4.21) with  $m > 0$  for  $l$  ( $l = -M/2, \dots, M/2 - 1$ ) and  $t_m \leq t \leq t_{m+1}$ :

(i) For  $\gamma^2 - 4(\mu_l^2 + 1) > 0$

$$\begin{aligned} \tilde{\phi}_l^m(t) = & \frac{1}{e^{-k\lambda_1} - e^{-k\lambda_2}} \left[ \frac{(|\psi^m|^2)_l}{\mu_l^2 + 1} (e^{-k\lambda_2} - 1) + \tilde{\phi}_l^{m-1}(t_{m-1}) - \tilde{\phi}_l^{m-1}(t_m) e^{-k\lambda_2} \right] e^{\lambda_1(t-t_m)} \\ & + \frac{1}{e^{-k\lambda_2} - e^{-k\lambda_1}} \left[ \frac{(|\psi^m|^2)_l}{\mu_l^2 + 1} (e^{-k\lambda_1} - 1) + \tilde{\phi}_l^{m-1}(t_{m-1}) - \tilde{\phi}_l^{m-1}(t_m) e^{-k\lambda_1} \right] e^{\lambda_2(t-t_m)} \\ & + \frac{(|\psi^m|^2)_l}{\mu_l^2 + 1}; \end{aligned} \quad (4.22)$$

(ii) for  $\gamma^2 - 4(\mu_l^2 + 1) = 0$

$$\begin{aligned} \widetilde{\phi}_l^m(t) = & \left[ \frac{t - t_m}{k} \left( \widetilde{\phi}_l^{m-1}(t_m) - \frac{(\widetilde{|\psi^m|^2})_l}{\mu_l^2 + 1} + e^{-\frac{k\gamma}{2\varepsilon}} \left( \frac{(\widetilde{|\psi^m|^2})_l}{\mu_l^2 + 1} - \widetilde{\phi}_l^{m-1}(t_{m-1}) \right) \right) \right. \\ & \left. + \widetilde{\phi}_l^{m-1}(t_m) - \frac{(\widetilde{|\psi^m|^2})_l}{\mu_l^2 + 1} \right] e^{-\frac{\gamma(t-t_m)}{2\varepsilon}} + \frac{(\widetilde{|\psi^m|^2})_l}{\mu_l^2 + 1}; \end{aligned} \quad (4.23)$$

and (iii) for  $\gamma^2 - 4(\mu_l^2 + 1) < 0$

$$\begin{aligned} \widetilde{\phi}_l^m(t) = & e^{-\frac{\gamma(t-t_m)}{2\varepsilon}} \left[ \left( \widetilde{\phi}_l^{m-1}(t_m) - \frac{(\widetilde{|\psi^m|^2})_l}{\mu_l^2 + 1} \right) (\cos(\beta(t - t_m)) + \cot(\beta k) \sin(\beta(t - t_m))) \right. \\ & \left. + e^{-\frac{\gamma k}{2\varepsilon}} \left( \frac{(\widetilde{|\psi^m|^2})_l}{\mu_l^2 + 1} - \widetilde{\phi}_l^{m-1}(t_{m-1}) \right) \frac{\sin(\beta(t - t_m))}{\sin(\beta k)} \right] + \frac{(\widetilde{|\psi^m|^2})_l}{\mu_l^2 + 1}. \end{aligned} \quad (4.24)$$

From time  $t = t_m$  to  $t = t_{m+1}$ , we combine the splitting steps via the standard Strang splitting [61, 5, 8]:

$$\begin{aligned} \phi_j^{m+1} &= \sum_{l=-M/2}^{M/2-1} (\widetilde{\phi^{m+1}})_l e^{i\mu_l(x_j-a)}, \\ \psi_j^* &= \sum_{l=-M/2}^{M/2-1} e^{-ik\mu_l^2/2} (\widetilde{\psi^m})_l e^{i\mu_l(x_j-a)}, \\ \psi_j^{**} &= e^{-\nu k + ik(\phi_j^m + \phi_j^{m+1})/2} \psi_j^*, \\ \psi_j^{m+1} &= \sum_{l=-M/2}^{M/2-1} e^{-ik\mu_l^2/2} (\widetilde{\psi^{**}})_l e^{i\mu_l(x_j-a)}, \quad 0 \leq j \leq M-1, \quad m \geq 0; \end{aligned} \quad (4.25)$$

where  $\widetilde{U}_l$ , the Fourier coefficients of a vector  $U = (U_0, U_1, U_2, \dots, U_M)^T$  with  $U_0 = U_M$ , are defined as

$$\widetilde{U}_l = \frac{1}{M} \sum_{j=0}^{M-1} U_j e^{-i\mu_l(x_j-a)}, \quad l = -\frac{M}{2}, \dots, \frac{M}{2} - 1, \quad (4.26)$$

and (i) for  $\gamma^2 - 4(\mu_l^2 + 1) > 0$

$$\widetilde{(\phi^{m+1})}_l = \begin{cases} \frac{\varepsilon(e^{\lambda_1 k} - e^{\lambda_2 k})}{\sqrt{\gamma^2 - 4(\mu_l^2 + 1)}} (\widetilde{\phi^{(1)}})_l + \frac{\varepsilon(\lambda_1 e^{\lambda_2 k} - \lambda_2 e^{\lambda_1 k})}{\sqrt{\gamma^2 - 4(\mu_l^2 + 1)}} (\widetilde{\phi^{(0)}})_l & m = 0 \\ + \left( \frac{\varepsilon(\lambda_2 e^{\lambda_1 k} - \lambda_1 e^{\lambda_2 k})}{\sqrt{\gamma^2 - 4(\mu_l^2 + 1)}} + 1 \right) \frac{(\widetilde{|\psi^{(0)}|^2})_l}{\mu_l^2 + 1}, & \\ -e^{(\lambda_1 + \lambda_2)k} (\widetilde{\phi^{m-1}})_l + (e^{\lambda_1 k} + e^{\lambda_2 k}) (\widetilde{\phi^m})_l & m \geq 1 \\ + (e^{\lambda_1 k} - 1)(e^{\lambda_2 k} - 1) \frac{(\widetilde{|\psi^m|^2})_l}{\mu_l^2 + 1}; & \end{cases} \quad (4.28)$$

(ii) for  $\gamma^2 - 4(\mu_l^2 + 1) = 0$

$$\widetilde{(\phi^{m+1})}_l = \begin{cases} \left(1 + \frac{\gamma k}{2\varepsilon}\right) e^{-\frac{\gamma k}{2\varepsilon}} \widetilde{(\phi^{(0)})}_l + k e^{-\frac{\gamma k}{2\varepsilon}} \widetilde{(\phi^{(1)})}_l & m = 0 \\ - \left( \left(1 + \frac{\gamma k}{2\varepsilon}\right) e^{-\frac{\gamma k}{2\varepsilon}} - 1 \right) \frac{(|\psi^{(0)}|^2)_l}{\mu_l^2 + 1}, & \\ \\ 2e^{-\frac{k\gamma}{2\varepsilon}} \widetilde{(\phi^m)}_l - e^{-\frac{\gamma k}{\varepsilon}} \widetilde{(\phi^{m-1})}_l & m \geq 1 \\ + \left( e^{-\frac{\gamma k}{2\varepsilon}} - 1 \right)^2 \frac{(|\psi^m|^2)_l}{\mu_l^2 + 1}; & \end{cases} \quad (4.29)$$

and (iii) for  $\gamma^2 - 4(\mu_l^2 + 1) < 0$

$$\widetilde{(\phi^{m+1})}_l = \begin{cases} \left( \cos(\beta k) + \frac{\gamma}{2\beta\varepsilon} \sin(\beta k) \right) e^{-\frac{\gamma k}{2\varepsilon}} \widetilde{(\phi^{(0)})}_l + \frac{\sin(\beta k)}{\beta} e^{-\frac{\gamma k}{2\varepsilon}} \widetilde{(\phi^{(1)})}_l & m = 0 \\ - \left( \left( \cos(\beta k) + \frac{\gamma}{2\beta\varepsilon} \sin(\beta k) \right) e^{-\frac{\gamma k}{2\varepsilon}} - 1 \right) \frac{(|\psi^{(0)}|^2)_l}{\mu_l^2 + 1}, & \\ \\ -e^{-\frac{\gamma k}{\varepsilon}} \widetilde{(\phi^{m-1})}_l + 2 \cos(\beta k) e^{-\frac{\gamma k}{2\varepsilon}} \widetilde{(\phi^m)}_l & m \geq 1 \\ - \left( 2 \cos(\beta k) e^{-\frac{\gamma k}{2\varepsilon}} - e^{-\frac{\gamma k}{\varepsilon}} - 1 \right) \frac{(|\psi^m|^2)_l}{\mu_l^2 + 1}. & \end{cases} \quad (4.30)$$

The initial conditions (4.5) are discretized as

$$\psi_j^0 = \psi^{(0)}(x_j), \quad \phi_j^0 = \phi^{(0)}(x_j), \quad \phi_j^{(1)} = \phi^{(1)}(x_j), \quad 0 \leq j \leq M. \quad (4.31)$$

Note that the spatial discretization error of the above method is of spectral order accuracy in  $h$ , and the time discretization error is demonstrated to be of second order accuracy in  $k$  in section 4.3.1 from our numerical results.

### 4.1.3 Crank-Nicolson leap-frog time-splitting spectral discretizations (CN-LF-TSSP)

Another way to discretize the Klein-Gordon equation (4.2) in the KGS is by using a pseudospectral method for spatial derivatives, followed by application of a Crank-Nicolson/leap-frog method for linear/nonlinear terms for time derivatives:

$$\begin{aligned} \varepsilon^2 \frac{\phi_j^{m+1} - 2\phi_j^m + \phi_j^{m-1}}{k^2} + \varepsilon \gamma \frac{\phi_j^{m+1} - \phi_j^{m-1}}{2k} - D_{xx}^f \left( \beta \phi^{m+1} + (1 - 2\beta) \phi^m + \beta \phi^{m-1} \right)_{x=x_j} \\ + \left( \beta \phi_j^{m+1} + (1 - 2\beta) \phi_j^m + \beta \phi_j^{m-1} \right) - |\psi_j^m|^2 = 0, \quad 0 \leq j \leq M, \quad m \geq 0, \end{aligned} \quad (4.32)$$

where  $0 \leq \beta \leq 1/2$  is a constant;  $D_{xx}^f$ , a spectral differential operator approximation of  $\partial_{xx}$ , is defined as

$$D_{xx}^f U|_{x=x_j} = - \sum_{l=-M/2}^{M/2-1} \mu_l^2 \widetilde{U}_l e^{i\mu_l(x_j-a)}. \quad (4.33)$$

When  $\beta = 0$  in (4.32), the discretization (4.32) to the equation (4.2) is *explicit*. When  $0 < \beta \leq 1/2$ , the discretization is *implicit*, but can be solved *explicitly*. In fact, suppose

$$\phi_j^m = \sum_{l=-M/2}^{M/2-1} (\widetilde{\phi^m})_l e^{i\mu_l(x_j-a)}, \quad j = 0, \dots, M, \quad m = 0, 1, \dots \quad (4.34)$$

Plugging (4.34) into (4.32) and using the orthogonality of the Fourier functions, we obtain for  $m \geq 1$

$$\begin{aligned} \varepsilon^2 \frac{(\widetilde{\phi^{m+1}})_l - 2(\widetilde{\phi^m})_l + (\widetilde{\phi^{m-1}})_l}{k^2} + \varepsilon\gamma \frac{(\widetilde{\phi^{m+1}})_l - (\widetilde{\phi^{m-1}})_l}{2k} - (|\widetilde{\psi^m}|^2)_l \\ + (\mu_l^2 + 1) \left( \beta(\widetilde{\phi^{m+1}})_l + (1 - 2\beta)(\widetilde{\phi^m})_l + \beta(\widetilde{\phi^{m-1}})_l \right) = 0, \quad 0 \leq j \leq M. \end{aligned} \quad (4.35)$$

Solving the above equation, we get

$$\begin{aligned} (\widetilde{\phi^{m+1}})_l = \frac{4\varepsilon^2 + 2(2\beta - 1)(\mu_l^2 + 1)k^2}{2k^2\beta(\mu_l^2 + 1) + \varepsilon\gamma k + 2\varepsilon^2} (\widetilde{\phi^m})_l - \left( 1 - \frac{2\varepsilon\gamma k}{2k^2\beta(\mu_l^2 + 1) + \varepsilon\gamma k + 2\varepsilon^2} \right) (\widetilde{\phi^{m-1}})_l \\ + \frac{2k^2}{2k^2\beta(\mu_l^2 + 1) + \varepsilon\gamma k + 2\varepsilon^2} (|\widetilde{\psi^m}|^2)_l, \quad -\frac{M}{2} \leq l < \frac{M}{2}, \quad m \geq 1. \end{aligned} \quad (4.36)$$

From time  $t = t_m$  to  $t = t_{m+1}$ , we combine the splitting steps via the standard Strang splitting [61, 5, 8]:

$$\phi_j^{m+1} = \sum_{l=-M/2}^{M/2-1} (\widetilde{\phi^{m+1}})_l e^{i\mu_l(x_j-a)}, \quad (4.37)$$

$$\psi_j^* = \sum_{l=-M/2}^{M/2-1} e^{-ik\mu_l^2/2} (\widetilde{\psi^m})_l e^{i\mu_l(x_j-a)},$$

$$\psi_j^{**} = e^{-\nu k + ik(\phi_j^m + \phi_j^{m+1})/2} \psi_j^*$$

$$\psi_j^{m+1} = \sum_{l=-M/2}^{M/2-1} e^{-ik\mu_l^2/2} (\widetilde{\psi^{**}})_l e^{i\mu_l(x_j-a)}, \quad 0 \leq j \leq M-1, \quad m \geq 0. \quad (4.38)$$

The initial conditions are discretized as

$$\psi_j^0 = \psi^{(0)}(x_j), \quad \phi_j^0 = \phi^{(0)}(x_j), \quad \frac{\phi_j^1 - \phi_j^{-1}}{2k} = \phi^{(1)}(x_j), \quad 0 \leq j \leq M-1. \quad (4.39)$$

This implies that

$$\begin{aligned} (\widetilde{\phi^1})_l &= \frac{2\varepsilon^2 + (2\beta - 1)(\mu_l^2 + 1)k^2}{2(\varepsilon^2 + \beta(\mu_l^2 + 1)k^2)} (\widetilde{\phi^{(0)}})_l + \frac{k(2k^2\beta(\mu_l^2 + 1) - \varepsilon\gamma k + 2\varepsilon^2)}{2(\varepsilon^2 + \beta(\mu_l^2 + 1)k^2)} (\widetilde{\phi^{(1)}})_l \\ &\quad + \frac{k^2}{2(\varepsilon^2 + \beta(\mu_l^2 + 1)k^2)} (\widetilde{|\psi^{(0)}|^2})_l. \end{aligned} \quad (4.40)$$

Note that the spatial discretization error of the method is of spectral order accuracy in  $h$  and the time discretization error is demonstrated to be second order accurate in  $k$  in section 4.3.1 from our numerical results.

## 4.2 Properties of numerical methods

### 4.2.1 For plane wave solution

Choose the initial data in (4.3)-(4.4) as

$$\phi^{(0)} = d, \quad \phi^{(1)} = 0, \quad a < x < b, \quad (4.41)$$

$$\psi^{(0)} = \sqrt{d} \exp\left(i\frac{2\pi r x}{b-a}\right), \quad a < x < b, \quad (4.42)$$

then the generalized KGS (3.37)-(3.38) admits the plane wave solution (3.40). In this case, our numerical method TSSP gives exact solution provided  $M \geq 2(|r| + 1)$ . Plugging (4.41)-(4.42) into (4.39), we get

$$\phi_j^{-1} = \phi_j^1, \quad (4.43)$$

$$\psi_j^0 = \sqrt{d} \exp\left(i\frac{2\pi r x_j}{b-a}\right), \quad j = 0, 1, 2, \dots, M-1. \quad (4.44)$$

and note (4.27), we also get

$$\widetilde{\psi}_l^0 = \sqrt{d} e^{i\mu_l r a} \delta_{lr}, \quad l = -\frac{M}{2}, \dots, \frac{M}{2} - 1, \quad (4.45)$$

with

$$\delta_{lr} = \begin{cases} 0, & l \neq r, \\ 1, & l = r, \end{cases} \quad \mu_r = \frac{2\pi r}{b-a}. \quad (4.46)$$

Plugging (4.43), (4.44) and (4.45) into (4.37)-(4.38) with  $m = 1$ , we have

$$\phi_j^1 = \phi_j^0 = d, \quad (4.47)$$

$$\psi_j^* = \sqrt{d} e^{i\mu_r x_j} e^{-ik\mu_r^2/2}, \quad (4.48)$$

and

$$\psi_j^{**} = \sqrt{d} e^{i\mu_r x_j} e^{-ik\mu_r^2/2} e^{-\nu k + ikd} = \sqrt{d} e^{i\mu_r x_j} e^{-i(k\mu_r^2/2 - kd)}, \quad \nu = 0. \quad (4.49)$$

Then we obtain

$$\psi_j^1 = \sqrt{d} e^{-i(k\mu_r^2 - kd - \mu_r a)}, \quad \nu = 0. \quad (4.50)$$

By induction, we can obtain

$$\phi_j^{m+1} = d, \quad (4.51)$$

$$\psi_j^{m+1} = \sqrt{d} e^{-i(t\mu_r^2 - t d - \mu_r a)}, \quad \nu = 0, \quad (4.52)$$

with

$$t = t_{m+1} = (m+1)k, \quad m = 1, 2, \dots. \quad (4.53)$$

Here we use the identity

$$\sum_{j=0}^{M-1} e^{i2\pi(r-l)j/M} = \begin{cases} 0, & r-l \neq nM, \\ M, & r-l = nM. \end{cases} \quad \text{for } n \text{ integer} \quad (4.54)$$

Thus in this case our numerical method TSSP really gives exact results provided that the number of grid points  $M \geq 2(|r| + 1)$ .

## 4.2.2 Conservation and decay rate

Define the usual  $l^2$ -norm and mean value of a vector  $U = (U_0, U_1, \dots, U_M)^T$  which is a discretization of a periodic function  $U(x)$  on the interval  $[a, b]$  with  $U_j = U(x_j)$

( $j = 0, 1, \dots, M$ ) as

$$\|U\|_{l^2} = \sqrt{\frac{b-a}{M} \sum_{j=0}^{M-1} |U_j|^2}, \quad N(U) = \frac{b-a}{M} \sum_{j=0}^{M-1} U_j. \quad (4.55)$$

For the discretizations (4.25)-(4.26) and (4.37)-(4.38), we have the following result for dynamics of wave energy in discretized level:

**Theorem 4.1.** The discretizations PSAS-TSSP(4.25)-(4.26) and CN-LF-TSSP (4.37)-(4.38) for KGS possess the following properties:

$$\|\psi^m\|_{l^2}^2 = e^{-2\nu t_m} \|\psi^0\|_{l^2}^2 = e^{-2\nu t_m} \|\psi^{(0)}\|_{l^2}^2, \quad m = 0, 1, 2, \dots. \quad (4.56)$$

**Proof.** From (4.38) in the scheme TSSP, noting (4.27), we have

$$\begin{aligned} \frac{M}{b-a} \|\psi^{m+1}\|_{l^2}^2 &= \sum_{j=0}^{M-1} |\psi_j^{m+1}|^2 = \sum_{j=0}^{M-1} \left| \sum_{l=-M/2}^{M/2-1} e^{-ik\mu_l^2/2} (\widetilde{\psi^{**}})_l e^{i\mu_l(x_j-a)} \right|^2 \\ &= M \sum_{l=-M/2}^{M/2-1} \left| e^{-ik\mu_l^2/2} (\widetilde{\psi^{**}})_l \right|^2 = M \sum_{l=-M/2}^{M/2-1} \left| (\widetilde{\psi^{**}})_l \right|^2 \\ &= \frac{1}{M} \sum_{l=-M/2}^{M/2-1} \left| \sum_{j=0}^{M-1} \psi_j^{**} e^{-i\mu_l(x_j-a)} \right|^2 = \sum_{j=0}^{M-1} |\psi_j^{**}|^2 \\ &= \sum_{j=0}^{M-1} \left| e^{-\nu k + ik(\phi_j^m + \phi_j^{m+1})/2} \psi_j^* \right|^2 = e^{-2\nu k} \sum_{j=0}^{M-1} |\psi_j^*|^2 \\ &= e^{-2\nu k} \sum_{j=0}^{M-1} \left| \sum_{l=-M/2}^{M/2-1} e^{-k\mu_l^2/2} (\widetilde{\psi^*})_l e^{i\mu_l(x_j-a)} \right|^2 \\ &= e^{-2\nu k} M \sum_{l=-M/2}^{M/2-1} \left| e^{-i\mu_l^2/2} (\widetilde{\psi^*})_l \right|^2 = e^{-2\nu k} M \sum_{l=-M/2}^{M/2-1} \left| (\widetilde{\psi^*})_l \right|^2 \\ &= \frac{e^{-2\nu k}}{M} \sum_{l=-M/2}^{M/2-1} \left| \psi_j^* e^{-i\mu_l(x_j-a)} \right|^2 = e^{-2\nu k} \sum_{j=0}^{M-1} |\psi_j^m|^2 \\ &= \frac{M e^{-2\nu k}}{b-a} \|\psi^m\|_{l^2}^2 = \dots \\ &= \frac{M e^{-2\nu t_{m+1}}}{b-a} \|\psi^0\|_{l^2}^2, \quad m \geq 1. \end{aligned} \quad (4.57)$$

Thus, the equality (4.56) is proved. Here, we use the identities

$$\sum_{j=0}^{M-1} e^{i2\pi(k-l)j/M} = \begin{cases} 0, & k-l \neq nM, \\ 1, & k-l = nM, \end{cases} \quad \text{for } n \text{ integer,} \quad (4.58)$$

and

$$\sum_{l=-M/2}^{M/2-1} e^{i2\pi(k-j)l/M} = \begin{cases} 0, & k-j \neq nM, \\ 1, & k-j = nM, \end{cases} \quad \text{for } n \text{ integer.} \quad (4.59)$$

□

### 4.2.3 Dynamics of mean value of meson field

When  $\nu = 0$ , for the discretization PSAS-TSSP (4.25)-(4.26), we have the following results for dynamics of mean value of the meson field in discretized level:

**Theorem 4.2.** When  $\nu = 0$ , the discretization PSAS-TSSP (4.25)-(4.26) for KGS possesses the following property:

(i) when  $\gamma > 2$

$$\begin{aligned} N(\phi^{m+1}) &= D(0) + \frac{N(\phi^{(1)}) - \lambda_2^0(N(\phi^{(0)}) - D(0))}{\lambda_1^0 - \lambda_2^0} e^{\lambda_1^0 t_{m+1}} \\ &\quad + \frac{-N(\phi^{(1)}) + \lambda_1^0(N(\phi^{(0)}) - D(0))}{\lambda_1^0 - \lambda_2^0} e^{\lambda_2^0 t_{m+1}}; \end{aligned} \quad (4.60)$$

(ii) when  $\gamma = 2$

$$\begin{aligned} N(\phi^{m+1}) &= D(0) + (N(\phi^{(0)}) - D(0)) e^{\lambda_0 t_{m+1}} \\ &\quad + (N(\phi^{(1)}) - \lambda_0(N(\phi^{(0)}) - D(0))) t_{m+1} e^{\lambda_0 t_{m+1}}; \end{aligned} \quad (4.61)$$

and (iii) when  $0 \leq \gamma < 2$

$$\begin{aligned} N(\phi^{m+1}) &= D(0) + e^{\lambda_0 t_{m+1}} \left[ (N(\phi^{(0)}) - D(0)) \cos(\beta_0 t_{m+1}) \right. \\ &\quad \left. + \frac{N(\phi^{(1)}) - \lambda_0(N(\phi^{(0)}) - D(0))}{\beta_0} \sin(\beta_0 t_{m+1}) \right]; \end{aligned} \quad (4.62)$$

where

$$D(0) = N(|\psi_0|^2) = \frac{b-a}{M} \sum_{j=0}^{M-1} |\psi^{(0)}(x_j)|^2. \quad (4.63)$$

**Proof.** From (4.55), (4.25) and (4.27), noticing the orthogonality of the discrete Fourier series, we have

$$\begin{aligned} N(\phi^{m+1}) &= \frac{b-a}{M} \sum_{j=0}^{M-1} \phi_j^{m+1} = \frac{b-a}{M} \sum_{j=0}^{M-1} \sum_{l=-M/2}^{M/2-1} (\widetilde{\phi^{m+1}})_l e^{i\mu_l(x_j-a)} \\ &= \frac{b-a}{M} \sum_{l=-M/2}^{M/2-1} (\widetilde{\phi^{m+1}})_l \sum_{j=0}^{M-1} e^{i\mu_l(x_j-a)} = (b-a) (\widetilde{\phi^{m+1}})_0. \end{aligned} \quad (4.64)$$

Similarly, from (4.56) with  $\nu = 0$ , we have

$$(|\widetilde{\psi^{m+1}}|^2)_0 = \frac{1}{M} \sum_{j=0}^{M-1} |\psi_j^{m+1}|^2 = \frac{\|\psi^{m+1}\|_{l^2}^2}{b-a} = \frac{\|\psi^0\|_{l^2}^2}{b-a} = (|\widetilde{\psi^{(0)}}|^2)_0, \quad m \geq 0.$$

(i) When  $\gamma > 2$ , denote  $p = e^{\lambda_1^0 k}$  and  $q = e^{\lambda_2^0 k}$ . From (4.28) and (4.16) with  $l = 0$ , (3.36) and (4.65), we obtain

$$\begin{aligned} (\widetilde{\phi^{m+1}})_0 &= -pq(\widetilde{\phi^{m-1}})_0 + (p+q)(\widetilde{\phi^m})_0 + (p-1)(q-1)(|\widetilde{\psi^m}|^2)_0 \\ &= -pq(\widetilde{\phi^{m-1}})_0 + (p+q)(\widetilde{\phi^m})_0 + (p-1)(q-1)(|\widetilde{\psi^{(0)}}|^2)_0, \quad m \geq 1; \end{aligned} \quad (4.65)$$

$$(\widetilde{\phi^1})_0 = \frac{p-q}{\lambda_1^0 - \lambda_2^0} (\widetilde{\phi^{(1)}})_0 + \frac{\lambda_1^0 q - \lambda_2^0 p}{\lambda_1^0 - \lambda_2^0} (\widetilde{\phi^{(0)}})_0 + \left(1 + \frac{\lambda_2^0 p - \lambda_1^0 q}{\lambda_1^0 - \lambda_2^0}\right) (|\widetilde{\psi^{(0)}}|^2)_0. \quad (4.66)$$

Rewrite (4.65), by induction, we obtain for  $m \geq 1$ :

$$\begin{aligned} &(\widetilde{\phi^{m+1}})_0 - p(\widetilde{\phi^m})_0 + (p-1)(|\widetilde{\psi^{(0)}}|^2)_0 \\ &= q \left( (\widetilde{\phi^m})_0 - p(\widetilde{\phi^{m-1}})_0 + (p-1)(|\widetilde{\psi^{(0)}}|^2)_0 \right) \\ &= q^m \left( (\widetilde{\phi^1})_0 - p(\widetilde{\phi^{(0)}})_0 + (p-1)(|\widetilde{\psi^{(0)}}|^2)_0 \right). \end{aligned} \quad (4.67)$$

From (4.67), by induction again, we get

$$\begin{aligned} (\widetilde{\phi^{m+1}})_0 &= \sum_{r=0}^m \left[ p^r q^{m-r} \left( (\widetilde{\phi^1})_0 - p(\widetilde{\phi^{(0)}})_0 \right) + p^r (q^{m-r} - 1)(p-1)(|\widetilde{\psi^{(0)}}|^2)_0 \right] \\ &\quad + p^{m+1} (\widetilde{\phi^{(0)}})_0 \\ &= \frac{q^{m+1} - p^{m+1}}{q-p} (\widetilde{\phi^1})_0 + \frac{qp^{m+1} - pq^{m+1}}{q-p} (\widetilde{\phi^{(0)}})_0 \\ &\quad + \frac{p^{m+1} - q^{m+1} + pq^{m+1} - qp^{m+1} + q-p}{q-p} (|\widetilde{\psi^{(0)}}|^2)_0. \end{aligned} \quad (4.68)$$

Combining (4.64), (4.68) and (4.66), noticing (4.65) and (4.55), we obtain

$$\begin{aligned}
N(\phi^{m+1}) &= \frac{q^{m+1} - p^{m+1}}{q - p} \left[ \frac{p - q}{\lambda_1^0 - \lambda_2^0} N(\phi^{(1)}) + \frac{\lambda_1^0 q - \lambda_2^0 p}{\lambda_1^0 - \lambda_2^0} N(\phi^{(0)}) \right. \\
&\quad \left. + \left( 1 + \frac{\lambda_2^0 p - \lambda_1^0 q}{\lambda_1^0 - \lambda_2^0} \right) N(|\psi^{(0)}|^2) \right] + \frac{qp^{m+1} - pq^{m+1}}{q - p} N(\phi^{(0)}) \\
&\quad + \frac{p^{m+1} - q^{m+1} + pq^{m+1} - qp^{m+1} + q - p}{q - p} N(|\psi^{(0)}|^2) \\
&= \frac{p^{m+1} - q^{m+1}}{\lambda_1^0 - \lambda_2^0} N(\phi^{(1)}) + \frac{\lambda_1^0 q^{m+1} - \lambda_2^0 p^{m+1}}{\lambda_1^0 - \lambda_2^0} N(\phi^{(0)}) \\
&\quad + \left( 1 - \frac{\lambda_1^0 q^{m+1} - \lambda_2^0 p^{m+1}}{\lambda_1^0 - \lambda_2^0} \right) N(|\psi^{(0)}|^2) \\
&= N(|\psi^{(0)}|^2) + \frac{-N(\phi^{(1)}) + \lambda_1^0 (N(\phi^{(0)}) - N(|\psi^{(0)}|^2))}{\lambda_1^0 - \lambda_2^0} e^{\lambda_2^0 t_{m+1}} \\
&\quad + \frac{N(\phi^{(1)}) - \lambda_2^0 (N(\phi^{(0)}) - N(|\psi^{(0)}|^2))}{\lambda_1^0 - \lambda_2^0} e^{\lambda_1^0 t_{m+1}}. \tag{4.69}
\end{aligned}$$

Thus (4.60) is a combination of (4.69) and (4.63).

(ii) When  $\gamma = 2$ , denote  $p = e^{\lambda_0 k}$ . From (4.29) and (4.16) with  $l = 0$ , (3.36) and (4.65), we obtain

$$\begin{aligned}
\widetilde{(\phi^{m+1})}_0 &= -p^2 \widetilde{(\phi^{m-1})}_0 + 2p \widetilde{(\phi^m)}_0 + (p - 1)^2 \widetilde{(|\psi^m|^2)}_0 \\
&= -p^2 \widetilde{(\phi^{m-1})}_0 + 2p \widetilde{(\phi^m)}_0 + (p - 1)^2 \widetilde{(|\psi^{(0)}|^2)}_0, \quad m \geq 1; \tag{4.70}
\end{aligned}$$

$$\widetilde{(\phi^1)}_0 = kp \widetilde{(\phi^{(1)})}_0 + (1 - \lambda_0 k)p \widetilde{(\phi^{(0)})}_0 + (1 - (1 - \lambda_0 k)p) \widetilde{(|\psi^{(0)}|^2)}_0. \tag{4.71}$$

Rewrite (4.70), by induction, we obtain for  $m \geq 1$ :

$$\begin{aligned}
&\widetilde{(\phi^{m+1})}_0 - p \widetilde{(\phi^m)}_0 + (p - 1) \widetilde{(|\psi^{(0)}|^2)}_0 \\
&= p \left( \widetilde{(\phi^m)}_0 - p \widetilde{(\phi^{m-1})}_0 + (p - 1) \widetilde{(|\psi^{(0)}|^2)}_0 \right) \\
&= p^m \left( \widetilde{(\phi^1)}_0 - p \widetilde{(\phi^{(0)})}_0 + (p - 1) \widetilde{(|\psi^{(0)}|^2)}_0 \right). \tag{4.72}
\end{aligned}$$

From (4.72), by induction again, we get

$$\begin{aligned}
\widetilde{(\phi^{m+1})}_0 &= \sum_{r=0}^m \left[ p^m \left( \widetilde{(\phi^1)}_0 - p \widetilde{(\phi^{(0)})}_0 \right) + p^r (p^{m-r} - 1)(p-1) \widetilde{(|\psi^{(0)}|^2)}_0 \right] \\
&\quad + p^{m+1} \widetilde{(\phi^{(0)})}_0 \\
&= (m+1)p^m \widetilde{(\phi^1)}_0 - mp^{m+1} \widetilde{(\phi^{(0)})}_0 \\
&\quad + (1 - p^{m+1} + (m+1)(p-1)p^m) \widetilde{(|\psi^{(0)}|^2)}_0. \tag{4.73}
\end{aligned}$$

Combining (4.64), (4.73) and (4.71), noticing (4.65) and (4.55), we obtain

$$\begin{aligned}
N(\phi^{m+1}) &= (m+1)p^m [kpN(\phi^{(1)}) + (1 - \lambda_0 k)pN(\phi^{(0)}) + (1 - (1 - \lambda_0 k)p)N(|\psi^{(0)}|^2)] \\
&\quad - mp^{m+1}N(\phi^{(0)}) + [1 - p^{m+1} + (m+1)(p-1)p^m]N(|\psi^{(0)}|^2) \\
&= (m+1)kp^{m+1}N(\phi^{(1)}) + (1 - (m+1)\lambda_0 k)p^{m+1}N(\phi^{(0)}) \\
&\quad + [1 - p^{m+1} + (m+1)\lambda_0 kp^{m+1}]N(|\psi^{(0)}|^2) \\
&= N(|\psi^{(0)}|^2) + [N(\phi^{(0)}) - N(|\psi^{(0)}|^2)]e^{\lambda_0 t_{m+1}} \\
&\quad + [N(\phi^{(1)}) - \lambda_0(N(\phi^{(0)}) - N(|\psi^{(0)}|^2))]t_{m+1}e^{\lambda_0 t_{m+1}}. \tag{4.74}
\end{aligned}$$

Thus (4.61) is a combination of (4.74) and (4.63).

(iii) When  $0 \leq \gamma < 2$ , denote  $p = e^{(\lambda_0 + i\beta_0)k}$  and  $q = e^{(\lambda_0 - i\beta_0)k}$ . From (4.28) and (4.16) with  $l = 0$ , (3.36) and (4.65), we obtain

$$\begin{aligned}
\widetilde{(\phi^{m+1})}_0 &= -pq\widetilde{(\phi^{m-1})}_0 + (p+q)\widetilde{(\phi^m)}_0 + (p-1)(q-1)\widetilde{(|\psi^m|^2)}_0 \\
&= -pq\widetilde{(\phi^{m-1})}_0 + (p+q)\widetilde{(\phi^m)}_0 + (p-1)(q-1)\widetilde{(|\psi^{(0)}|^2)}_0, \quad m \geq 1; \tag{4.75}
\end{aligned}$$

$$\begin{aligned}
\widetilde{(\phi^1)}_0 &= \frac{\sin(\beta_0 k)e^{\lambda_0 k}}{\beta_0} \widetilde{(\phi^{(1)})}_0 + \left( \cos(\beta_0 k) - \frac{\lambda_0}{\beta_0} \sin(\beta_0 k) \right) e^{\lambda_0 k} \widetilde{(\phi^{(0)})}_0 \\
&\quad + \left[ 1 - \left( \cos(\beta_0 k) - \frac{\lambda_0}{\beta_0} \sin(\beta_0 k) \right) e^{\lambda_0 k} \right] \widetilde{(|\psi^{(0)}|^2)}_0. \tag{4.76}
\end{aligned}$$

Rewrite (4.75), by induction, we obtain for  $m \geq 1$ :

$$\begin{aligned}
&\widetilde{(\phi^{m+1})}_0 - p \widetilde{(\phi^m)}_0 + (p-1)\widetilde{(|\psi^{(0)}|^2)}_0 \\
&= q \left( \widetilde{(\phi^m)}_0 - p \widetilde{(\phi^{m-1})}_0 + (p-1)\widetilde{(|\psi^{(0)}|^2)}_0 \right) \\
&= q^m \left( \widetilde{(\phi^1)}_0 - p \widetilde{(\phi^{(0)})}_0 + (p-1)\widetilde{(|\psi^{(0)}|^2)}_0 \right). \tag{4.77}
\end{aligned}$$

From (4.77), by induction again, we get

$$\begin{aligned}
(\widetilde{\phi^{m+1}})_0 &= \sum_{r=0}^m \left[ p^r q^{m-r} \left( (\widetilde{\phi^1})_0 - p (\widetilde{\phi^{(0)}})_0 \right) + p^r (q^{m-r} - 1)(p-1) (\widetilde{|\psi^{(0)}|^2})_0 \right] \\
&\quad + p^{m+1} (\widetilde{\phi^{(0)}})_0 \\
&= \frac{q^{m+1} - p^{m+1}}{q-p} (\widetilde{\phi^1})_0 + \frac{qp^{m+1} - pq^{m+1}}{q-p} (\widetilde{\phi^{(0)}})_0 \\
&\quad + \frac{p^{m+1} - q^{m+1} + pq^{m+1} - qp^{m+1} + q - p}{q-p} (\widetilde{|\psi^{(0)}|^2})_0. \tag{4.78}
\end{aligned}$$

Combining (4.64), (4.78) and (4.76), noticing (4.65) and (4.55), we obtain

$$\begin{aligned}
N(\phi^{m+1}) &= \frac{q^{m+1} - p^{m+1}}{q-p} \left[ \left( 1 - \left( \cos(\beta_0 k) - \frac{\lambda_0}{\beta_0} \sin(\beta_0 k) \right) e^{\lambda_0 k} \right) N(|\psi^{(0)}|^2) \right. \\
&\quad \left. + \frac{\sin(\beta_0 k) e^{\lambda_0 k}}{\beta_0} N(\phi^{(1)}) + \left( \cos(\beta_0 k) - \frac{\lambda_0}{\beta_0} \sin(\beta_0 k) \right) e^{\lambda_0 k} N(\phi^{(0)}) \right] \\
&\quad + \frac{qp^{m+1} - pq^{m+1}}{q-p} N(\phi^{(0)}) + \frac{p^{m+1} - q^{m+1} + pq^{m+1} - qp^{m+1} + q - p}{q-p} N(|\psi^{(0)}|^2) \\
&= e^{\lambda_0(m+1)k} \left( \cos((m+1)\beta_0 k) - \frac{\lambda_0}{\beta_0} \sin((m+1)\beta_0 k) \right) N(\phi^{(0)}) \\
&\quad + \left[ 1 - e^{\lambda_0(m+1)k} \left( \cos((m+1)\beta_0 k) - \frac{\lambda_0}{\beta_0} \sin((m+1)\beta_0 k) \right) \right] N(|\psi^{(0)}|^2) \\
&\quad + e^{\lambda_0(m+1)k} \left( \frac{\sin((m+1)\beta_0 k)}{\beta_0} \right) N(\phi^{(1)}) \\
&= N(|\psi^{(0)}|^2) + e^{\lambda_0 t_{m+1}} \left[ (N(\phi^{(0)}) - N(|\psi^{(0)}|^2)) \cos(\beta_0 t_{m+1}) \right. \\
&\quad \left. + \frac{N(\phi^{(1)}) - \lambda_0 (N(\phi^{(0)}) - N(|\psi^{(0)}|^2))}{\beta_0} \sin(\beta_0 t_{m+1}) \right]. \tag{4.79}
\end{aligned}$$

Thus (4.62) is a combination of (4.79) and (4.63).  $\square$

#### 4.2.4 Stability analysis

By using the standard von Neumann analysis for the discretization PSAS-TSSP (4.25)-(4.26) and CN-LP-TSSP (4.37)-(4.38), we have

**Theorem 4.3.** The discretization PSAS-TSSP (4.25)-(4.26) is unconditionally stable for any parameter value  $\gamma \geq 0$ , time step  $k > 0$  and mesh size  $h > 0$ . When

$1/4 \leq \beta \leq 1/2$  and  $\gamma = 0$ , the discretization CN-LP-TSSP (4.37)-(4.38) is unconditionally stable; and when  $0 \leq \beta < 1/4$  and  $\gamma = 0$ , it is conditionally stable under the stability condition

$$k \leq \frac{2h\varepsilon}{\sqrt{(1-4\beta)(\pi^2 + h^2)}}. \quad (4.80)$$

**Proof.** For the discretization PSAS-TSSP (4.25)-(4.26), setting  $(|\widetilde{\psi^m}|^2)_l = 0$  and plugging  $\widetilde{\phi}_l^{m+1} = \mu \widetilde{\phi}_l^m = \mu^2 \widetilde{\phi}_l^{m-1}$  into (4.28), (4.29) and (4.30) with  $|\mu|$  the amplification factor, we obtain:

(i) When  $\gamma^2 - 4(\mu_l^2 + 1) > 0$ , the characteristic equation for  $\mu$  is

$$\mu^2 - (e^{\lambda_1 k} + e^{\lambda_2 k})\mu + e^{(\lambda_1 + \lambda_2)k} = 0. \quad (4.81)$$

Solving the above equation, we have

$$\mu_1 = e^{\lambda_1 k}, \quad \mu_2 = e^{\lambda_2 k}. \quad (4.82)$$

Thus the amplification factor satisfies

$$G_l = \max\{|\mu_1|, |\mu_2|\} = e^{\frac{-\gamma + \sqrt{\gamma^2 - 4(\mu_l^2 + 1)}}{2}} \leq 1, \quad l = -\frac{M}{2}, \dots, \frac{M}{2} - 1. \quad (4.83)$$

(ii) When  $\gamma^2 - 4(\mu_l^2 + 1) = 0$ , the characteristic equation for  $\mu$  is

$$\mu^2 - 2e^{-\frac{\gamma k}{2}}\mu + e^{-\gamma k} = 0. \quad (4.84)$$

Solving the above equation, we have

$$\mu = e^{-\frac{\gamma k}{2}}.$$

Thus the amplification factor satisfies

$$G_l = |\mu| = e^{-\frac{\gamma k}{2}} \leq 1, \quad l = -\frac{M}{2}, \dots, \frac{M}{2} - 1. \quad (4.85)$$

(iii) When  $\gamma^2 - 4(\mu_l^2 + 1) < 0$ , the characteristic equation for  $\mu$  is

$$\mu^2 - 2\cos(\beta k)e^{-\frac{\gamma k}{2}}\mu + e^{-\gamma k} = 0. \quad (4.86)$$

Solving the above equation, we have

$$\mu = e^{-\frac{\gamma k}{2}} [\cos(\beta k) \pm i \sin(\beta k)]. \quad (4.87)$$

Thus the amplification factor satisfies

$$G_l = |\mu| = e^{-\frac{\gamma k}{2}} \sqrt{\cos^2(\beta k) + \sin^2(\beta k)} = e^{-\frac{\gamma k}{2}} \leq 1, \quad l = -\frac{M}{2}, \dots, \frac{M}{2} - 1. \quad (4.88)$$

(4.83), (4.85) and (4.88), together with (4.56), imply that PSAS-TSSP is unconditionally stable for any time step  $k > 0$ , mesh size  $h > 0$  and parameter values  $\gamma \geq 0$ .

Similarly for the discretization CN-LF-TSSP (4.37)-(4.38), noting (4.36), we have the characteristic equation

$$\mu^2 - 2 \left( 1 - \frac{(\mu_l^2 + 1)k^2 + \varepsilon\gamma k}{2k^2\beta(\mu_l^2 + 1) + \varepsilon\gamma k + 2\varepsilon^2} \right) \mu + 1 - \frac{2\varepsilon\gamma k}{2k^2\beta(\mu_l^2 + 1) + \varepsilon\gamma k + 2\varepsilon^2} = 0. \quad (4.89)$$

Solving the above equation, we obtain

$$\begin{aligned} \mu = & 1 - \frac{(\mu_l^2 + 1)k^2 + \varepsilon\gamma k}{2k^2\beta(\mu_l^2 + 1) + \varepsilon\gamma k + 2\varepsilon^2} \\ & \pm \sqrt{\left( 1 - \frac{(\mu_l^2 + 1)k^2 + \varepsilon\gamma k}{2k^2\beta(\mu_l^2 + 1) + \varepsilon\gamma k + 2\varepsilon^2} \right)^2 - 1 + \frac{2\varepsilon\gamma k}{2k^2\beta(\mu_l^2 + 1) + \varepsilon\gamma k + 2\varepsilon^2}}. \end{aligned}$$

When  $1/4 \leq \beta \leq 1/2$  and  $\gamma = 0$ , we have

$$\left| 1 - \frac{(\mu_l^2 + 1)k^2}{2k^2\beta(\mu_l^2 + 1) + 2\varepsilon^2} \right| \leq 1, \quad k > 0.$$

Thus

$$\mu = 1 - \frac{(\mu_l^2 + 1)k^2}{2k^2\beta(\mu_l^2 + 1) + 2\varepsilon^2} \pm i \sqrt{1 - \left( 1 - \frac{(\mu_l^2 + 1)k^2}{2k^2\beta(\mu_l^2 + 1) + 2\varepsilon^2} \right)^2}.$$

This implies that the amplification factor satisfies

$$\begin{aligned} G_l &= |\mu| = \sqrt{\left( 1 - \frac{(\mu_l^2 + 1)k^2}{2k^2\beta(\mu_l^2 + 1) + 2\varepsilon^2} \right)^2 + 1 - \left( 1 - \frac{(\mu_l^2 + 1)k^2}{2k^2\beta(\mu_l^2 + 1) + 2\varepsilon^2} \right)^2} \\ &= 1, \quad l = -M/2, \dots, M/2 - 1. \end{aligned}$$

This, together with (4.56), implies that CN-LP-TSSP with  $1/4 \leq \beta \leq 1/2$  is unconditionally stable. On the other hand, when  $0 \leq \beta < 1/4$  and  $\gamma = 0$ , we need the stability condition

$$\left| 1 - \frac{(\mu_l^2 + 1)k^2}{2k^2\beta(\mu_l^2 + 1) + 2\varepsilon^2} \right| \leq 1, \quad l = -M/2, \dots, M/2 - 1.$$

This implies that

$$k \leq \min_{-M/2 \leq l \leq M/2-1} \sqrt{\frac{4\varepsilon^2}{(1-4\beta)(1+\mu_l^2)}} = \frac{2h\varepsilon}{\sqrt{(1-4\beta)(\pi^2 + h^2)}}.$$

Thus we get the stability condition (4.80).  $\square$

## 4.3 Numerical results of the Klein-Gordon-Schrödinger equation

In this section, we will compare the accuracy and stability of different numerical methods for the Klein-Gordon-Schrödinger equations with a solitary wave solution, and also present the numerical results for plane waves, soliton-soliton collisions in 1D, 2D problems and the generalized KGS with a damping term.

### 4.3.1 Comparisons of different methods

**Example 4.1.** The standard KGS with a solitary wave solution in 1D, i.e., we choose  $d = 1$ ,  $\varepsilon = 1$ ,  $\nu = 0$  in (1.4)-(1.6). The initial data in (1.6) is chosen as

$$\psi^{(0)}(x) = \psi_+(\mathbf{x}, t = 0), \quad \phi^{(0)}(x) = \phi_+(x, t = 0), \quad (4.90)$$

$$\phi^{(1)}(x) = \partial_t \phi_+(x, t = 0), \quad x \in \mathbb{R}; \quad (4.91)$$

where  $\psi_+$  and  $\phi_+$  are given in (3.41)-(3.42).

We present computations for two different regimes of acoustic speed, i.e.,  $1/\varepsilon$ .

Case I. O(1)-acoustic speed, i.e.,  $\varepsilon = 1$ . In our computation, we take  $B = 1$  in (3.41)-(3.42) and solve the problem on the interval  $[-32, 32]$ , i.e.,  $a = -32$  and

	Mesh	$h = 1.0$	$h = 1/2$	$h = 1/4$
PSAS-TSSP	$e_1$	1.341	5.031E-3	9.006E-8
	$e_2$	1.056	8.342E-2	7.476E-7
CN-LF-TSSP ( $\beta = 0$ )	$e_1$	1.341	5.031E-3	8.418E-7
	$e_2$	1.056	8.342E-3	7.491E-7
CN-LF-TSSP ( $\beta = 1/4$ )	$e_1$	1.341	5.031E-3	9.327E-8
	$e_2$	1.056	8.342E-3	7.510E-7
CN-LF-TSSP ( $\beta = 1/2$ )	$e_1$	1.341	5.081E-3	1.140E-7
	$e_2$	1.056	8.342E-3	7.587E-7

Table 4.1: Spatial discretization errors  $e_1(t)$  and  $e_2(t)$  at time  $t = 2$  for different mesh sizes  $h$  under  $k = 0.0001$ . I: For  $\gamma = 0$ .

$b = 32$  with periodic boundary conditions. When  $\gamma = 0$ , the KGS admits the well-known solitary wave solution (3.41)-(3.42) as exact solution. When  $\gamma > 0$ , there is no analytical solution and we let  $\psi$  and  $\phi$  be the ‘exact’ solutions which are obtained numerically by using our numerical method with a very fine mesh and small time step size, e.g.  $h = \frac{1}{32}$  and  $k = 0.0001$ . Let  $\psi_{h,k}$  and  $\phi_{h,k}$  be the numerical solution obtained by using a method with mesh size  $h$  and time step  $k$ . To quantify the numerical methods, we define the error functions as

$$e_1(t) = \|\psi(\cdot, t) - \psi_{h,k}(t)\|_{l^2}, \quad e_2(t) = \|\phi(\cdot, t) - \phi_{h,k}(t)\|_{l^2},$$

$$e(t) = \frac{\|\psi(\cdot, t) - \psi_{h,k}(t)\|_{l^2}}{\|\psi(\cdot, t)\|_{l^2}} + \frac{\|\phi(\cdot, t) - \phi_{h,k}(t)\|_{l^2}}{\|\phi(\cdot, t)\|_{l^2}} = \frac{e_1(t)}{\|\psi(\cdot, t)\|_{l^2}} + \frac{e_2(t)}{\|\phi(\cdot, t)\|_{l^2}}.$$

First we test the discretization error in space. In order to do this, we choose a very small time step, e.g.,  $k = 0.0001$ , such that the error from time discretization is negligible compared to the spatial discretization error, and solve the KGS with different methods under different mesh size  $h$  and  $\gamma$ . Table 4.1 lists the numerical errors of  $e_1(t)$  and  $e_2(t)$  at  $t = 2$  with different mesh sizes  $h$  and parameter values  $\gamma$  for different numerical methods.

Then we test the discretization error in time. Table 4.2 shows the numerical errors

	Mesh	$h = 1.0$	$h = 1/2$	$h = 1/4$
PSAS-TSSP	$e_1$	0.823	4.094E-3	1.127E-6
	$e_2$	0.715	3.324E-3	1.729E-6
CN-LF-TSSP ( $\beta = 0$ )	$e_1$	0.823	4.094E-3	1.612E-6
	$e_2$	0.715	3.324E-3	1.078E-6
CN-LF-TSSP ( $\beta = 1/4$ )	$e_1$	0.823	4.094E-3	1.625E-6
	$e_2$	0.715	3.324E-3	1.105E-6
CN-LF-TSSP ( $\beta = 1/2$ )	$e_1$	0.823	4.094E-3	1.622E-6
	$e_2$	0.715	3.324E-3	1.120E-6

Table 4.1: (cont'd): II: For  $\gamma = 0.5$ .

$e_1(t)$  and  $e_2(t)$  at  $t = 1.0$  under different time steps  $k$  and mesh sizes  $h$  for different numerical methods.

Finally we test the conservation of conserved quantities. Table 4.3 presents the quantities and numerical errors at different times with mesh size  $h = \frac{1}{8}$  and time step  $k = 0.0001$  for different numerical methods.

From Tables 4.1-4.2, we can draw the following observations: Our new numerical methods PSAS-TSSP and CN-LF-TSSP are of spectral-order accuracy in space discretization and second-order accuracy in time. Moreover, PSAS-TSSP and CN-LP-TSSP with  $\beta = 1/2$  or  $\beta = 1/4$  are unconditionally stable, where CN-LP-TSSP with  $\beta = 0$  is conditionally stable. Both numerical methods conserve the wave energy  $D$  exactly and the Hamiltonian  $H$  very well (up to 8 significant digits). Furthermore, these two methods are explicit, easy to program, less memory requirement, easy to extend to 2D & 3D cases, and keep most properties of KGS in the discretized level. In the following next section, we always use PSAS-TSSP for solving KGS.

Case II. “nonrelativistic limit” regime, i.e.,  $0 < \varepsilon \ll 1$ . We choose  $B = 1$  and  $\gamma = 0$  in (3.41)-(3.42). Here we test the  $\varepsilon$ -resolution of different numerical methods when  $\varepsilon \rightarrow 0$ . Two types of initial data are chosen:

	h	Error	$k = \frac{1}{25}$	$k = \frac{1}{100}$	$k = \frac{1}{400}$	$k = \frac{1}{1600}$
PSAS-TSSP	$\frac{1}{4}$	$e_1$	7.414E-3	4.728E-4	2.971E-5	1.861E-6
		$e_2$	2.409E-3	1.538E-4	9.681E-6	7.421E-7
	$\frac{1}{8}$	$e_1$	7.414E-3	4.728E-4	2.971E-5	1.859E-6
		$e_2$	2.409E-3	1.538E-4	9.672E-6	6.054E-7
CN-LF-TSSP ( $\beta = 0$ )	$\frac{1}{4}$	$e_1$	7.935E-3	5.067E-4	3.185E-5	1.995E-6
		$e_2$	7.882E-4	5.086E-5	3.242E-5	4.738E-7
	$\frac{1}{8}$	$e_1$	7.935E-3	5.067E-4	3.185E-5	1.993E-6
		$e_2$	7.882E-4	5.086E-5	3.212E-6	2.013E-7
CN-LF-TSSP ( $\beta = 1/4$ )	$\frac{1}{4}$	$e_1$	6.714E-3	4.269E-4	2.681E-5	1.680E-6
		$e_2$	5.690E-3	3.622E-4	2.275E-5	1.486E-6
	$\frac{1}{8}$	$e_1$	6.714E-3	4.269E-4	2.681E-5	1.678E-6
		$e_2$	5.690E-3	3.622E-4	2.274E-5	1.423E-6
CN-LF-TSSP ( $\beta = 1/2$ )	$\frac{1}{4}$	$e_1$	6.737E-3	4.284E-4	2.690E-5	1.685E-6
		$e_2$	1.061E-2	6.752E-4	4.237E-5	2.686E-6
	$\frac{1}{8}$	$e_1$	6.737E-3	4.284E-4	2.690E-5	1.683E-6
		$e_2$	1.061E-2	6.752E-4	4.237E-5	2.651E-6

Table 4.2: Temporal discretization errors  $e_1(t)$  and  $e_2(t)$  at time  $t = 1$  for different time steps  $k$ . I: For  $\gamma = 0$ .

- Type 1.  $O(\varepsilon)$ -wavelength in the initial data, i.e., we choose the initial data as (4.90)-(4.91) with  $\varepsilon$ .
- Type 2.  $O(1)$ -wavelength in the initial data, i.e., we choose the initial data as

$$\begin{aligned}\psi(x, 0) &= \psi^{(0)}(x) = \operatorname{sech}(x+p)e^{-2i(x+p)} + \operatorname{sech}(x-p)e^{-2i(x-p)}, \quad (4.92) \\ \phi(x, 0) &= \phi^{(0)}(x), \quad \partial_t \psi(x, 0) = 0, \quad -\infty < x < \infty, \quad (4.93)\end{aligned}$$

where  $\phi^{(0)}$  satisfies

$$-\phi_{xx}^{(0)}(x) + \phi^{(0)}(x) = |\psi^{(0)}(x)|^2, \quad -\infty < x < \infty. \quad (4.94)$$

	Error	$k = \frac{1}{4}$	$k = \frac{1}{8}$	$k = \frac{1}{16}$	$k = \frac{1}{32}$	$k = \frac{1}{64}$
PSAS-TSSP	$e_1$	4.135E-1	7.965E-2	1.885E-2	4.694E-3	1.173E-3
	$e_2$	9.913E-2	2.287E-2	5.500E-3	1.364E-3	3.402E-4
CN-LF-TSSP ( $\beta = 0$ )	$e_1$	3.948E-1	7.120E-2	1.656E-2	4.117E-3	1.028E-3
	$e_2$	5.475E-2	1.246E-2	2.957E-3	7.322E-4	1.827e-4
CN-LF-TSSP ( $\beta = 1/4$ )	$e_1$	3.848E-1	5.956E-2	1.321E-2	3.272E-3	8.166E-4
	$e_2$	2.058E-1	5.011E-2	1.235E-2	3.079E-3	7.690E-4
CN-LF-TSSP ( $\beta = 1/2$ )	$e_1$	3.966E-1	5.948E-2	1.323E-2	3.283E-3	8.16E-4
	$e_2$	3.517E-1	8.874E-2	2.216E-2	5.541E-3	1.385E-3

Table 4.2: (cont'd): II. For  $\gamma = 0.5$  and  $h = 1/4$ .

	Time	e	$D$	$H$
PSAS-TSSP	1.0	1.690E-8	12.0000000	11.7286127
	2.0	2.672E-8	12.0000000	11.7286128
CN-LF-TSSP $\beta = 0$	1.0	6.556E-9	12.0000000	11.7286127
	2.0	2.211E-8	12.0000000	11.7286128
CN-LF-TSSP $\beta = 1/4$	1.0	2.163E-8	12.0000000	11.7286127
	2.0	4.342E-8	12.0000000	11.7286128
CN-LF-TSSP $\beta = 1/2$	1.0	2.473E-8	12.0000000	11.7286127
	2.0	4.815E-8	12.0000000	11.7286128

Table 4.3: Conserved quantities analysis:  $k = 0.0001$  and  $h = \frac{1}{8}$ .

We take  $p = 8$  in (4.92). Figure 4.1 shows the numerical results of PSAS-TSSP at  $t = 1$  when we choose the meshing strategy  $h = O(\varepsilon)$  and  $k = O(\varepsilon)$ :  $\Gamma_0 = (\varepsilon_0, h_0, k_0) = (0.125, 0.25, 0.04)$ ,  $\Gamma_0/4$ ,  $\Gamma_0/16$ ; and  $h = O(\varepsilon)$  and  $k = 0.04$ -independent of  $\varepsilon$ :  $\Gamma_0 = (\varepsilon_0, h_0) = (0.125, 0.25)$ ,  $\Gamma_0/4$ ,  $\Gamma_0/16$  for Type 1 initial data; and Figure 4.2 shows similar results for Type 2 initial data. In addition, CN-LF-TSSP with  $\beta = 1/4$  or  $1/2$  gives similar numerical results at the same meshing strategies.

From Tables 4.1-4.3 and Figures 4.1-4.2, we can draw the following observations:

(i) In  $O(1)$ -speed of light regime, i.e.,  $\varepsilon = O(1)$  fixed, our new numerical methods PSAS-TSSP and CN-LP-TSSP are of spectral-order accuracy in space discretization and second-order accuracy in time. Moreover, PSAS-TSSP and CN-LF-TSSP with  $\beta = 1/2$  or  $\beta = 1/4$  are unconditionally stable, where CN-LF-TSSP with  $\beta = 0$  is conditionally stable. Both numerical methods conserve the wave energy  $D$  exactly and the Hamiltonian  $H$  very well (up to 8 significant digits). Furthermore, these two methods are explicit, easy to program, less memory requirement, easy to extend to 2D & 3D cases, and keep most properties of KGS in the discretized level.

(ii) in the “nonrelativistic” limit regime, i.e.,  $0 < \varepsilon \ll 1$ , the  $\varepsilon$ -resolution of our numerical methods PSAS-TSSP and CN-LF-TSSP with  $\varepsilon = 1/4$  or  $1/2$  is  $h = O(\varepsilon)$  and  $k = O(\varepsilon)$  for  $O(\varepsilon)$ -wavelength, and resp.,  $h = O(1)$  and  $k = O(1)$  for  $O(1)$ -wavelength, initial data. The method CN-LF-TSSP with  $\beta = 0$  gives correct numerical results only at meshing strategy  $h = O(\varepsilon)$  and  $k = O(\varepsilon^2)$  for  $O(\varepsilon)$ -wavelength, and resp.,  $h = O(1)$  and  $k = O(\varepsilon)$  for  $O(1)$ -wavelength, initial data.

### 4.3.2 Application of our numerical methods

#### Plane wave solution of the standard KGS

**Example 4.2.** The standard KGS with a plane-wave solution, i.e., we choose  $d = 1$ ,  $\varepsilon = 1$ ,  $\nu = 0$  and  $\gamma = 0$  in (1.4)-(1.6) and consider the problem on the interval  $[a, b]$  with  $a = 0$  and  $b = 2\pi$ . The initial condition is taken as

$$\psi(x, 0) = \psi^{(0)}(x) = e^{i7x}, \quad \phi(x, 0) = \phi^{(0)}(x) = 1, \quad \phi_t(x, 0) = \phi^{(1)}(x) = 0. \quad (4.95)$$

It is easy to see that KGS (4.1)-(4.2) with periodic boundary conditions (4.3)-(4.4) and initial condition (4.95) admits the plane wave solution

$$\psi(x, t) = e^{i(7x-48t)}, \quad \phi(x, t) = 1, \quad a \leq x \leq b, \quad t \geq 0. \quad (4.96)$$

We solve this problem by using the PSAS-TSSP (4.25)-(4.26) with mesh size  $h = \frac{\pi}{8}$ , time step  $k = 0.001$ . Figure 4.3 shows the numerical results at  $t = 2$  and  $t = 4$ .

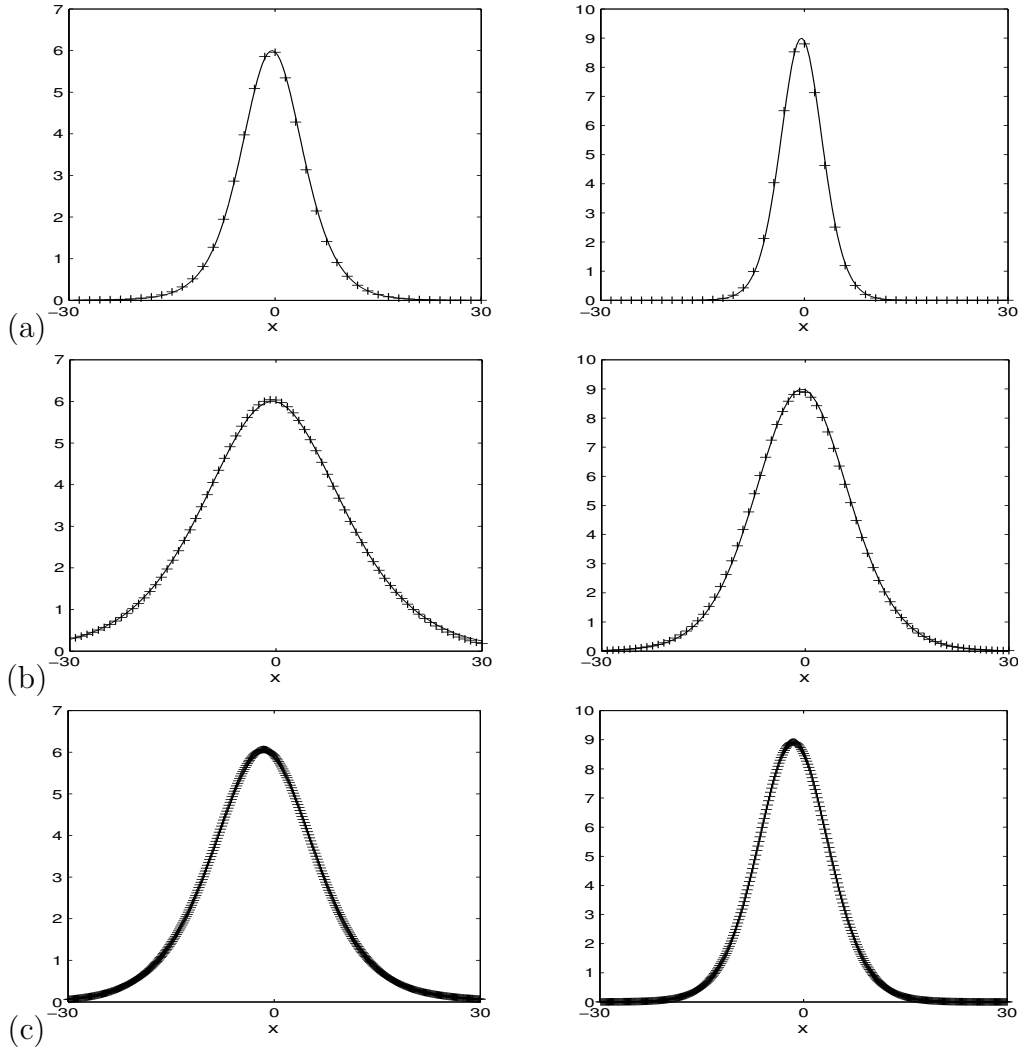


Figure 4.1: Numerical solutions of the meson field  $\phi$  (left column) and the nucleon density  $|\psi|^2$  (right column) at  $t = 1$  for Example 1 with Type 1 initial data in the “nonrelativistic” limit regime by PSAS-TSSP. ‘-’: exact solution given in (4.96), ‘+ + +’: numerical solution. I. With the meshing strategy  $h = O(\varepsilon)$  and  $k = O(\varepsilon)$ : (a)  $\Gamma_0 = (\varepsilon_0, h_0, k_0) = (0.125, 0.25, 0.04)$ , (b)  $\Gamma_0/4$ , and (c)  $\Gamma_0/16$ .

From Figure 4.3, we can see that the PSAS-TSSP method for KGS really provides the exact plane-wave solution of the KGS equations (4.1)-(4.5).

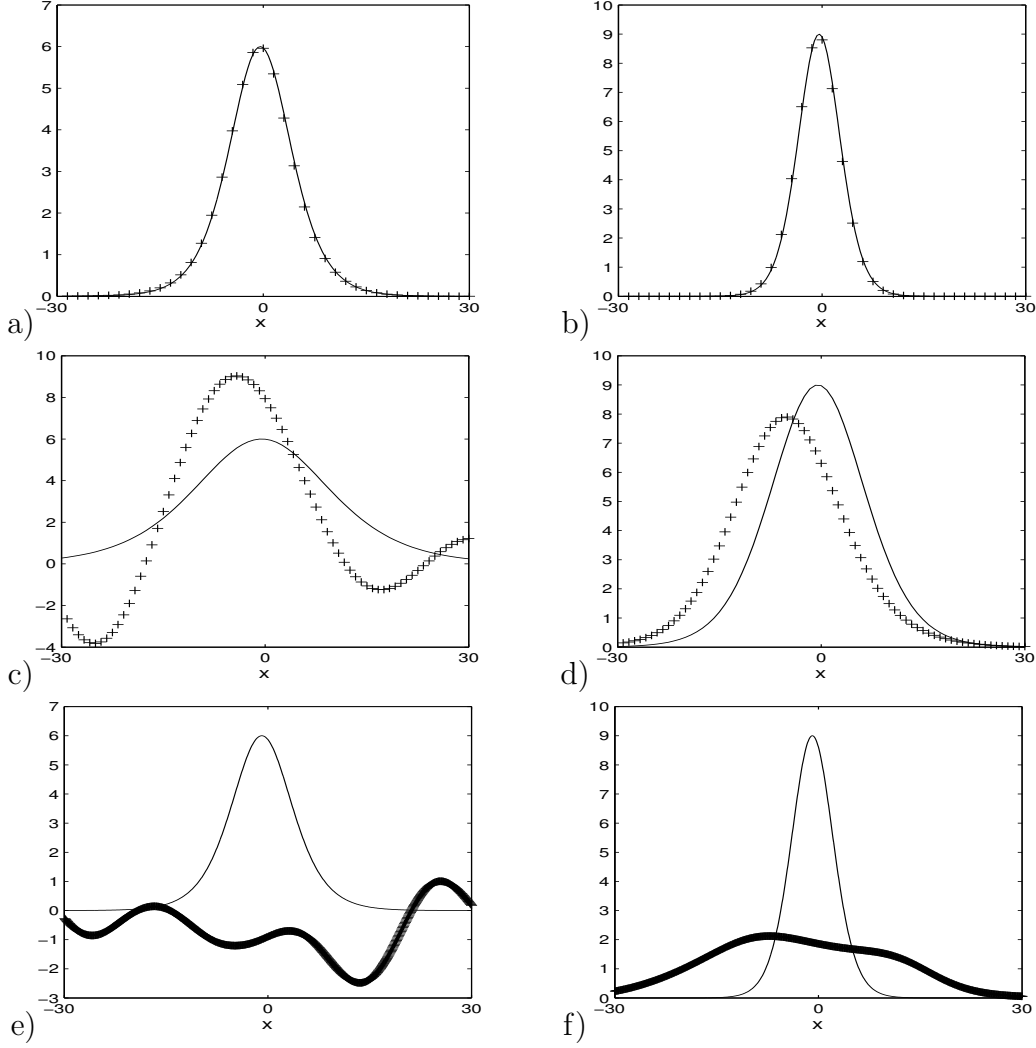


Figure 4.1: (cont'd): II. With the meshing strategy  $h = O(\varepsilon)$  and  $k = 0.04$ -independent of  $\varepsilon$ : (d)  $\Gamma_0 = (\varepsilon_0, h_0) = (0.125, 0.25)$ , (e)  $\Gamma_0/4$ , and (f)  $\Gamma_0/16$ .

### Soliton-Soliton collisions of standard KGS

**Example 4.3.** Interaction between solitary wave solutions in 1D for the standard KGS, i.e., we choose  $d = 1$ ,  $\varepsilon = 1$ ,  $\nu = 0$  and  $\gamma = 0$  in (1.4)-(1.6). The initial condition is chosen as

$$\psi(x, 0) = \psi_+(x + p, t = 0) + \psi_-(x - p, t = 0), \quad (4.97)$$

$$\phi(x, 0) = \phi_+(x + p, t = 0) + \phi_-(x - p, t = 0), \quad x \in \mathbb{R}, \quad (4.98)$$

$$\partial_t \phi(x, 0) = \partial_t \phi_+(x + p, t = 0) + \partial_t \phi_-(x - p, t = 0), \quad (4.99)$$

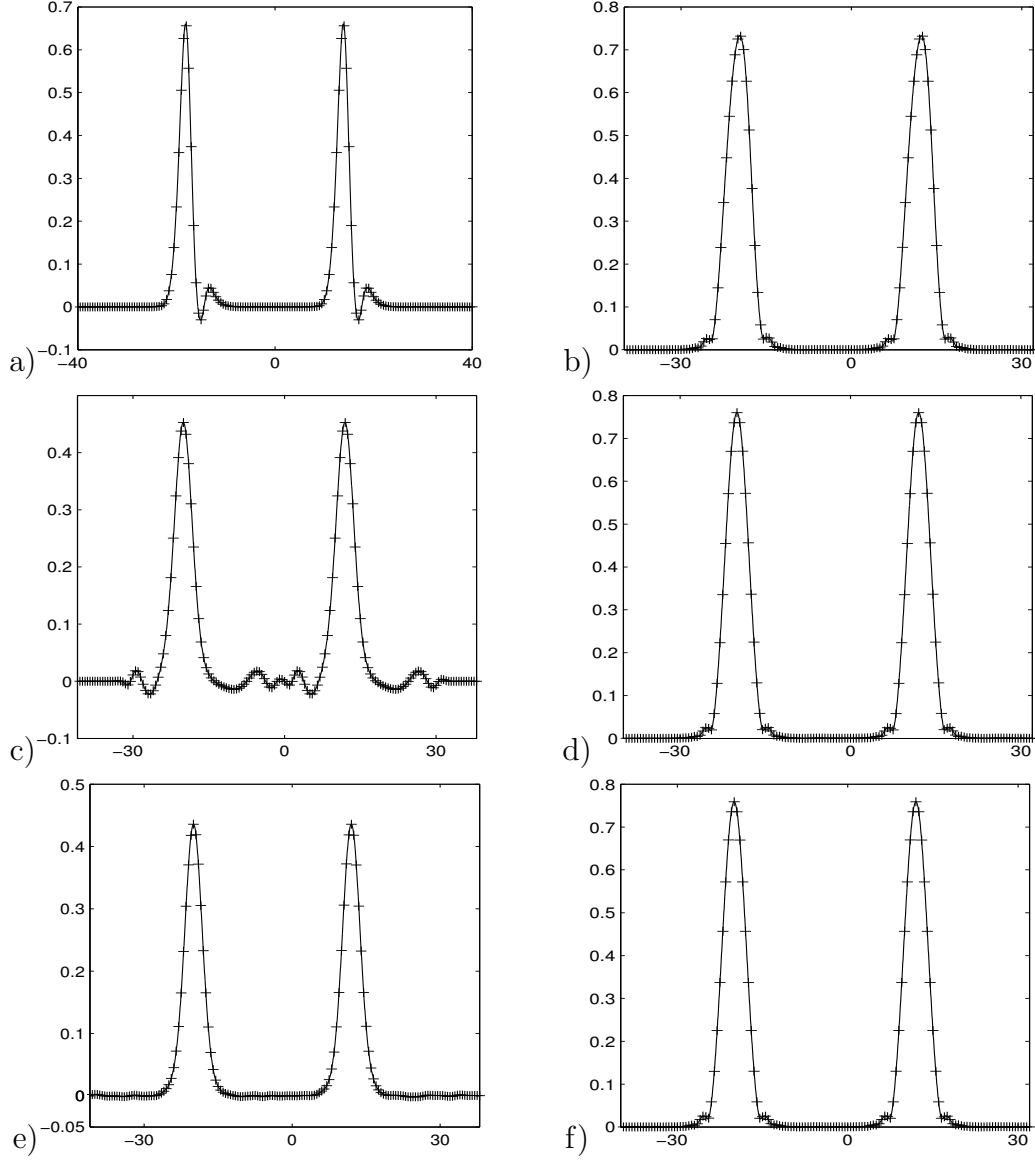


Figure 4.2: Numerical solutions of the density  $|\psi(x,t)|^2$  and the meson field  $\phi(x,t)$  at  $t = 1$  in the nonrelativistic limit regime by PSAS-TSSP with the same mesh ( $h = 1/2$  and  $k = 0.005$ ). '-': 'exact' solution, '+ + +': numerical solution. The left column corresponds to the meson field  $\phi(x,t)$ : (a)  $\varepsilon = 1/2$ , (c)  $\varepsilon = 1/16$ . (e)  $\varepsilon = 1/128$ . The right column corresponds to the density  $|\psi(x,t)|^2$ : (b)  $\varepsilon = 1/2$ , (d)  $\varepsilon = 1/16$ . (f)  $\varepsilon = 1/128$ .

where  $\psi_{\pm}$  and  $\phi_{\pm}$  are defined as in (3.41) and (3.42), and  $x = \pm p$  are initial locations of the two solitons.

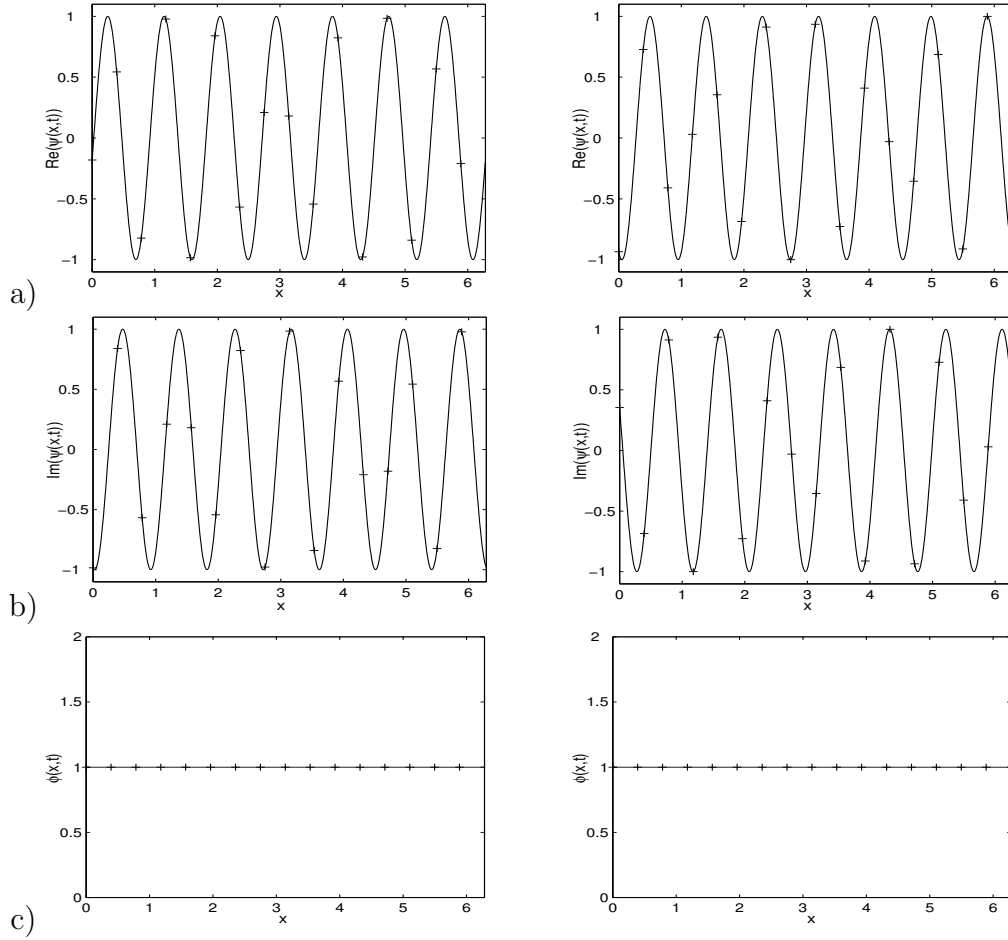


Figure 4.3: Numerical solutions for plane wave of KGS in Example 4.2 at time  $t = 2$  (left column) and  $t = 4$  (right column). '−': exact solution given in (4.96), '+ + +': numerical solution. (a): Real part of nucleon field  $Re(\psi(x, t))$ ; (b): imaginary part of nucleon field  $Im(\psi(x, t))$ ; (c): meson field  $\phi$ .

We solve the problem in the interval  $[-40, 40]$ , i.e.,  $a = -40$  and  $b = 40$  with mesh size  $h = 5/128$  and time step  $k = 0.001$  by using our method PSAS-TSSP, and take  $p = 8$  and  $B = 1$ . Figure 4.4 shows the values of  $|\psi(x, t)|$  and  $\phi(x, t)$  at different times. From Figure 4.4, the time  $t = 9.2$  corresponds to the time when the two solitons are at the same location and the time  $t = 18.5$  corresponds to the time when the collision is nearing completion (cf. Figure 4.4). From the figure we can see that during the collision, waves are emitted, and that after the collision the two

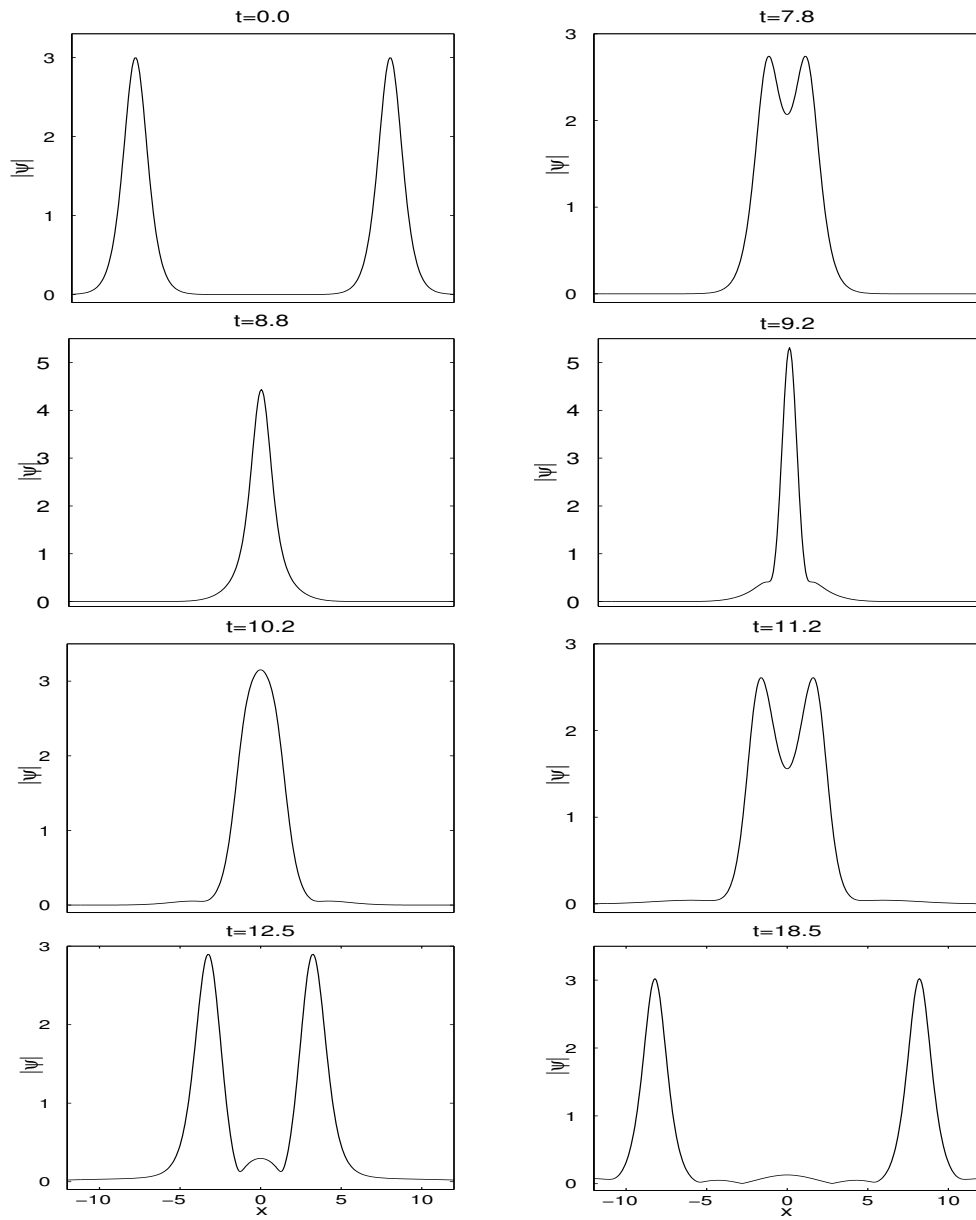
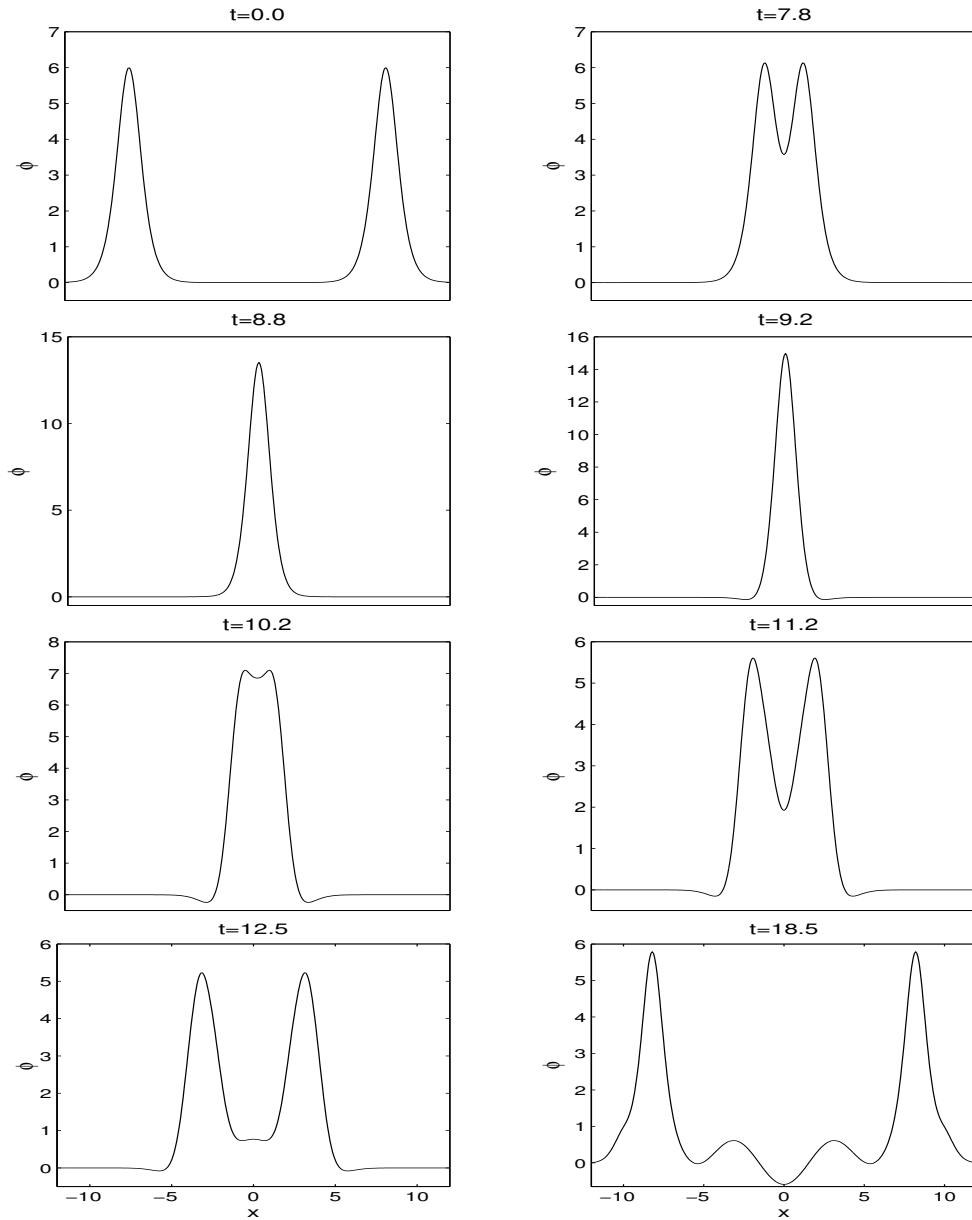


Figure 4.4: Numerical solutions of soliton-soliton collision in standard KGS in Example 4.3 I: Nucleon density  $|\psi(x, t)|$ .

solitons have a reduced peak value.

Figure 4.5: (cont'd): II. Meson field  $\phi(x, t)$ .

### Soliton-soliton collisions of KGS with damping term

**Example 4.4.** Soliton-soliton collision in 1D of KGS with damping term, i.e., we choose  $d = 1$ ,  $\varepsilon = 1$  and  $\nu = 0$  in (1.4)-(1.6). The initial condition is chosen as (4.97)-(4.98). Again, we solve the problem in the interval  $[-40, 40]$ , i.e.,  $a = -40$  and  $b = 40$  with mesh size  $h = 5/128$  and time step  $k = 0.001$  by using our method

PSAS-TSSP, and take  $p = 8$  and  $B = 1$ . Figure 4.6 displays time evolution of  $|\psi(x, t)|^2$  and  $\phi(x, t)$  for different values of  $\gamma$ . Figure 4.7 shows time evolution of the Hamiltonian  $H(t)$  and mean value of the meson field  $N(t)$  for different values of  $\gamma$ . From Figures 4.6-4.7, we can draw the following conclusions: (i) When  $\gamma = 0$ , the collision between two solitons seems quite elastic (cf. Figure 4.6 top row) although there are some waves are emitted; when  $\gamma > 0$  but small, damping effect can be observed in the collision and the emission of the sound waves is inconspicuous; when  $\gamma > 0$  and large, a soliton wave which is a bound state of the KGS is generated after the collision (cf. 4.6 3 last row). This observation seems new for the KGS. (ii). When  $\gamma = 0$ , the Hamiltonian is conserved; when  $\gamma > 0$ , it decreases when time increases and converges to a constant when time goes infity (cf. Figure 4.7 left). (iii) When  $\gamma = 0$ , the mean value of the meson field changes periodically; where it oscillates and decays when  $\gamma > 0$  (cf. Figure 4.7 right). These agree very well with the analytical results in section 2. (iv) The results here also demonstrate the efficiency and high resolution of our numerical method for studying soliton-soliton collision in KGS.

### Soliton-soliton collisions of KGS in “nonrelativistic limit” regime

**Example 4.5.** Soliton-soliton collision in 1D of KGS in “nonrelativistic limit” regime, i.e., we choose  $d = 1$ ,  $\gamma = 0$  and  $\nu = 0$  in (1.4)-(1.6). Let

$$\psi^{(0)}(x) = \operatorname{sech}(x + p)e^{-2i(x+p)} + \operatorname{sech}(x - p)e^{-2i(x-p)}, \quad (4.100)$$

$$\phi^{(0)}(x) = -|\operatorname{sech}(x + p)|^2 - |\operatorname{sech}(x - p)|^2, \quad x \in \mathbb{R}. \quad (4.101)$$

We solve the KGS (1.4)-(1.6) in one dimension with the initial conditions

$$\psi^{KGS}(x, 0) = \psi^{(0)}(x), \quad \phi^{KGS}(x, 0) = \phi^{(0)}(x), \quad \partial_t \phi^{KGS}(x, 0) = 0, \quad x \in \mathbb{R}, \quad (4.102)$$

in the interval  $[-128, 128]$ . We take  $p = 16.0$ . Figures 4.9-4.10 show that there are many oscillations when  $\varepsilon \rightarrow 0$ , which are quite different from the numerical results obtained by the different initial conditions (4.92)-(4.94).

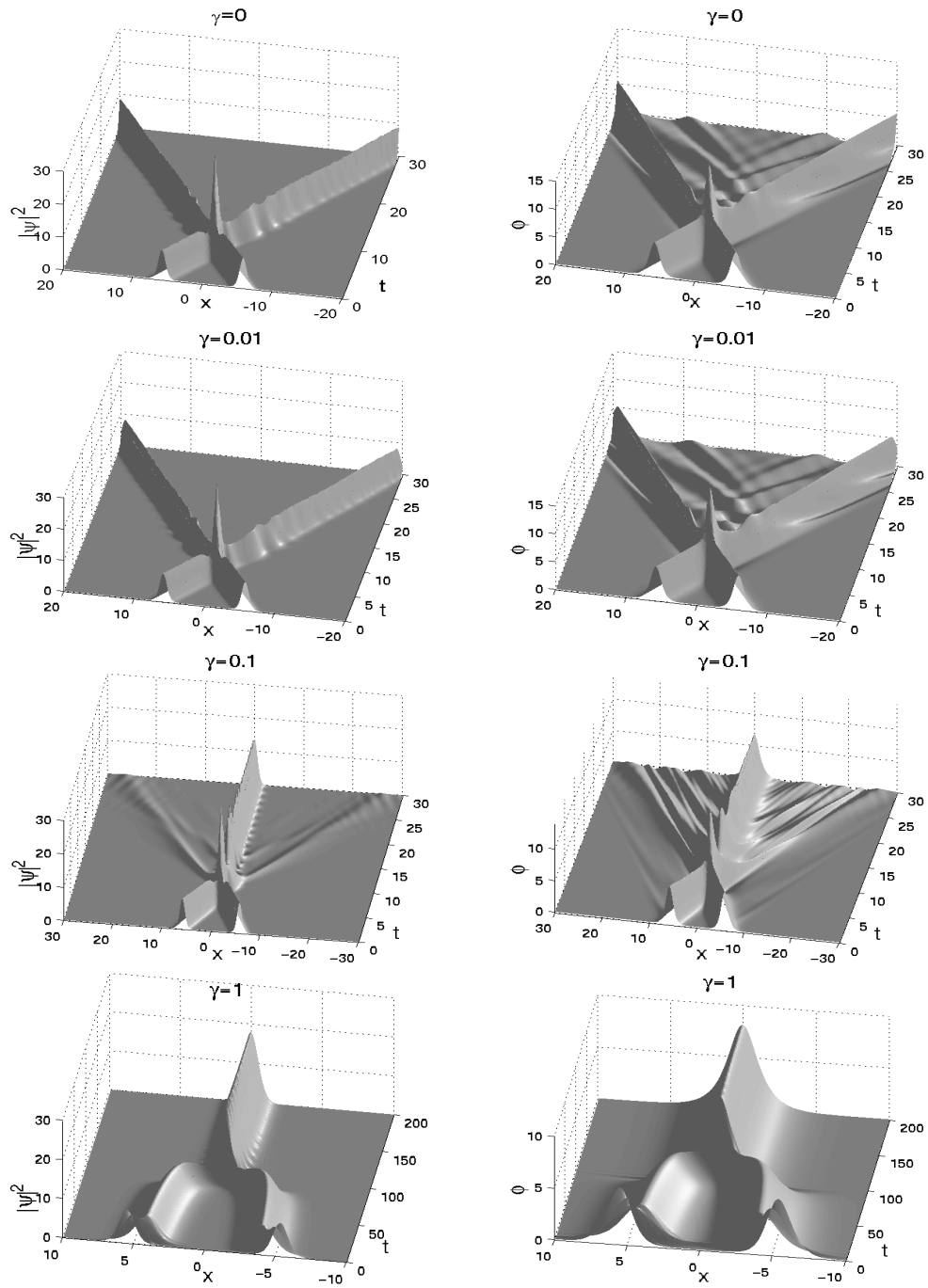


Figure 4.6: Time evolution of nucleon density  $|\psi(x,t)|^2$  (left column) and meson field  $\phi(x,t)$  (right column) for soliton-soliton collision of KGS in Example 4.4 for different values of  $\gamma$ .

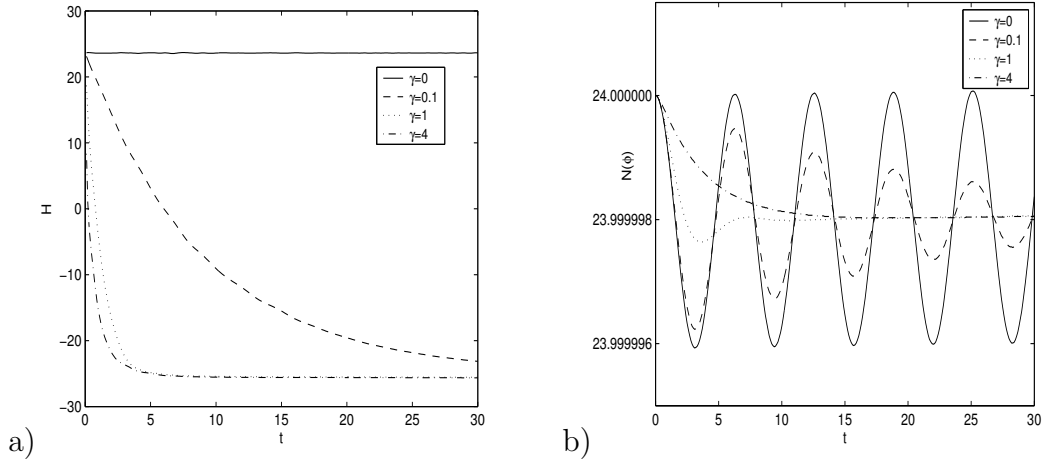


Figure 4.7: Time evolution of the Hamiltonian  $H(t)$  ('left') and mean value of the meson field  $N(t)$  ('right') in Example 4.4 for different values of  $\gamma$ .

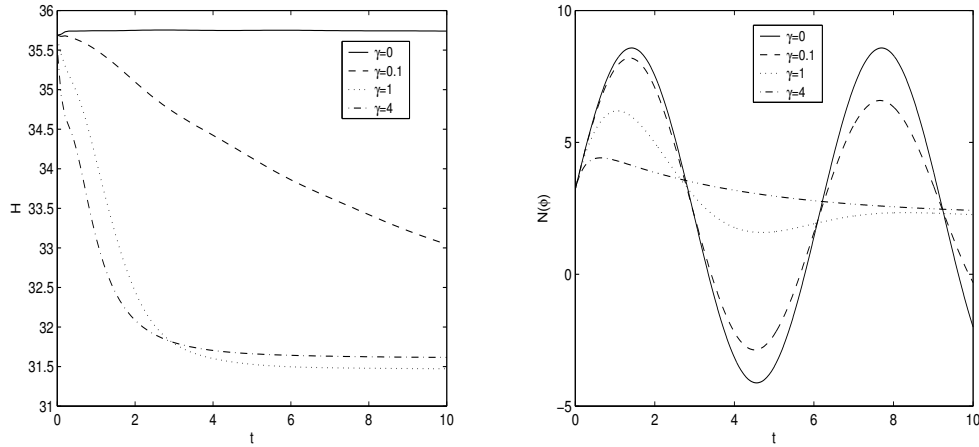


Figure 4.8: Time evolution of the Hamiltonian  $H(t)$  ('left') and mean value of the meson field  $N(t)$  ('right') in Example 4.6 for different values of  $\gamma$ .

### Solution of 2D standard KGS

**Example 4.6.** Dynamics of KGS in 2D, i.e., we choose  $d = 2$ ,  $\nu = 0$  and  $\varepsilon = 1$  in (1.4)-(1.6). The initial condition is taken as

$$\psi(x, y, 0) = \frac{2}{e^{x^2+2y^2} + e^{-(x^2+2y^2)}} e^{i5/\cosh(\sqrt{4x^2+y^2})},$$

$$\phi(x, y, 0) = e^{-(x^2+y^2)}, \quad \phi_t(x, y, 0) = \frac{e^{-(x^2+y^2)}}{2}, \quad (x, y) \in \mathbb{R}^2.$$

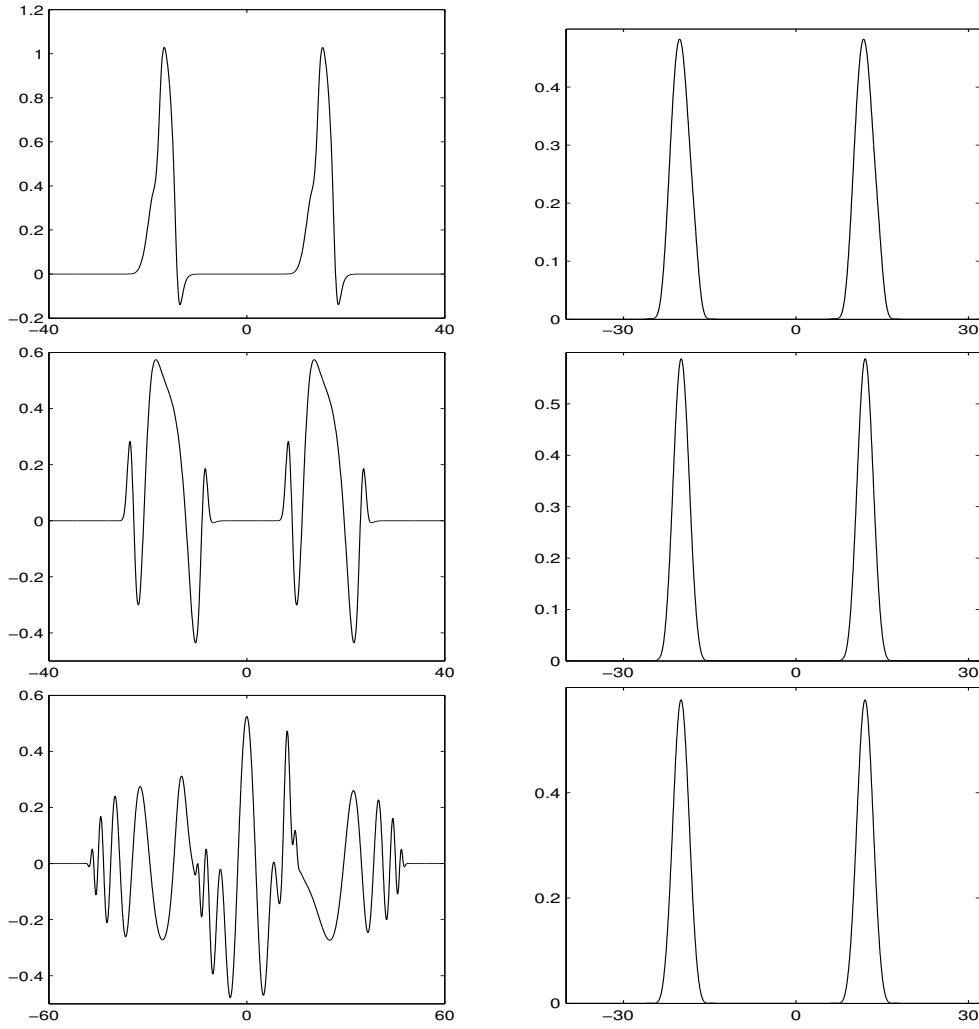


Figure 4.9: Numerical solutions of the nucleon density  $|\psi(x, y, t)|^2$  (right column) and meson field  $\phi(x, y, t)$  (left column) in Example 4.5 at  $t = 1$ . 1th row:  $\varepsilon = 1/2$ ; 2nd row:  $\varepsilon = 1/8$ ; 3rd row :  $\varepsilon = 1/32$ .

We solve this problem on the rectangle  $[-64, 64]^2$  with mesh size  $h = 1/16$  and time step  $k = 0.001$  by using our method PSAS-TSSP. Figure 4.11 shows the surface plots of  $\phi$  and  $|\psi|^2$  with  $\gamma = 0$  at different times. Figure 4.8 depicts time evolution of the Hamiltonian  $H(t)$  and mean value of the meson field  $N(t)$  for different values of  $\gamma$ .

From Figures 4.8-4.11, we can draw the following conclusions: (i). When  $\gamma = 0$ , the Hamiltonian is conserved; when  $\gamma > 0$ , it decreases when time increases and

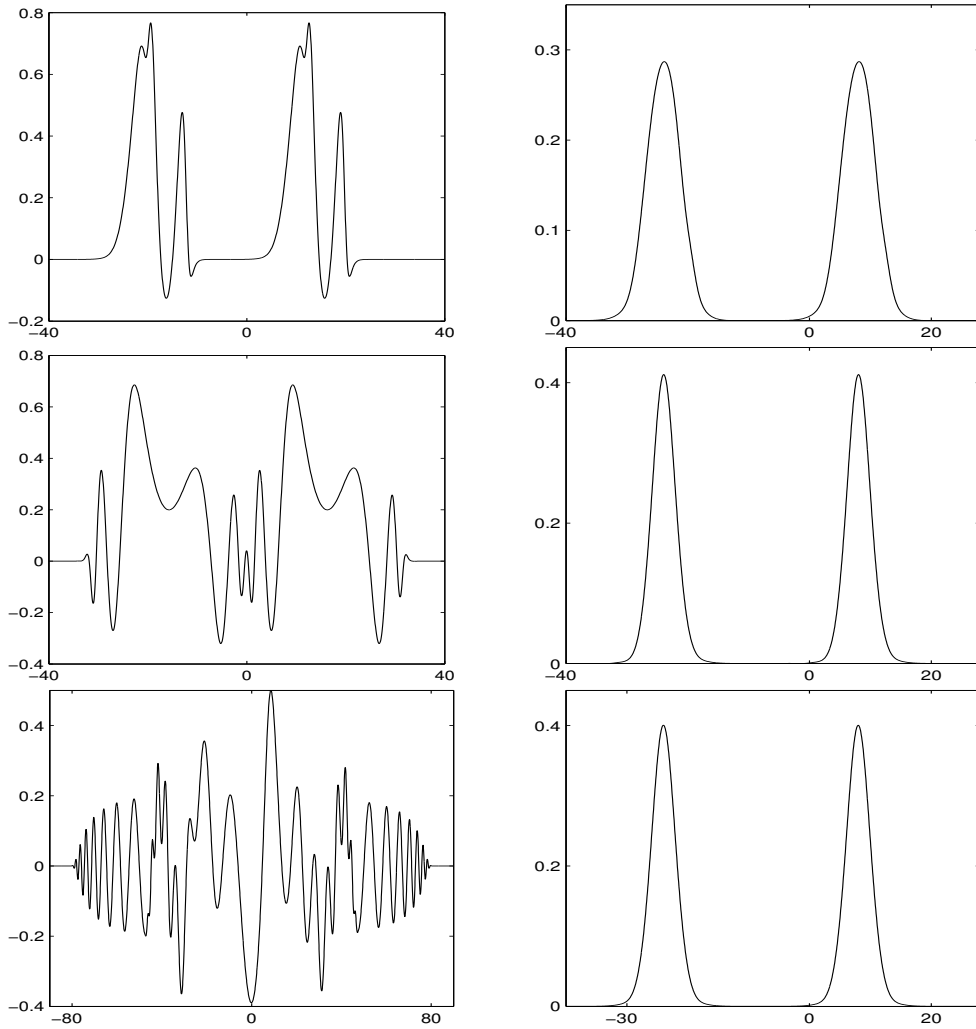


Figure 4.10: Numerical solutions of the nucleon density  $|\psi(x, y, t)|^2$  (right column) and meson field  $\phi(x, y, t)$  (left column) in Example 4.5 at  $t = 2$ . 1th row:  $\varepsilon = 1/2$ ; 2nd row:  $\varepsilon = 1/8$ ; 3rd row :  $\varepsilon = 1/32$ .

converges to a constant when time goes infinity (cf. Figure 4.8 left). (ii) When  $\gamma = 0$ , the mean value of the meson field changes periodically; where it oscillates and decays when  $\gamma > 0$  (cf. Figure 4.8 right). These agree very well with the analytical results in section 2. (iii) The results here also demonstrate the efficiency and high resolution of our numerical method for studying dynamics of KGS in 2D & 3D.

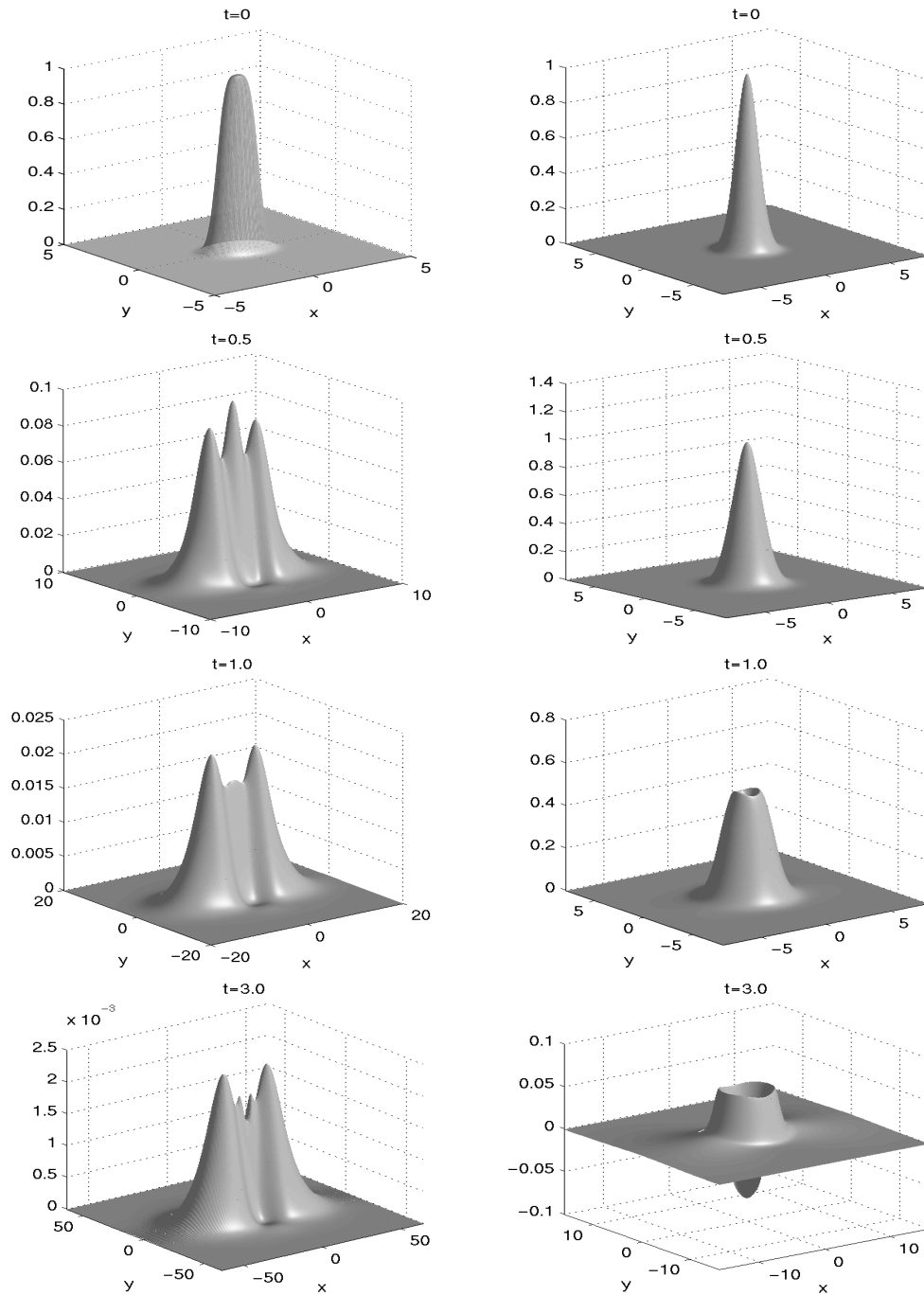


Figure 4.11: Surface plots of the nucleon density  $|\psi(x, y, t)|^2$  (left column) and meson field  $\phi(x, y, t)$  (right column) in Example 4.6 with  $\gamma = 0$  at different times.

# Application to the Schrödinger-Yukawa equations

In this chapter, we will extend our numerical method, time-splitting spectral method (TSSP) to the Schrödinger-Yukawa equations and also present the numerical results of the Schrödinger-Yukawa equations in 1D and 2D cases.

## 5.1 Introduction to the Schrödinger-Yukawa equations

The generalized Schrödinger-Yukawa equations are

$$i\eta\partial_t\psi = -\eta^2\theta\Delta\psi + C\phi\psi - \alpha|\psi|^{\frac{2}{d}}\psi - i\gamma\psi + V_{\text{ext}}\psi, \quad \mathbf{x} \in \mathbb{R}^d, \quad t > 0, \quad (5.1)$$

$$\Delta\phi = -|\psi|^2 + \beta\phi, \quad \mathbf{x} \in \mathbb{R}^d, \quad t > 0, \quad (5.2)$$

$$\psi(\mathbf{x}, 0) = \psi^{(0)}(\mathbf{x}), \quad \phi(\mathbf{x}, 0) = \phi^{(0)}(\mathbf{x}), \quad \mathbf{x} \in \mathbb{R}^d. \quad (5.3)$$

where  $\eta$  is the scaled Planck constant,  $C > 0$  is a fixed constant,  $\alpha > 0$ ,  $\theta$ ,  $\beta$  are real parameters and  $V_{\text{ext}}$  is a given external potential, for example a confining potential.

When  $\eta = 1$ ,  $\theta = \frac{1}{2}$ ,  $\alpha = 0$ ,  $V_{\text{ext}} = 0$ ,  $\beta = 0$ , we can get the well-known Schrödinger-Yukawa (S-Y) equations

$$i \partial_t \psi + \Delta \psi + \phi \psi + i \nu \psi = 0, \quad \mathbf{x} \in \mathbb{R}^d, \quad t > 0, \quad (5.4)$$

$$-\Delta \phi + \phi = |\psi|^2, \quad \mathbf{x} \in \mathbb{R}^d, \quad t > 0; \quad (5.5)$$

which can be also derived from (1.4) and (1.5) when  $\varepsilon \rightarrow 0$  (corresponding to infinite speed of light or ‘nonrelativistic’ limit regime).

When  $\theta = \frac{1}{2}$ ,  $\gamma = 0$ ,  $\beta = 0$ , the system of (5.1) and (5.2) reduces to the well-known Schrödinger-Poisson- $X\alpha$  (S-P- $X\alpha$ ) model, which has been firstly derived in [1, 13] as a local one particle approximation of the time dependent Hartree-Fock equations. It describes the time evolution of electrons in a quantum model respecting the Pauli principle in an approximate fashion. It reads

$$i \eta \partial_t \psi = -\frac{\eta^2}{2} \Delta \psi + C \phi \psi - \alpha |\psi|^{\frac{2}{a}} \psi + V_{\text{ext}} \psi, \quad \mathbf{x} \in \mathbb{R}^d, \quad t > 0, \quad (5.6)$$

$$\Delta \phi = -|\psi|^2, \quad \mathbf{x} \in \mathbb{R}^d, \quad t > 0. \quad (5.7)$$

It is an NLS with two nonlinear terms of different nature: the nonlocal Hartree potential and a local power term, with focusing sign and an exponent that is sub-critical for finite time blowup. Such “time dependent density functional theory” models yield approximations of the time-dependent Hartree-Fock (TDHF) equations that are much easier to solve numerically: firstly, for large number of particles  $N$  the system of coupled NLS of the TDHF system becomes too large, and secondly, the exchange terms are very costly to calculate.

## 5.2 Numerical method for the Schrödinger-Yukawa equations

For  $d = 1$ , the Schrödinger-Yukawa equations with periodic boundary conditions can be written as

$$i\eta\partial_t\psi = -\eta^2\theta\Delta\psi + C\phi\psi - \alpha|\psi|^2\psi - i\nu\psi + V_{\text{ext}}\psi, \quad a < x < b, t > 0 \quad (5.8)$$

$$\Delta\phi = -|\psi|^2 + \beta\phi, \quad a < x < b, \quad t > 0, \quad (5.9)$$

$$\psi(a, t) = \psi(b, t), \quad \partial_x\psi(a, t) = \partial_x\psi(b, t), \quad t \geq 0, \quad (5.10)$$

$$\phi(a, t) = \phi(b, t), \quad \partial_x\phi(a, t) = \partial_x\phi(b, t), \quad t \geq 0, \quad (5.11)$$

$$\psi(x, 0) = \psi^{(0)}(x), \quad \phi(x, 0) = \phi^{(0)}(x), \quad a \leq x \leq b. \quad (5.12)$$

The idea to construct the TSSP for the KGS (1.4)-(1.6) can be easily extended to the Schrödinger-Yukawa equations (5.1)-(5.2). The details of the numerical scheme are shown below. From time  $t = t_m$  to  $t = t_{m+1}$ , we use the Strang splitting formula:

$$\phi_j^{m+1} = \begin{cases} \frac{1}{M} \sum_{-M/2 \leq l \leq M/2-1} \frac{1}{\mu_l^2 + \beta} (\widetilde{|\psi^m|^2})_l e^{i\mu_l(x_j - a)}, & \beta \neq 0, \\ \frac{1}{M} \sum_{-M/2 \leq l \leq M/2-1, l \neq 0} \frac{1}{\mu_l^2 + \beta} (\widetilde{|\psi^m|^2})_l e^{i\mu_l(x_j - a)}, & \beta = 0, \end{cases} \quad (5.13)$$

$$j = 0, 1, 2, \dots, M-1. \quad (5.14)$$

$$\psi_j^* = \frac{1}{M} \sum_{l=-M/2}^{M/2-1} e^{-i\eta\mu_l^2 k/2} (\widetilde{\psi^m})_l e^{i\mu_l(x_j - a)}, \quad j = 0, 1, 2, \dots, M-1. \quad (5.15)$$

$$\psi^{**} = \begin{cases} e^{-i[C(\phi_j^m + \phi_j^{m+1})/2 + V_{\text{ext}}(x_j) + \alpha(e^{-2\nu k} - 1)|\psi_j^*|^2/2\nu - i\nu]k/\eta} \psi_j^*, & \nu \neq 0, \\ e^{-i[C(\phi_j^m + \phi_j^{m+1})/2 + V_{\text{ext}}(x_j) - \alpha|\psi_j^*|^2 - i\nu]k/\eta} \psi_j^*, & \nu = 0, \end{cases} \quad (5.16)$$

$$j = 0, 1, 2, \dots, M-1. \quad (5.17)$$

$$\psi_j^{n+1} = \frac{1}{M} \sum_{l=-M/2}^{M/2-1} e^{i\eta\mu_l^2 k/2} (\widetilde{\psi^{**}})_l e^{i\mu_l(x_j - a)}, \quad j = 0, 1, 2, \dots, M-1; \quad (5.18)$$

where  $\widetilde{U}_l$  ( $l = -M/2, \dots, M/2 - 1$ ), the Fourier coefficients of a vector  $U = (U_0, U_1, \dots, U_M)^T$  with  $U_0 = U_M$ , are defined as

$$\mu_l = \frac{2\pi l}{b-a}, \quad \widetilde{U}_l = \sum_{j=0}^{M-1} U_j e^{-i\mu_l(x_j - a)}, \quad l = -\frac{M}{2}, \dots, \frac{M}{2} - 1. \quad (5.19)$$

## 5.3 Numerical results of the Schrödinger-Yukawa equations

In this section, we study the convergence of KGS to S-Y in the "nonrelativistic limit" ( $0 < \varepsilon \ll 1$ ), where the parameter  $\varepsilon$  is inversely proportional to the acoustic speed. We also present the numerical solution of the Schrödinger-Yukawa equations in the 1D case.

### 5.3.1 Convergence of KGS to S-Y in "nonrelativistic limit" regime

**Example 5.1.** Reduction from the Klein-Gordon-Schrödinger equations to the Schrödinger-Yukawa equations, i.e., we choose  $d = 1$ ,  $\nu = 0$  and  $\gamma = 0$  in (1.4)-(1.6). Let

$$\psi^{(0)}(x) = \operatorname{sech}(x+p)e^{-2i(x+p)} + \operatorname{sech}(x-p)e^{-2i(x-p)}, \quad (5.20)$$

and  $\phi^{(0)}(x)$  satisfies

$$-\phi_{xx}^{(0)}(x) + \phi^{(0)}(x) = -|\psi^{(0)}(x)|^2. \quad (5.21)$$

We solve the KGS (1.4)-(1.6) in one dimension with the initial conditions

$$\psi^{\text{KGS}}(x, 0) = \psi^{(0)}(x), \quad \phi^{\text{KGS}}(x, 0) = \phi^{(0)}(x), \quad \partial_t \phi^{\text{KGS}}(x, 0) = 0, \quad x \in \mathbb{R}, \quad (5.22)$$

and the S-Y (5.1)-(5.2) in one dimension with the initial condition

$$\psi^{\text{SY}}(x, 0) = \psi^{(0)}(x). \quad (5.23)$$

in the interval  $[-80, 80]$  with mesh size  $h = 5/128$  and time step  $k = 0.00005$ . We take  $p = 8$ . Let  $\psi^{\text{KGS}}$  and  $\phi^{\text{KGS}}$  be the numerical solutions of the KGS (1.4)-(1.6),  $\psi^{\text{SY}}$  and  $\phi^{\text{SY}}$  be of the S-Y (5.1)-(5.2) by using PSAS-TSSP and TSSP respectively. Table 5.1 shows the errors between the solutions of the KGS and its reduction S-Y at time  $t = 1.0$  under different  $\varepsilon$ .

	$\varepsilon = 1/4$	$\varepsilon/2$	$\varepsilon/4$	$\varepsilon/8$
$\ \phi^{\text{KGS}} - \phi^{\text{SY}}\ _{l^2}$	0.357	3.26E-2	7.762E-3	1.809E-3
$\ \psi^{\text{KGS}} - \psi^{\text{SY}}\ _{l^2}$	3.261E-2	7.597E-3	1.399E-3	3.373E-4
$ H^{\text{KGS}} - H^{\text{SY}} $	0.165	3.314E-2	8.721E-3	2.492E-3

Table 5.1: Error analysis between KGS and its reduction S-Y: Errors are computed at time  $t = 1$  under  $h = 5/128$  and  $k = 0.00005$ .

From Table 5.1, we can see that the meson field  $\phi^{\text{KGS}}$ , nucleon density  $|\psi^{\text{KGS}}|^2$ , and the Hamiltonian  $H^{\text{KGS}}$  of the KGS (1.4)-(1.6) converge to  $\phi^{\text{SY}}$  in  $l^2$ -norm,  $\psi^{\text{SY}}$  in  $l^2$ -norm,  $H^{\text{SY}}$  of the Schrödinger-Yukawa equations (5.1)-(5.2) quadratically when  $\varepsilon \rightarrow 0$ .

### 5.3.2 Applications

**Example 5.2.** 1-D S-P-X $\alpha$  model, i.e., we choose  $d = 1$ ,  $\varepsilon = 1$ ,  $\theta = 1/2$ ,  $V_{\text{ext}} \equiv 0$  and  $C = 1$  in (5.1)-(5.2). Note that the local interaction term in (5.1) is the “focusing cubic NLS interaction” in the case  $d = 1$ . The initial condition is hence taken the same as in the simulations of [55]

$$\psi(x, t = 0) = A_I(x)e^{iS_I(x)/\varepsilon}, \quad x \in \mathbb{R}, \quad (5.24)$$

where  $A_I(x) = e^{-x^2}$ ,  $(S_I(x))_x = -\tanh(x)$ . Note that  $S_I$  is such that the initial phase is “compressive”. This means that even the linear evolution develops caustics in finite time. We solve this problem either on the interval  $x \in [-4, 4]$  or on  $x \in [-8, 8]$  depending on the time for which the solution is calculated.

We present numerical results for four different regimes of  $\alpha$ :

Case I.  $\alpha = 0$ , i.e., Schrödinger-Poisson regime;

Case II.  $\alpha = \varepsilon$ , i.e., Schrödinger-Poisson equation with  $O(\varepsilon)$  cubic nonlinearity;

Case III.  $\alpha = \sqrt{\varepsilon}$ , i.e., Schrödinger-Poisson equation with  $O(\sqrt{\varepsilon})$  cubic nonlinearity;

Case IV.  $\alpha = 1$ , i.e., Schrödinger-Poisson equation with  $O(1)$  cubic nonlinearity.

Figure 5.1 displays comparisons of the position density  $n(x, t) = |\psi(x, t)|^2$  at fixed time for the above different parameter regimes with different  $\varepsilon$ . Figure 5.2 plots the evolution of the position density of the wave function for  $\alpha = 1$  and  $\varepsilon = 0.025$ . Figure 5.3 shows the analogous results for the attractive Hartree integration, i.e.,  $C = -1$ ,  $\alpha = 0.5$  and  $\varepsilon = 0.025$ .

From Figure 5.1, we can see that before the break (part a) and b)), the result is essentially independent of  $\varepsilon$ . After the break the behavior of the position density  $n(x, t)$  changes substantially with respect to the different regimes of  $\alpha$ . For  $\alpha = 0$  the solution stays smooth. For  $\alpha = \varepsilon$  it also stays smooth, but it concentrates at the origin. For  $\alpha = \sqrt{\varepsilon}$  a pronounced structure of peaks develop, they look like the soliton structure typical for the NLS [43]. The number of peaks is doubled when  $\varepsilon$  is halved. For  $\alpha = 1$ , the number of peaks increases again and they occur at different locations than that for  $\alpha = \sqrt{\varepsilon}$ .

We can see that the scaling  $\alpha = O(\sqrt{\varepsilon})$  is critical in the sense that the solution has a substantially behavior than for the smaller scales of  $\alpha$ . Beyond this scaling, the semiclassical limit can not be obtained by naive numerics.

Figure 5.3 is a test to see what happens if the Hartree potential is attractive instead of repulsive, with all other parameters kept the same, i.e., Figure 5.2 and Figure 5.3 differ only by the sign of  $C$ . The resulting effect corresponds to the physical intuition that the pattern of caustics that is typical for focusing NLS would be enhanced and focused in physical space by an additional attractive force.

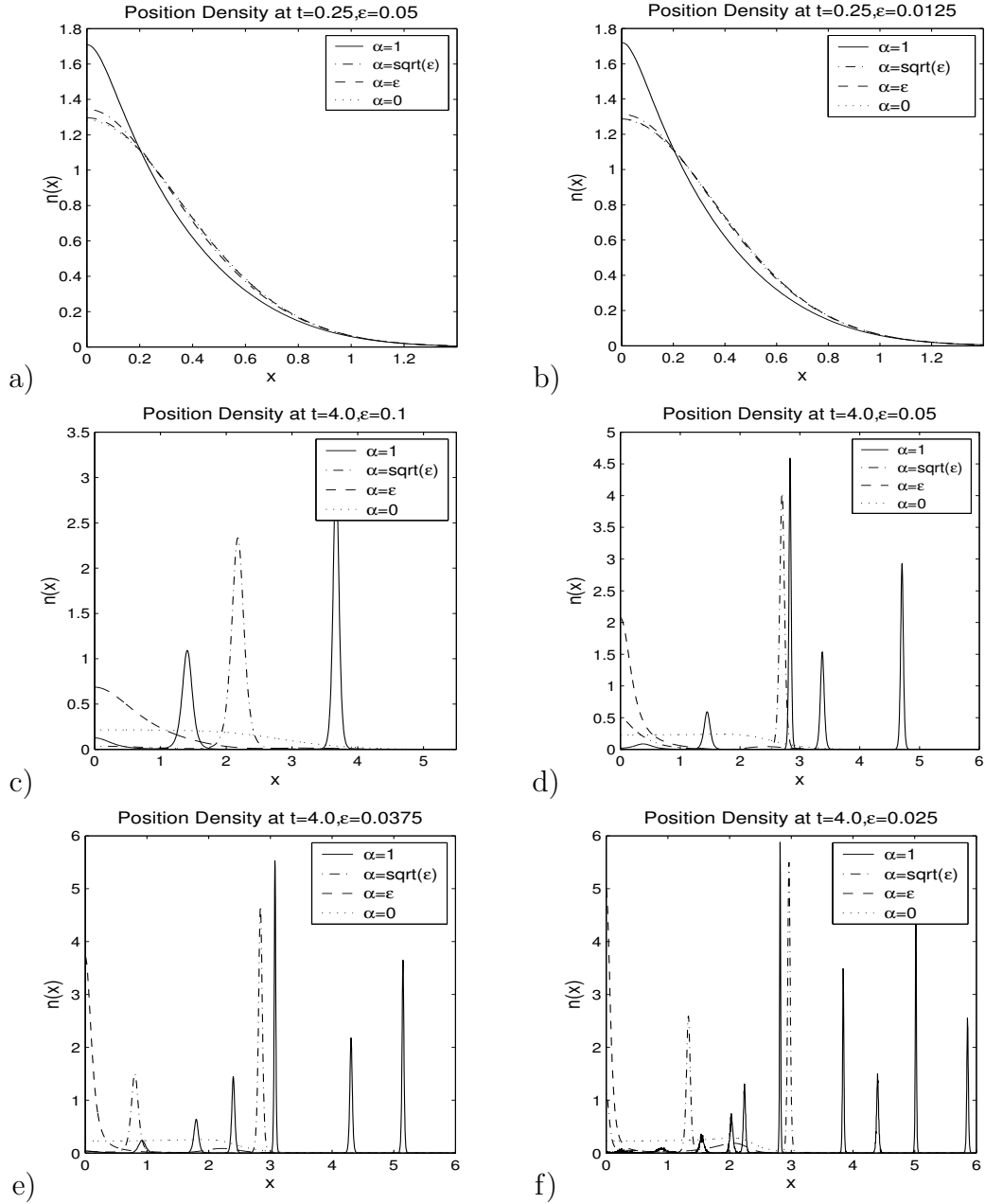


Figure 5.1: Numerical results for different scales of the  $X\alpha$  term in Example 5.2, i.e.,  $\alpha = 1, \sqrt{\epsilon}, \epsilon, 0$ . a) and b) : small time  $t = 0.25$ , pre-break, a) for  $\epsilon = 0.05$ , b) for  $\epsilon = 0.0125$ . c)-f): large time,  $t = 4.0$ , post-break. c) for  $\epsilon = 0.1$ , d) for  $\epsilon = 0.05$ , e) for  $\epsilon = 0.0375$ , f)  $\epsilon = 0.025$ .

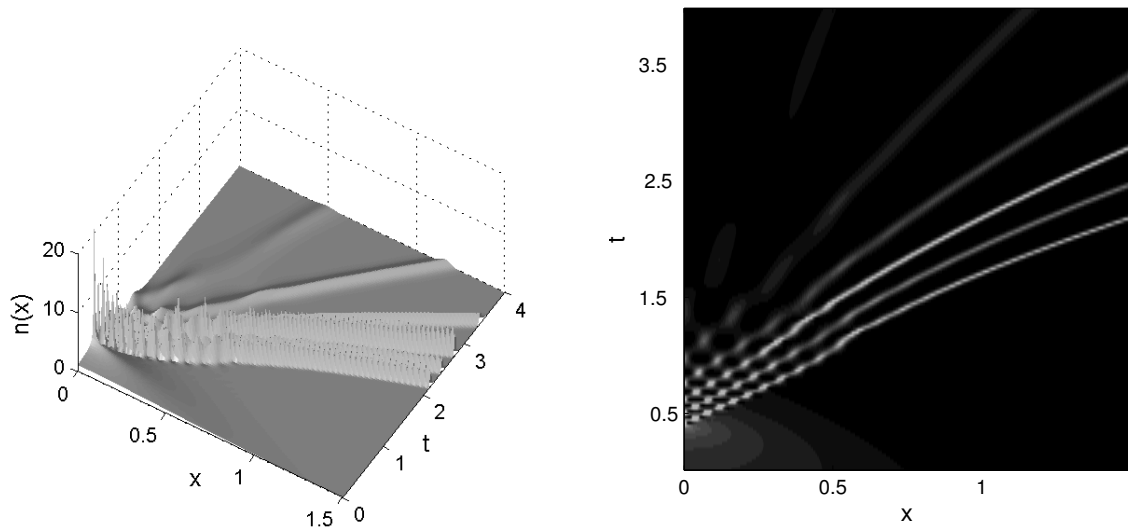


Figure 5.2: Time evolution of the position density for  $X\alpha$  term at  $O(1)$  in Example 5.2, i.e.,  $\alpha = 0.5$ , with  $\varepsilon = 0.025$ ,  $h = 1/512$  and  $k = 0.0005$ . a) surface plot; b) pseudocolor plot.

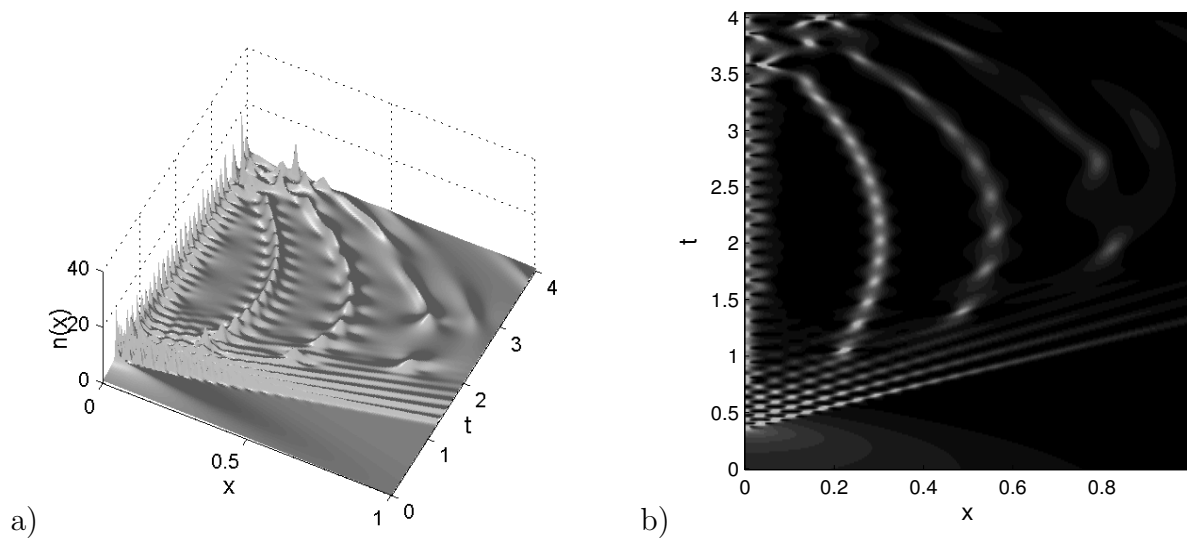


Figure 5.3: Time evolution of the position density for attractive Hartree interaction in Example 5.2.  $C = -1$ ,  $\alpha = 0.5$ ,  $\varepsilon = 0.025$ ,  $k = 0.00015$ . a) surface plot; b) pseudocolor plot.

# Chapter 6

## Conclusion

We began with the derivation of the Klein-Gordon equation (KG) which describes scalar (or pseudoscalar) spinless particles and analyzed its properties and presented Crank-Nicolson leap-frog spectral method (CN-LF-SP) for numerical discretization of the nonlinear Klein-Gordon equation. Numerical results for the Klein-Gordon equation demonstrated that the method is of spectral-order accuracy in space and second-order accuracy in time and it is much better than the other numerical methods proposed in the literature. It also preserves the system energy, linear momentum and angular momentum very well in the discretized level.

We continued with the derivation of the Klein-Gordon-Schrödinger equations (KGS) which describes a system of conserved scalar nucleons interacting with neutral scalar mesons coupled through the Yukawa interaction and analyzed its properties. Two new and efficient numerical methods are proposed for numerical discretization of the Klein-Gordon-Schrödinger equations. They are phase space analytical solver+time-splitting spectral method (PSAS-TSSP) and Crank-Nicolson leap-frog time-splitting spectral method (CN-LF-TSSP). These methods are explicit, unconditionally stable, of spectral accuracy in space and second order accuracy in time, easy to extend to high dimensions, easy to program, less memory-demanding, and time reversible and time transverse invariant. Furthermore, they conserve (or keep the same decay

rate of) the wave energy in KGS when there is no damping (or a linear damping) term, give exact results for plane-wave solutions of KGS, and keep the same dynamics of the mean value of the meson field in discretized level. We also applied our new numerical methods to study numerically soliton-soliton interaction of KGS in 1D and dynamics of KGS in 2D. We numerically found that, when a large damping term is added to the Klein-Gordon equation, bound state of KGS can be obtained from the dynamics of KGS when time goes to infinity.

Finally, we extended our numerical method, time-splitting spectral method (TSSP) to the Schrödinger-Yukawa equations and presented the numerical results of the Schrödinger-Yukawa equations in 1D and 2D cases.

---

## Bibliography

---

- [1] M.J. Ablowitz and P.A. Clarkson, Solitons, nonlinear evolution equations and inverse scattering, Cambridge University Press, London, 1991.
- [2] M.J. Ablowitz, B.M. Herbst and C. Schober, On the numerical solution of the sine-Gordon equation, *J. Comput. Phys.*, 126 (1996), pp. 299-314.
- [3] M.J. Ablowitz, M.D. Kruskal and J.F. Ladik, Solitary wave collisions, *SIAM J. Appl. Math.*, 36 (1979), pp. 428-437.
- [4] J. Argyris, M. Haase and J.C. Heinrich, Finite element approximation to two-dimensional sine-Gordon solitons, *Comput. Methods Appl. Mech. Eng.*, 86 (1991), pp. 1-26.
- [5] W. Bao and D. Jaksch, An explicit unconditionally stable numerical method for solving damped nonlinear Schrödinger equations with a focusing nonlinearity, *SIAM J. Numer. Anal.*, 41 (2003), pp. 1406-1426.
- [6] W. Bao, D. Jaksch and P.A. Markowich, Numerical solution of the Gross-Pitaevskii equation for Bose-Einstein condensation, *J. Comput. Phys.*, 187 (2003), pp. 318-342.

- 
- [7] W. Bao, D. Jaksch and P.A. Markowich, Three Dimensional Simulation of Jet Formation in Collapsing Condensates, *J. Phys. B: At. Mol. Opt. Phys.*, 37 (2004), pp. 329-343.
- [8] W. Bao, S. Jin and P.A. Markowich, On time-splitting spectral approximations for the Schrödinger equation in the semiclassical regime, *J. Comput. Phys.*, 175 (2002), pp. 487-524.
- [9] W. Bao, S. Jin and P.A. Markowich, Numerical study of time-splitting spectral discretizations of nonlinear Schrödinger equations in the semiclassical regimes, *SIAM J. Sci. Comput.*, 25 (2003), pp. 27-64.
- [10] W. Bao and X.G. Li, An efficient and stable numerical method for the Maxwell-Dirac system, *J. Comput. Phys.*, 199 (2004), pp. 663-687.
- [11] W. Bao, F.F. Sun and G.W. Wei, Numerical methods for the generalized Zakharov system, *J. Comput. Phys.*, 190 (2003), pp. 201-228.
- [12] W. Bao and F.F. Sun, Efficient and stable numerical methods for the generalized and vector Zakharov system, *SIAM J. Sci. Comput.*, 26 (2005), pp. 1057-1088.
- [13] C. Bardos, F. Golse and N.J. Mauser, Weak coupling limit of the N-particle Schrödinger equation, *Math. Analysis and Application*, 7 (2000), pp. 275-293.
- [14] A. Barone, F. Esposito, C.J. Magee and A.C. Scott, Theory and applications of the sine-Gordon equation, *Riv. Nuovo Cimento*, 1 (1971), pp. 227-267.
- [15] P. Bechouche, N.J. Mauser and S. Selberg, Non-relativistic limit of Klein-Gordon-Maxwell, *American J. of Math.*, 126 (2004), pp. 31-64.
- [16] P. Bechouche, N.J. Mauser and S. Selberg, Nonrelativistic limit of Klein-Gordon-Maxwell to Schrödinger-Poisson, preprint.

- 
- [17] P. Biler, Attractors for the system of Schrödinger and Klein-Gordon equations with Yukawa coupling, *SIAM J. Math. Anal.*, 21 (1990), pp. 1190-1212.
- [18] J.G. Caputo, N. Flytzanis and Y. Gaididei, Split mode method for the elliptic 2D sine-Gordon equation: application to Josephson junction in overlap geometry, *Int. J. Mod. Phys. C*, 9 (1998), pp. 301-323.
- [19] P.L. Christiansen and P.S. Lomdahl, Numerical study of 2+1 dimensional sine-Gordon solitons, *Physica D*, 2 (1981), pp. 482-494.
- [20] R.J. Cirincione and P.R. Chernoff, Dirac and Klein-Gordon equations: convergence of solutions in the nonrelativistic limit, *Commun. Math. Phys.*, 79 (1981), pp. 33-46.
- [21] C. Dariescu and M.A. Dariescu, Transition and regeneration rates in charged boson stars via perturbative calculations, *Int. Journal of Modern Phy. A*, 20 (2005), pp. 2326-2330.
- [22] A. Darwish and E.G. Fan, A series of new explicit exact solutions for the coupled Klein-Gordon-Schrödinger equations, *Chaos, Solitons & Fractals*, 20 (2004), pp. 609-617.
- [23] R.F. Dashen, B. Hasslacher and A. Neveu, Nonperturbative methods and extended hadron models in field theory II. Two-dimensional model and extended hadrons, *Phys. Rev. D*, 10 (1974), pp. 4130-4138.
- [24] K. Djidjeli, W.G. Price and E.H. Twizell, Numerical solutions of a damped sine-Gordon equation in two space variables, *J. Eng. Math.*, 29 (1995), pp. 347-369.
- [25] R.K. Dodd, J.C. Eilbeck, J.D. Gibbon and H.C. Morris, *Solitons and nonlinear wave equations*, Academic Press, London, 1982.
- [26] B. Fornberg and T.A. Driscoll, A fast spectral algorithm for nonlinear wave equations with linear dispersion, *J. Comput. Phys.* 155 (1999), pp. 456-467.

- 
- [27] F. Fucito, F. Marchesoni, E. Marinari, G. Parisi, L. Peliti, S. Ruffo and A. Vulpiani, Approach to equilibrium in a chain of nonlinear oscillators, *J. Physique*, 43 (1982), pp. 707-713.
- [28] I. Fukuda and M. Tsutsumi, On the Yukawa-coupled Klein-Gordon-Schrödinger equations in three space dimensions, *Proc. Japan Acad.*, 51 (1975), pp. 402-405.
- [29] I. Fukuda and M. Tsutsumi, On coupled Klein-Gordon-Schrödinger equations II, *J. Math. Anal. Appl.*, 66 (1978), pp. 358-378.
- [30] I. Fukuda and M. Tsutsumi, On coupled Klein-Gordon-Schrödinger equations III, *Math. Japan*, 24 (1979), pp. 307-321.
- [31] J.D. Gibbon, I.N. James and I.M. Moroz, The sine-Gordon equation as a model for a rapidly rotating baroclinic fluid, *Phys. Scripta*, 20 (1979), pp. 402-408.
- [32] J. Ginibre and G. Velo, The global Cauchy problem for the nonlinear Klein-Gordon equation, *Math. Z.*, 189 (1985), pp. 487-505.
- [33] B.L. Guo, Global solution for some problem of a class of equations in interaction of complex Schrödinger field and real Klein-Gordon field, *Sci. China Ser. A*, 25 (1982), pp. 97-107.
- [34] B.L. Guo and C.X. Miao, Asymptotic behavior of coupled Klein-Gordon-Schrödinger equations, *Sci. China Ser. A*, 25 (1995), pp. 705-714.
- [35] B.L. Guo and Y.S. Li, Attractor for dissipative Klein-Gordon-Schrödinger equations in  $R^3$ , *J. Diff. Eq.*, 136 (1997), pp. 356-377.
- [36] B.Y. Guo, X. Li and L. Vazquez, A Legendre spectral method for solving the nonlinear Klein-Gordon equation, *Comput. Appl. Math.*, 15 (1996), pp. 19-36.
- [37] N. Hayashi and W. von Wahl, On the global strong solutions of coupled Klein-Gordon-Schrödinger equations, *J. Math. Soc. Jpn.*, 39 (1987), pp. 489-497.

- 
- [38] F.T. Hioe, Periodic solitary waves for two coupled nonlinear Klein-Gordon and Schrödinger equations, *J. Phys. A: Math. Gen.*, 36 (2003), pp. 7307-7330.
- [39] Z. Huang, S. Jin, P.A. Markowich, C. Sparber and C. Zheng, A time-splitting spectral scheme for the Maxwell-Dirac system, *J. Comput. Phys.*, 208 (2005), pp. 761–789.
- [40] S. Jiménez and L. Vázquez, Analysis of four numerical schemes for a nonlinear Klein-Gordon equation, *App. Math. Comput.*, 35 (1990), pp. 61-94.
- [41] S. Jiménez, Comportamiento de Ciertas Cadenas de Osciladores No Lineales, Ph.D. Thesis, Univ. Complutense de Madrid, Spain, 1988.
- [42] S. Jin, P.A. Markowich and C. Zheng, Numerical simulation of a generalized Zakharov system, *J. Comput. Phys.*, 201 (2004), pp. 376–395.
- [43] , S. Kamvissis, K.T.R. McLaughlin and P.D. Miller, Semiclassical soliton ensembles for the focusing nonlinear Schrödinger equation, *Annals of Mathematics Studies* 154, Princeton University Press, Princeton, 2003.
- [44] D. Kaya, An implementation of the ADM for generalized one-dimensional Klein-Gordon equation, *Appl. Math. Comput.*, 166 (2005), pp. 426-433.
- [45] M.E. Khalifa and M. Elgamal, A numerical solution to Klein-Gordon equation with Dirichlet boundary condition, *Appl. Math. Comput.*, 160 (2005), pp. 451-475.
- [46] A.Q.M. Khaliq, B. Abukhodair and Q. Sheng, A predictor-corrector scheme for the sine-Gordon equation, *Numer. Methods Partial Differ. Eqns.*, 16 (2000), pp. 133-146.
- [47] K.R. Khusnutdinova and D.E. Pelinovsky, On the exchange of energy in coupled Klein-Gordon equations, *Wave Motion*, 38 (2003), pp. 1-10.

- 
- [48] O.M. Kiselev, Perturbation of a solitary wave of the nonlinear Klein-Gordon equation, *Siberian Math. J.*, 41 (2000), pp. 345-358.
- [49] G.L. Lamb, *Elements of soliton theory*, Wiley, New York, 1980.
- [50] Y. Li and B. Guo, Asymptotic smoothing effect of solutions to weakly dissipative Klein-Gordon-Schrödinger equations, *J. Math. Anal. Appl.*, 282 (2003), pp. 256-265.
- [51] X.Q. Liu and S. Jiang, Exact solutions of multi-component nonlinear Schrödinger and Klein-Gordon equations, *Appl. Math. Comp.*, 160 (2005), pp. 875-880.
- [52] X. Lu and R. Schmid, Symplectic integration of sine-Gordon type systems, *Math. Comput. Simul.*, 50 (1999), pp. 255-263.
- [53] K.N. Lu and B.X. Wang, Global attractors for the Klein-Gordon-Schrödinger equation in unbounded domains, *J. Diff. Eq.*, 170 (2001), pp. 281-316.
- [54] V.G. Makhankov, Dynamics of classical solitons (in non-integrable systems), *Phys. Lett. C*, 35 (1978), pp. 1-128.
- [55] P. Miller and S. Kamvissis, On the semiclassical limit of the focusing nonlinear Schrödinger equation, *Phys. Lett. A*, 247 (1998), pp. 75-86.
- [56] M. Ohta, Stability of stationary states for the coupled Klein-Gordon-Schrödinger equations, *Non. Anal.*, 27 (1996), pp. 455-461.
- [57] T. Ozawa, K. Tsutaya and Y. Tsutsumi, Well-posedness in energy space for the Cauchy problem of the Klein-Gordon-Zakharov equations with different propagation speeds in three space dimensions, *Math. Ann.*, 313 (1999), pp. 127-140.

- 
- [58] T. Ozawa, and Y. Tsutsumi, Asymptotic behaviour of solutions for the coupled Klein-Gordon-Schrödinger equations, *Adv. Stud. Pure Math.*, 23 (1994), pp. 295-305.
- [59] A.C. Scott, *Active and nonlinear wave propagation in electronics*, Springer, New York, 1978.
- [60] R. Shankar, *Principles of quantum mechanics*, Kluwer Academic/Plenum Publishers, New York.
- [61] G. Strang, On the construction and comparison of difference schemes, *SIAM J. Numer. Anal.*, 5 (1968), pp. 505-517.
- [62] W.A. Strauss and L. Vázquez, Numerical solution of a nonlinear Klein-Gordon equation, *J. Comput. Phys.*, 28 (1978), pp. 271-278.
- [63] T.R. Taha and M.J. Ablowitz, Analytical and numerical aspects of certain nonlinear evolution equations, III. Numerical, nonlinear Schrödinger equation, *J. Comput. Phys.*, 55 (1984), pp. 203-230.
- [64] K. Veselic, On the nonrelativistic limit of the bound states of the Klein-Gordon equation, *J. Math. Anal. Appl.*, 96 (1983), pp. 63-84.
- [65] Q.F. Wang and D.Z. Cheng, Numerical solution of damped nonlinear Klein-Gordon equations using variational method and finite element approach, *Appl. Math. Comput.*, 162 (2005), pp. 381-401.
- [66] Y.H. Wang, B. Wang, High-order multi-symplectic schemes for the nonlinear Klein-Gordon equation, *Appl. Math. Comput.*, 166 (2005), pp. 608-632.
- [67] M.L. Wang and Y.B. Zhou, The periodic wave solutions for the Klein-Gordon-Schrödinger equations, *Phys. Lett. A*, 318 (2003), pp. 84-92.
- [68] R.A. Weder, Scattering theory for the Klein-Gordon equation, *J. Functional Analysis*, 27 (1978), pp. 100-117.

- [69] X.M. Xiang, Spectral method for solving the system of equations of Schrödinger-Klein-Gordon field, *J. Comput. Appl. Math.*, 21 (1988), pp. 161-171.
- [70] L.M. Zhang, Convergence of a conservative difference scheme for a class of Klein-Gordon-Schrödinger equations in one space dimension *Appl. Math. Comput.*, 163 (2005), pp. 343-355.